PROTEOMICS OF OXIDATIVE STRESS USING INDUCIBLE CYP2E1 EXPRESSING HEPG2 CELLS AND 3T3-L1 ADIPOCYTES AS MODEL SYSTEMS

A Dissertation

by

BILLY WALKER NEWTON

Submitted to the Office of Graduate Studies of
Texas A&M University
in partial fulfillment of the requirements for the degree of

DOCTOR OF PHILOSOPHY

May 2011

Major Subject: Chemical Engineering

Proteomics of Oxidative Stress Using Inducible CYP2E1 Expressing HepG2 Cells and 3T3-L1 Adipocytes as Model Systems

Copyright 2011 Billy Walker Newton

PROTEOMICS OF OXIDATIVE STRESS USING INDUCIBLE CYP2E1 EXPRESSING HEPG2 CELLS AND 3T3-L1 ADIPOCYTES AS MODEL SYSTEMS

A Dissertation

by

BILLY WALKER NEWTON

Submitted to the Office of Graduate Studies of
Texas A&M University
in partial fulfillment of the requirements for the degree of

DOCTOR OF PHILOSOPHY

Approved by:

Chair of Committee,	Arul Jayaraman
Committee Members,	David H. Russell
	Mariah Hahn
	Zhilei Chen
Head of Department,	Michael V. Pishko

May 2011

Major Subject: Chemical Engineering

ABSTRACT

Proteomics of Oxidative Stress Using Inducible CYP2E1 Expressing HepG2 Cells and 3T3-L1 Adipocytes as Model Systems.

(May 2011)

Billy Walker Newton, B.S.; M.S., Texas A&M University

Chair of Advisory Committee: Dr. Arul Jayaraman

The overall goal of this research was to investigate oxidative stress related changes to the proteomes of 3T3-L1 adipocytes and an inducible CYP2E1 expressing HepG2 cells. Enhanced oxidative stress in hypertrophic adipocytes is associated with metabolic dysregulation and insulin resistance. Because mitochondria generate reactive oxygen species (ROS), we monitored changes to the adipocyte mitochondrial proteome during differentiation and enlargement. We labeled mitochondrial extracts from 3T3-L1 cells that were 0, 4, 7, 10, 14, and 18 days post differentiation with iTRAQ, followed by MS based identification. We found citric acid cycle proteins such as pyruvate carboxylase, citrate synthase, as well as beta-oxidation enzymes; cartinine acyl transferase and long-chain enoyl-CoA hydratase up-regulated from 7 through 18 days post differentiation onset. These data indicate TCA up-regulation for enhanced metabolic and citrate output necessary for lipid synthesis in adipocytes. Paradoxically, the data also show the simultaneous increase in the fatty acid oxidation, indicating a metabolic overdrive state. Biochemical assays showing peaks in ATP and ROS generation in 3 day old adipocytes

provide further evidence of this overdrive state. A second peak in ROS generation occurred in 10 day old adipocytes; concurrent ATP generation reduced to near pre-adipocyte levels and this may indicate a metabolic shift that may be responsible for increased oxidative stress in hypertrophic adipocytes.

We developed a doxycycline inducible CYP2E1 expressing HepG2 cell line using the pTet-On/pRevTRE expression system to allow greater control and sensitivity in the generation CYP2E1 mediated oxidative stress. Our cell line (RD12) demonstrated stability and tight expression control. After induction, RD12 cells showed 30 percent higher CYP2E1 activity when compared to the constitutive E47 cell line. RD12 cells showed 30% greater toxicity than E47 cells and 25% less free glutathione when exposed to 20 mM acetaminophen, indicating RD12 cells are more sensitive to the effects reactive intermediates and oxidative stress generated by CYP2E1.

We conducted a survey of the toxicity of dietary fatty acids (oleic, linoleic, and palmitic) on HepG2 cells to determine fatty acid doses that induced metabolic changes, but did not cause excessive cell death. The dose of 0.20 mM linoleic and palmitic acid for 48 hours produced low toxicity, but oleic acid actually produced lower toxicity than untreated cells. After exposure cells were treated with a pro-oxidant to determine which fatty acid increased the susceptibility to protein carbonylation. The carbonylated protein isolation procedure indicated the palmitic acid may induce more carbonylation than oleic acid, but greater efficiency in the isolation procedure is required for a confidant determination.

DEDICATION

I would like to dedicate this work to my wife, to my mother and to my father. Without all of their love, support and belief in me, this effort would not be possible. They kept me going through all of the long days and nights in the lab, when things went right, and when they did not. These are the people I do not want to let down.

ACKNOWLEDGEMENTS

I would like to thank my committee chair, Dr. Arul Jayaraman, and my committee members, Dr. David Russell, Dr. Mariah Hahn, and Dr. Zhilei Chen, for their guidance and support throughout the course of this research.

I thank Dr. Jayaraman for being an excellent advisor during my studies at Texas A&M. He has been patient, caring and helpful during my research. He has taught me to be thoughtful and diligent in my writing and data analysis. He has encouraged and been supportive of the development of my own ideas and conclusions regarding my work. My fondest memories are meeting with him and going over data and ideas for new experiments. It has been a privilege and a pleasure to work for him.

I thank Dr. Bill Russell, Stephanie Cologna, Dr. David Russell, and the rest of the staff at The Laboratory for Biological Mass Spectrometry – Texas A&M University (LBMS-TAMU). They performed all mass spectrometry for our experiments. Without their efforts and expertise, this work would not be possible. I also thank members of the Dr. Thomas Wood Lab and the Dr. Mariah Hahn Lab for the help. Thanks go to my wife for help and support in type-setting and proof-reading.

Thanks also go to my friends and colleagues and the department faculty and staff for making my time at Texas A&M University a great experience. I thank Towanna Arnold,

Dr. Pishko, and all the Chemical Engineering Department staff for their help. I thank Colby Moya, Thomas Richardson, Tarun Bansal, Manjunath Hegde, Fatih Senocak, Allison Liable, Shreya Maite, Sunny Kim, Derek Englert, and any others who helped me in performing my laboratory work.

I also want to extend my gratitude to the National Science Foundation, the American Heart Association, and the National Institutes of Health for their financial support of this research.

TABLE OF CONTENTS

Page

CHAPTER Page

Page

LIST OF FIGURES

FIGURE Page

LIST OF TABLES

CHAPTER I

INTRODUCTION

1.1. BACKGROUND

It is becoming increasingly evident that oxidative stress plays a major role in the manifestation of many (1) diseases (1), including Alzheimer's disease (2), atherosclerosis (3), type II diabetes (4), obesity (5), alcoholic and non-alcoholic liver disease (5, 6), and the aging process itself (7). Reactive oxygen species (ROS) are ubiquitous and an unavoidable consequence of aerobic respiration, and normal metabolism results in the generation of different ROS, such as the superoxide ion (8). In a normal cell, the ROS generated are normally cleared away by the cellular anti-oxidant machinery, and a state of oxidative stress arises when the rate of generation (and the deleterious effects) of reactive oxygen species (ROS) is much greater than their rate of removal by the antioxidant systems (8). The excess ROS present are capable of targeting all classes of biomolecules including DNA, protein, and lipids (1, 8). The accumulation of such oxidatively-damaged biomolecules can lead to cellular dysfunction and cell death, and oxidatively-modified proteins have been detected in neurons of Alzheimer's patients (9), adipose tissue of obese mice (10), and in liver tissue from alcohol-fed rats (11). Oxidative stress has also been linked to impaired glucose transport in adipocytes (12) and in the progression to steatohepatitis in hepatocytes (5).

This dissertation follows the style of *The Journal of the Federation of American Societies for Experimental Biology.*

Oxidative stress has been linked to impaired glucose transport in adipocytes (12) and in the progression of steatosis to steatohepatitis in hepatocytes (5). Characterizing ROS and oxidative stress, i.e., production and removal of free radicals, is challenging for two reasons. The half-life of free radicals is very short (10^{-9} s for the hydroxyl radical (8)) which makes accurate determination of ROS concentrations very difficult. In addition, the redox state of the cell can change very rapidly, such that a single measurement of ROS may not accurately represent the ROS concentration and its effects. An alternate approach to characterizing oxidative stress is to focus on the effects of these free radicals on biomolecules, especially proteins, since protein levels and modifications are more stable, i.e., like a molecular footprint, are more amenable to detection, and whole-proteome monitoring technologies are well established (13-15). Furthermore, since proteins provide structure and conduct biochemistry of cells and cellular dysfunction typically arises from changes in protein levels or activity, it is more pertinent to monitor changes in the proteome due to an imbalance of oxidative stress in cells.

Our overall goal is to develop and utilize model systems for characterizing oxidative stress modifications to the proteome and investigating their role in cellular dysfunction and disease. To accomplish this, we plan to conduct quantitative proteomic studies using two model systems - 3T3-L1 adipocytes and hepatocytes. These are both relevant and valid model systems, as oxidative stress and ROS affect the function of both adipose tissue and the liver (4-6, 12, 16).

1.2. MOTIVATION

It is estimated that approximately 21 million people in the U.S. have type II diabetes, and the annual total cost for treatment is over $80 billion (17). As of 2002, diabetes was the sixth leading cause of death listed on US death certificates (17), and 90 percent of new diabetes cases suffer from type II diabetes (18). Clearly type II diabetes is a major public health issue. Insulin resistance seen in type II diabetes has been linked to inflammation and oxidative stress in hypertrophic adipocytes (12, 19), and understanding mechanisms for these processes will lead to targets for improved therapy.

Alcoholic and non-alcoholic fatty liver diseases are also conditions where the accumulation fat in cells is linked to metabolic problems. While alcoholic and non-alcoholic fatty liver disease share different initial causes, there is believed to similarities in both conditions (such as enhanced oxidative stress and/or inflammation) that cause them to progress to serious conditions of steatohepatitis and eventually cirrhosis (5, 20-22). The healthcare treatment cost for alcohol related diseases, especially alcoholic liver disease and alcoholic cirrhosis is over $20 billion annually in the U.S. (23). Non-alcoholic fatty liver disease (NAFLD) is also a major growing public health problem (24), with one-third of diagnoses developing end-stage cirrhosis (25). NAFLD typically shares some of same symptoms associated with type II diabetes such as insulin resistance, obesity, and high triglycerides (5). The current studies involving 3T3-L1 adipocytes and CYP2E1 expressing hepatocytes are at a cellular and mechanistic level. The information provided on how oxidative stress manifests in cells can be used to help

understanding in other conditions associated with oxidative stress and the effects of ROS. These studies also provide information for targets of further study in the understanding the development and eventual treatment for diseases (type II diabetes, insulin resistance, and alcoholic and non-alcoholic liver disease) with severe public health consequences and costs.

1.3. RESEARCH OBJECTIVE, IMPORTANCE, AND NOVELTY

We looked at three systems to measure the effects of oxidative stress in 3 cell culture based models that moved from more natural to more engineered approaches as out lined in Figure 1.1. The first system was where ROS and oxidative stress occur naturally in differentiating and enlarging adipocytes, the second system aimed to determine if dietary fatty acids could modulate ROS and their effects, and last we sought to create a controllable system where ROS could induced at specific time points.

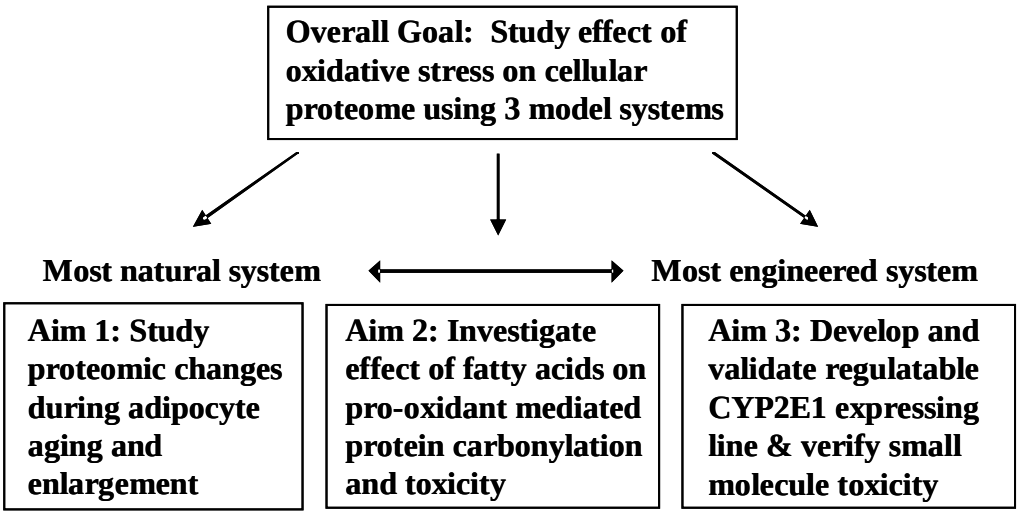

Figure 1.1. Outline of research goals.

The increase in adipose tissue mass arises in part due to progressive lipid loading and triglyceride accumulation in adipocytes. Enlarged adipocytes produce the highest levels of pro-inflammatory molecules and reactive oxygen species (ROS). Since mitochondria are the site for major metabolic processes, e.g., TCA cycle, that govern the extent of triglyceride accumulation as well as the primary site of ROS generation, we quantitatively investigated changes in the adipocyte mitochondrial proteome during different stages of differentiation and enlargement. Mitochondrial proteins from 3T3-L1 adipocytes at different stages of lipid accumulation (days 4 through 18) were digested and labeled using the iTRAQ 8-plex kit. The labeled peptides were fractionated using a liquid phase isoelectric fractionation system (MSWIFT) to increase the depth of proteome coverage, and analyzed using LC-MS/MS. While the 3T3-L1 adipocyte nuclear proteome and secreted proteome has been characterized during differentiation (through day 7) using SILAC (15), and the mitochondrial proteome studied in isoproternol-treated adipocytes at a single time point (26), the 3T3-L1 mitochondrial proteome has not been profiled from the pre-differentiated state through 18 day old hypertrophic adipocytes, as was undertaken in the current study.

The forced over-expression of CYP2E1 in hepatoma cells with a constitutive CMV promoter has been shown to lead to increased oxidative stress (27); however, forced constitutive expression of CYP2E1 also leads to adaptation of HepG2 to oxidative stress through an increase in the basal expression of anti-oxidant systems (28). Therefore we developed an inducible CYP2E1 expression system for two major reasons: 1) enhanced

sensitivity to CYP2E1 mediated oxidative stress, and 2) control over CYP2E1 induction to allow pre-treatment with pharmacological or labeling agents. These advantages will enhance investigations of effects of CYP2E1 generated ROS and oxidative stress, and development of inducible expression of CYP2E1 in HepG2 hepatocytes has not been reported.

Dietary fatty acids have modulated ROS in cells differently, with palmitic acid increasing ROS generation (29), and oleic acid inducing protection against added oxidants (30). We conducted a detailed survey of the toxicity of dietary fatty acids (oleic, linoleic, and palmitic) on HepG2 hepatocytes in order to determine fatty acid doses that induced metabolic changes, but did not cause excessive cell death. After fatty acid exposure cells were treated with the pro-oxidant *tert*-butyl hydroperoxide (*t*-BHP) to determine which fatty acid increased the susceptibility to protein carbonylation. A study determining the extent and type of protein carbonylation to the aforementioned fatty acids has not been reported.

The specific objectives in this course of study were to:

- Determine global mitochondrial proteome expression profiles from 3T3-L1 adipocytes that were 0,4,7,10,14,18 days post differentiation

- Conduct concurrent biochemical assays to determine lipid loading, ATP production, and ROS generation in 3T3-L1 adipocytes during differentiation and hypertrophy
- Develop a pRevTRE-CYP2E1 expression plasmid and verify its sequence and functionality
- Create a stable doxycycline inducible CYP2E1 expressing HepG2 hepatocyte cell line using the pRevTRE-CYP2E1 expression plasmid
- Characterize the controlled expression and enhanced oxidative stress sensitivity of doxycycline inducible CYP2E1 expressing HepG2 cell line
- Survey the cyto-toxic effects of fat pre-loading HepG2 hepatocytes with varying concentrations of dietary fatty acids (oleic, linoleic, and palmitic), both prior to and after the addition of the pro-oxidant *t*-BHP
- Isolate carbonylated protein from fatty acid and *t*-BHP treated HepG2 cells using affinity chromatography, in order to determine the extent and pattern of protein carbonylation produced by different fatty acids

CHAPTER II

LITERATURE REVIEW

2.1. METABOLISM AND GLUCOSE HOMEOSTASIS

Maintaining homeostasis in the human body requires interplay between various organs and systems to maintain appropriate metabolites levels. These metabolites, e.g., blood glucose, are maintained in a tight range despite periods of rapid ingestion of carbohydrate followed by periods of varying energy expenditure such as during physical activities or periods of extended fasting such as during sleep. Figure 2.1 demonstrates a typical blood glucose and insulin level during a 24-hour period. The maintenance of blood glucose within the reference range of 3.6 - 5.8 mmol (0.6 – 1.2 g/L) is perhaps the simple most important metabolic functions and is primarily carried out by the insulin/glucagon system (31).

Beta cells of pancreas produce insulin. Insulin is a 5300 Dalton peptide hormone whose primary function is to stimulate muscle and adipose tissue cells to take up glucose from the blood (31). The combination of muscle and adipose tissue cells represents 2/3 of total

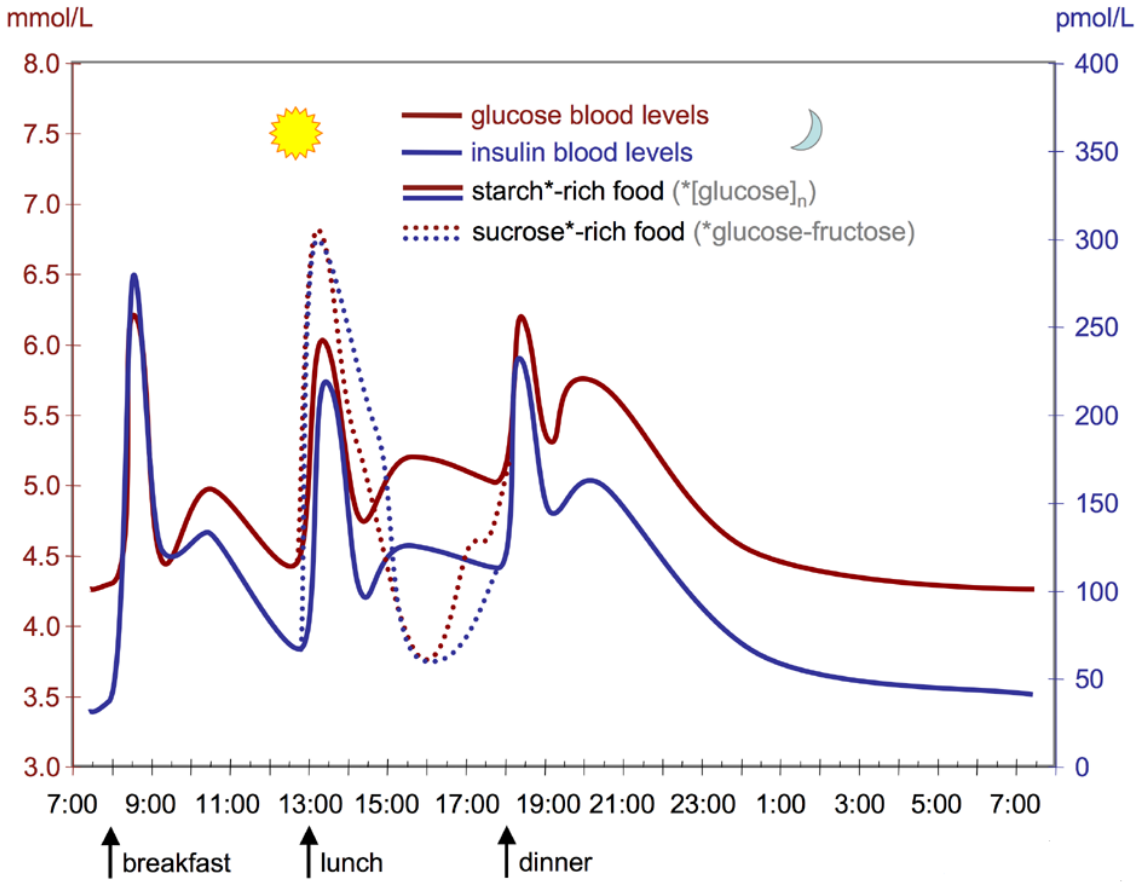

Figure 2.1. Typical 24-hour blood glucose and insulin levels (32).

body cells and the action of insulin lowers blood sugar (33). Insulin is also anabolic by promoting uptake of amino acid and protein synthesis (34). Glucose is the main source of energy for the brain since neuron cells in the brain are not able to use fat as fuel.

In contrast to insulin is the enzyme glucagon (35). Glucagon is secreted by pancreas when blood sugar levels are too low. Glucagon first stimulates breakdown of glycogen to glucose and induces glycogenesis in the liver. It also promotes synthesis of glucose from amino acids and triglycerides. Glucose produced from liver in turn can be excreted to the blood stream. This way, glucagon always stimulates insulin release. The glucose produced is available to be taken up by insulin dependent tissues.

Insulin binds to receptors on muscle cells (myocytes) and fat cells (adipocytes) and triggers signaling cascades that result in the localization of additional glut-4 glucose transporters to the plasma membrane. The activation of glut-4 in the membrane facilitates diffusion of glucose into these cells. Once in the cell, glucose enters the glycolysis pathway and is rapidly phosphorylated by a hexokinase so it cannot diffuse out of the cell. Table 2.1 shows all of the enzymes involved in a glycolysis. Hexokinases I-II are found in peripheral tissue and have low kinetic constant, K_m, so they are still able to function with low glucose level. They are allosterically inhibited by their product glucose-6-phosphate. Glucokinase (hexokinase IV) is only found in the liver and has much higher K_m, so it is only active at higher glucose concentration. It is not allosterically inhibited which allows the liver to regulate blood sugar levels.

Table 2.1. Glycolysis pathway (31).

Step	Substrate	Enzyme	Product
1	Glucose	*Hexokinase*	Glucose-6-phosphate
2	Glucose-6-phosphate	*Phosphoglucose isomerase*	Fructose 6-phosphate
3	Fructose 6-phosphate	*Phosphofructokinase*	Fructose 1,6-bisphosphate
4	Fructose 1,6-bisphosphate	*Fructose bisphosphate aldolase*	Glyceraldehyde 3-phosphate + Dihydroxyacetone phosphate
5	Dihydroxyacetone phosphate	*Triosephosphate isomerase*	Glyceraldehyde 3-phosphate
6	Glyceraldehyde 3-phosphate	*Glyceraldehyde phosphate dehydrogenase*	1,3-bisphosphoglycerate
7	1,3-bisphosphoglycerate	*Phosphoglycerate kinase*	3-phosphoglycerate
8	3-phosphoglycerate	*Phosphoglycerate mutase*	2-phosphoglycerate
9	2-phosphoglycerate	*Enolase*	Phosphoenolpyruvate
10	Phosphoenolpyruvate	*Pyruvate kinase*	Pyruvate

2.2. HYPERGLYCEMIA AND TYPE II DIABETES AND OBESITY

If glucose cannot be sufficiently removed from the blood stream, hyperglycemia results and this is the hallmark of diabetes mellitus. Diabetes type I, i.e., juvenile diabetes, results from destruction of the beta cells that produce insulin, typically at an early age. The exact reason for the destruction of beta cells remains unknown. Diabetes type I is characterized as a polygenic multifactorial process. Genetic susceptibility, diabetic triggers, and one or more antigens result an autoimmune response that destroy beta cells (36, 37). Environmental factors are important, as monozygotic twins of a parent with diabetes type I only both develop the disease about 50 percent of the time (36, 37). Currently, treatment of type I diabetes relies on the daily administration of exogenous insulin to control blood sugar level (17).

In contrast to type I diabetes, type II diabetes is a metabolism disorder. It typically appears later in life. It is increasingly being observed in adolescence and young adults (38). The resulting hyperglycemia found in type II diabetes comes from the existing insulin being unable to sufficiently control the blood glucose level (18). The normally insulin responsive tissue in type II diabetes are said to be “insulin resistant” (18) and develop a relative insulin deficiency, whereas in type I diabetes, the insulin producing cells no longer exist. In either case, hyperglycemia, if left untreated can lead to the development of debilitating conditions such as heart attack, stroke, kidney failure, blindness and limb amputation.

Type II diabetes is characterized as a combination of lifestyle and genetic factors. In one recent study, those who have high levels of activity, did not smoke, maintained a healthy weight, ate a diet high in fiber and low in saturated fat have an 89 percent lower rate of type II diabetes (39). Over 55 percent of type II case are associated with obesity (40). Type II diabetes when accompanied by co-morbidities of obesity, hypertension, and high triglycerides is often referred as metabolic syndrome (12, 41). There is a genetic component of type II diabetes. Having a first degree relation with it increases risk substantially and there is a specific mutation in the gene for islet amyloid peptide that results in earlier onset and severity of the disease (42, 43). But clearly, environmental and lifestyle factors are important as it has been shown in recent immigrants from populations with traditionally low incidents of type II diabetes have a substantial increase in type II diabetes when they adopt a Western lifestyle (33).

Much ongoing research aims to study the link between obesity, type II diabetes, and its associated insulin resistance. Adipose tissue, especially that from the mesenteric organs (visceral adipose tissue), is not thought of as simple fat storage depot but rather an organ capable of carrying out several metabolic reactions, such as lowering blood glucose, providing satiety signals, and excreting cytokines. Adipocytes have been shown to produce cytokines TNFα, IL-6 and IL-8 (44). Treatment of cultured adipocytes with TNFα decreased mitochondrial membrane potential, reduced ATP levels, and increased ROS production, implying it has role in adipocyte dysfunction (45). Adipocytes also produce the recently discovered adipocyte specific hormones leptin (46) and adiponectin

(47). The cytokine IL-6 is a major mediator of the inflammation response (48). Leptin is primarily produced in adipose tissue. It produces a satiety signal and reduces appetite. Leptin is found in high concentration in obese people and they are referred to as being leptin resistant, in the same sense as people with type II diabetes are insulin resistant (49). There is a strong correlation between adipocyte cell volume and the excretion of leptin, TNFα, IL-6, IL-8 (44), thus hypertrophic adipocytes are the most metabolically active. For this reason, studying metabolism and dysfunction in hypertrophic adipocytes can lead to better understanding of the metabolic dysregulation of adipose tissue. Adiponectin has been inversely correlated to body fat percentage and administration of adiponectin has lowered blood glucose levels and improved insulin sensitivity (50).

Oxidative stress has been linked to adipocytes and obesity. One study has shown the increased oxidative stress markers in the plasma and adipose tissue of obese mice (12). Another study shows the increased production of reactive oxygen species in cultured 3T3-L1 adipocytes to be proportional to the glucose concentration in culture media (19). Kobayashi et al. found cultured adipocytes to have a lower response to insulin after exposure to hydrogen peroxide (51). All of these taken together indicate the importance of oxidative stress in adipocytes and in glucose metabolism. In light of current research on the subject, type II diabetes and obesity are viewed as metabolic disorders with inflammatory and oxidative stress related components.

2.3. STEATOSIS

Steatosis is defined as the accumulation of fat in the liver that is manifested in a variety of conditions, and is categorized as either being related to alcoholic fatty liver disease (ALD) or non-alcoholic fatty liver disease (NAFLD) (6, 52). Steatosis is an important condition because it often marks the onset of possible problems with liver function that if left untreated could progress to more serious conditions such as steatohepatitis.

Steatosis is the first and most common pathology in ALD and occurs in up to 90 percent of alcoholics. Fatty liver is thought to be mainly a result of metabolic disturbances, such as decreased fatty acid oxidation, increased triglyceride synthesis, reduced fat export, and mobilization of extra-hepatic fat stores (16, 53-55). The metabolism of ethanol to acetaldehyde and its subsequent conversion to acetate produces NADH. The cellular accumulation of NADH increases substrate available for fatty acid synthesis, as well as disrupts mitochondrial beta oxidation, thereby leading to fat accumulation (56). Steatosis has long been considered a benign condition, as even severe cases of AS recovered after 3-4 weeks of alcohol withdrawal (57-59). However, more recent studies indicate that the metabolic changes taking place during the steatosis may also sensitize the cells to further injury (60-63). Lieber (54) suggested that metabolic changes of fatty liver alone may be insufficient to cause inflammation. It is now believed that degree of fat accumulation in the liver correlates to the susceptibility of subsequent liver damage (21). Researchers have shown that fatty liver is highly vulnerable to oxidative stress or injury mediated by endotoxins or cytokines, and Day has referred to this as the “two-hit”

hypothesis (60, 64, 65). While these studies show vulnerabilities of steatotic livers, one study also showed that a fatty liver induced by 5 weeks of ethanol exposure demonstrated enhanced capacity to regenerate and consequent decrease in hepatic injury (66). This was not due to reduced CYP2E1 activity, but possibly through activation of the transcription factor NF-κB (66).

Evidence exists that alcohol alone may not be enough to cause steatohepatitis and necrosis, and further studies are needed to understand mechanisms of AS, and identify biomarkers leading to subsequent pathological stages of ALD (6). While a detailed understanding of the mechanisms underlying the transition from AS to ASH is lacking, it is known that continued consumption of alcohol in humans eventually results in neutrophilic steatohepatitis (67, 68). Neutrophil infiltration into the liver is hallmark of ASH and contributes to the pathology of ALD. Alcoholic steatohepatitis reverts back to normal hepatic histopathology approximately only 10 percent of the time (69). Most patients with steatohepatitis (almost 50 percent) go on to develop fibrosis and cirrhosis (Figure 2.2). Steatohepatitis therefore represents a major rate limiting step in the progression towards cirrhosis and clinical liver disease (70, 71). It would be beneficial to patients with ALD to receive diagnosis and intervention before the onset of steatohepatitis and even cirrhosis. The term non-alcoholic steatohepatitis (NASH) was only recently coined in 1980 (72). NAFLD is now estimated to affect between 15 - 30 percent of adults in the U.S. (5) and parallels the incidence of obesity, insulin resistance, type II diabetes, high triglycerides, hypertension and other markers for the "metabolic

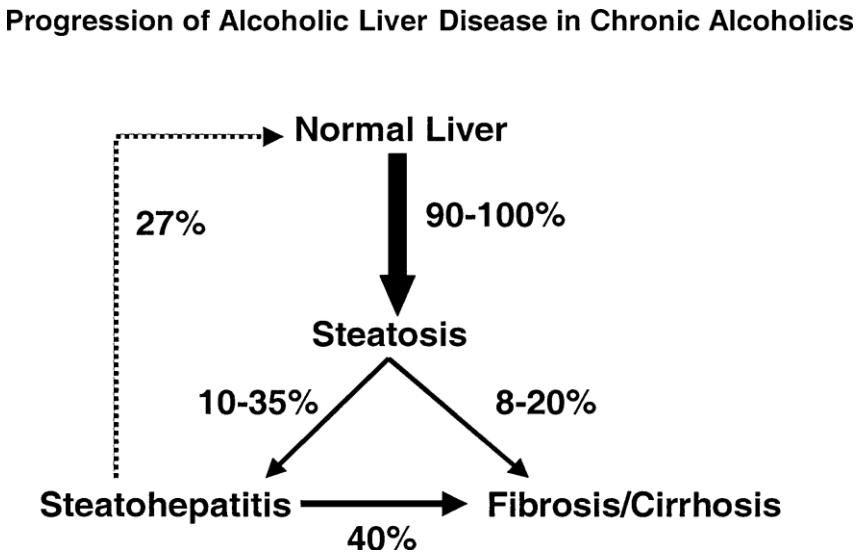

Figure 2.2. Progression of alcoholic liver disease. Consumption of ethanol produces hepatic pathology in sequence, ranging from steatosis (fatty liver) on one extreme, to fibrosis/cirrhosis on the opposite end of the spectrum (6).

syndrome" (5, 24). NAFLD strongly correlates with markers of the metabolic syndrome (73, 74), especially with insulin resistance in the liver and adipose tissue (75, 76). Non-alcoholic steatosis follows a similarity with alcoholic steatosis, in that not every case proceeds to steatohepatitis, or cirrhosis. Only 1 – 5 percent of non-alcoholic steatosis cases develop into cirrhosis (24). This is still a very significant number however, and further highlights the benefits early intervention in steatosis. The "two-hit" hypothesis outlined by Day (21, 24, 77) still applies to NASH.

NASH has been linked to mitochondrial dysfunction and production of increased ROS (78), and an increase in serum tumor necrosis factor alpha (TNFα) has been strongly linked to the progression of steatosis to NASH (79), and CYP2E1 activity has been found elevated in NASH patients (80). Current research is dedicated to understanding the mechanisms behind the progression of steatosis to NASH, as well as the underlying insulin resistance and dislypedemia found in NAFLD.

2.4. CYTOCHROME P450 2E1

The cytochrome P-450 (CYP) system is a large family of mono-oxygenase enzymes primarily found in the liver. The P-450 system is responsible for the modification and detoxification for a large variety of endogenous and exogenous substrates. Humans have more than 50 separate cytochrome P450 genes (81, 82). Many drugs or small molecules are inducers of P450 enzymes. Phenobarbitol induces CYP3A4 (83) and ethanol and pyrazole induce CYP2E1 (84-86). Steroid hormones are also an important class of endogenous substrates, e.g., CYP19A1 converts testosterone to estradiol (82). A major function of P450 catalyzed reactions is to hydroxylate compounds into a metabolite that can be easily excreted from the body. These reactions are referred to as phase I drug metabolism reactions. The addition of a hydroxyl group allows subsequent conjugation by phase II enzymes such glutathione-S transferase. This further detoxifies the compound and increases water solubility of metabolites, thereby, facilitating excretion. Not all xenobiotics are converted to water-soluble (harmless) intermediates, as compounds such as carbon tetrachloride and acetaminophen (86-88) are converted by P450 to a toxic intermediates which damage cells. For P450s to function catalytically, they need a source reducing equivalents such as NADPH cytochrome P450 reductase to reduce the heme iron.

Cytochrome P450 enzymes are regarded as a source of ROS (89, 90). While the overall P450 catalytic cycle is very efficient, small amounts of the superoxide anion radical (O_2^-) can be produced from premature decoupling of the oxygenated P450 complex.

Fridovich and others have estimated between 0.1 - 1.0 percent of molecular oxygen entering such cycles forms superoxide ions (90). Most of the oxygen decoupling happens between steps 3 and 4 in the P450 catalytic cycle represented in Figure 2.3.

Cytochrome P450 2E1 (CYP2E1) metabolizes a broad range of small molecules, including ethanol, pyrazole, aniline, p-nitrophenol, and acetaminophen (84, 85, 91). CYP2E1 is rapidly induced by ethanol. Cultured primary hepatocytes experience a nearly 200 percent increase in CYP2E1 activity after exposure to 100 mM ethanol for 12 hours (92). CYP2E1 has been highly studied as source of increased ROS and oxidative stress that occurs during chronic alcohol consumption (93, 94).

CYP2E1 displays high NADPH oxidase activity, as it produces superoxide ions at a higher rate than several other P450 enzymes, and this may result from poor coupling with NADPH-cytochrome P450 reductase (95, 96). CYP2E1 has been reported to generate the most lipid peroxidation in a study of five isolated P450 enzymes (96). CYP2E1 is primarily located in the endoplasmic reticulum (86), however it has been detected in the mitochondria, and one study estimated about 25 percent of total CYP2E1 is present in the mitochondrion (97). CYP2E1 expression is believed to have a high degree of post translation control, as incubation with the substrate methyl-pyrazole decreased the degradation rate (98). When CYP2E1 has been induced by chronic ethanol exposure, it takes part in what has been referred to as the microsomal ethanol oxidizing

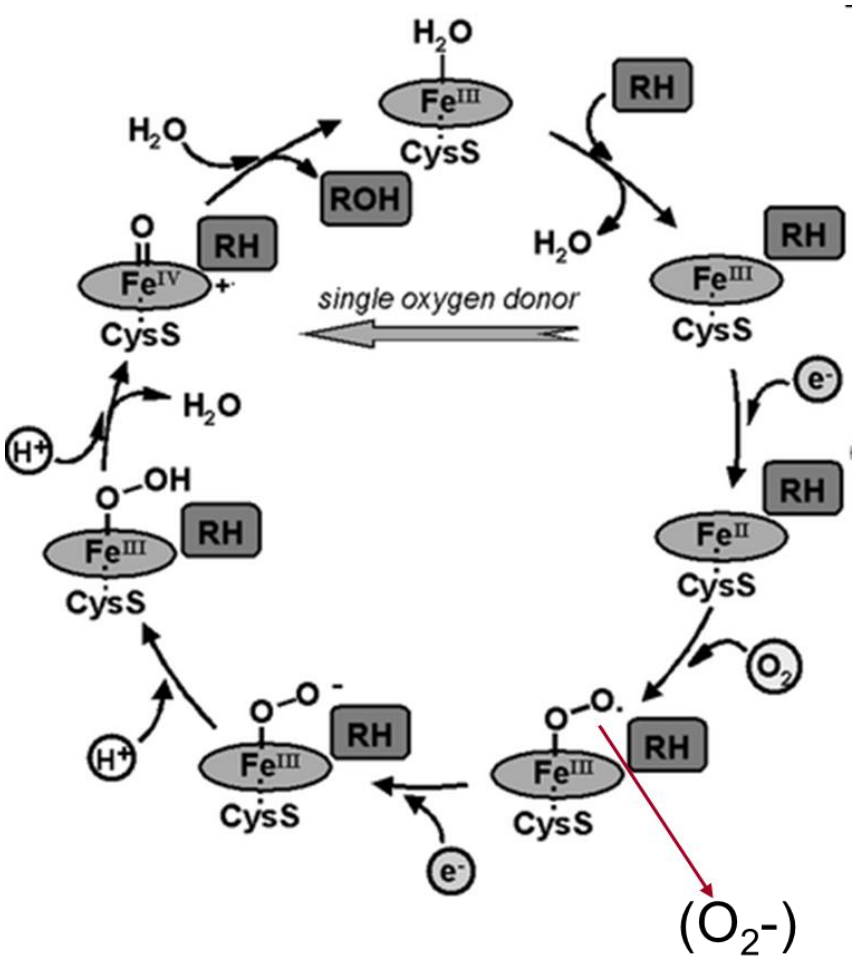

Figure 2.3. The catalytic cycle of cytochrome P450 2E1 (99).

system (MEOS), however this was found to likely only oxidize 10 percent of the ethanol when compared to alcohol dehydrogenase (100).

Alcohol is a major substrate for the CYP2E1 enzyme. Rats fed a Leiber-DiCarli ethanol based diet for 4 weeks experienced a 3-5 fold increase in CYP2E1 expression and a 2-3 fold increase superoxide ion production (101). A variety of metabolic or nutritional conditions can also induce CYP2E1 expression. Obese rats fed a high fat diet have elevated CYP2E1 levels (102) and diabetic rats have increased CYP2E1 mRNA (103), and this may be related to the fact that ketone bodies increase CYP2E1 expression (104). Ethanol-fed rats were more sensitive to the toxic effects of the endotoxin lipopolysaccaride and had higher TNFα levels in plasma when compared to control rats (6, 105, 106) Although CYP2E1 is implicated in ethanol-induced oxidative damage, there has been some controversy in the role of CYP2E1 in alcohol induced liver injury. Using an intra-gastric feeding model, Thurman et al. reported that endotoxin, activation of Kupffer cells, and cytokines such as TNFα play the largest role in the alcohol-induced liver injury (107, 108). More importantly, they also reported that inhibition with gadolinium chloride and CYP2E1-knockout mice suggest a limited role for CYP2E1 in alcohol-induced liver injury (109, 110) But using the same intra-gastric model Bardag-Gorce et al. (111) reported that ethanol-induced oxidative stress and inactivation of the proteasome complex were completely prevented in these mice (CYP2E1 knock-out and inhibited mice). Based these findings it was concluded that CYP2E1 induction was

responsible for the decrease in proteasome activity and accumulation of oxidatively-modified liver proteins.

Several cell lines, such as the HepG2 E47 line, have been engineered to constitutively-express CYP2E1 (27, 112). Sequential exposure of E47 cells to ethanol, polyunsaturated fatty acids (PUFA) and iron is required to induce toxicity and lipid peroxidation in E47 cells. Exposure to the glutathione pathway inhibitor, buthionine sulfoxamine (BSO), also increased toxicity in E47 cells with or without the addition of toxic enhancers (93). Another study found that the enhancer cocktail (ethanol, PUFA, and iron) also increased ROS levels in E47 cells and the amount of carbonylated proteins and detection of protein adducts bound to the lipid peroxidation product 4-hydroxynonenal (4-HNE) (113). E47 cells were found to have increased glutathione activity compared to control cells, and increased mRNA levels for gamma glutamyl cysteine synthetase, an enzyme involved in glutathione biosynthesis. The authors of this study believed that this high-level of anti-oxidant activity was a result of adaptation in E47 cells developed to compensate for persistent CYP2E1-mediated increase in oxidative stress. HepG2 cells transduced with an adenovirus to express CYP2E1 also exhibited more toxicity to acetaminophen than non CYP2E1- expressing controls (114). Acetaminophen is bioactivated by CYP2E1 to the toxic intermediate N-acetyl-p-benzoquinone imine, (NAPQI), and this intermediate was shown to produce protein adducts (87).

Overall, there is much evidence linking CYP2E1 enzyme activity to enhanced ROS production and oxidative stress. It is clear that the amount of tissue and cellular injury caused by this oxidative stress depends on the overall metabolic and nutritional state, as well as the presence of toxic enhancers such as poly-unsaturated fatty acids and iron. These factors and their role in the induction, activity, stabilization, and degradation rate of CYP2E1 may account for the variability seen between different research studies. Research will continue on the effects of ROS generated by CYP2E1 and this will lead to better understanding and potential treatment of oxidative stress related damage caused by ethanol and other conditions.

2.5. MITOCHONDRIAL FUNCTION AND REACTIVE OXYGEN SPECIES GENERATION

Mitochondria are the cellular powerhouse providing to ATP energy currency used by the rest of the cell (31). In addition, they are involved in other processes such as signaling, metabolite production, cell cycle and cell death. Mitochondria are enclosed in lipid bilayer double membrane and have their own proteome and genome. There have been over 900 separate proteins reported for rat mitochondria (115), and mitochondrial DNA only encode for approximately 37 of them (116) with the rest being encoded in the nucleus. These proteins must be imported through the TIM//TOM import complex. Mitochondrial proteins are translocated to the outer membrane (OMM), inner membrane (IMM), intermembrane space, cristae or inner matrix. The number of mitochondria varies per cell from approximately 100 to 800 in some cells such as hepatocytes (117).

The production of ATP in the mitochondria requires the operation of two major metabolic pathways: the citric acid cycle (TCA) and the electron transport chain (ETC). The purpose of the TCA cycle is to produce the reducing equivalents NADH and $FADH_2$, which are used by the ETC to drive ATP production. The majority of TCA cycle enzymes are located in mitochondrial matrix. The main input to the TCA cycle is pyruvate formed from glycolysis in the cytosol. Pyruvate goes through a branch point where the pyruvate either receives a carboxyl group from pyruvate carboxylase to enter the cycle as oxaloacetate or is decarboxylated by pyruvate dehydrogenase to become acetyl CoA as shown in Figure 2.4. This shunting of pyruvate through either path depends on the metabolic conditions in the cell. Generally every molecule of citrate exported requires a molecule of pyruvate to be converted to oxaloacetate. Fatty acid synthesis requires citrate and therefore a high rate of pyruvate conversion to oxaloacetate. Citrate is converted to aconitate and then to isocitrate by aconitase. Isocitrate dehydrogenase converts isocitrate to α-ketoglutarate, which is converted to succinyl CoA by α-ketoglutarase dehydrogenase. There is evidence that α-ketoglutarase dehydrogenase may be an important source of ROS, especially in neurons (118).

Oxaloacetate and acetyl CoA are combined to form citrate by citrate synthase. Citrate can also be considered a product of the TCA cycle, as well as other intermediates at certain time. Succinyl CoA synthetase strips the CoA group to form succinate. Succinate dehydrogenase converts succinate to fumarase and FAD^+ to $FADH_2$. By this action, succinate dehydrogenase also simultaneously participates in the ETC. Fumarase

converts fumarate to malate, which is coverted to oxaloacetate by malate dehydrogenase, thus completing the cycle. If all the above reactions are combined, then per pyruvate molecule, the balanced equation (31) is

$$\text{Pyruvate} + 4\ \text{NAD} + \text{FAD}^{+} + \text{GDP} + \text{P}_i + 2\ \text{H}_2\text{O} \rightarrow$$
$$4\ \text{NADH} + 3\text{H}^{+} + \text{FADH}_2 + \text{GTP} + 3\ \text{CO}_2 \qquad (1)$$

Carbon dioxide produced from respiration is produced in the TCA cycle. The electron transport chain is a series of protein complexes that uses the chemical energy in NADH (and to lesser extent $FADH_2$) to drive formation of electrochemical proton gradient. The potential of this gradient is, in turn, used to phosphorylate ADP to ATP. The ETC is carried out by series of protein complex in the IMM. In contrast to the OMM, the IMM is not freely permeable to small molecules, so that the electrochemical gradient is maintained. The ETC complex are represented by Figure 2.5.

ETC complex I (NADH dehydrogenase) is largest and most complicated enzyme complex in the ETC, consisting of 45 sub units (119). NADH dehydrogenase binds NADH at the flavin mononucleatide (FMN) prosthetic group and transfers two electrons along with two H^{+} ions creating $FMNH_2$. The electrons are passed through a series of seven iron-sulfur sub units to a site where ubiquinone (CoQ) is reduced to ubiquinol ($CoQH_2$) (119, 120). Koopman et al. and Murphy have written excellent reviews of the current understanding on how mitochondria, especially the ETC complex 1 produce

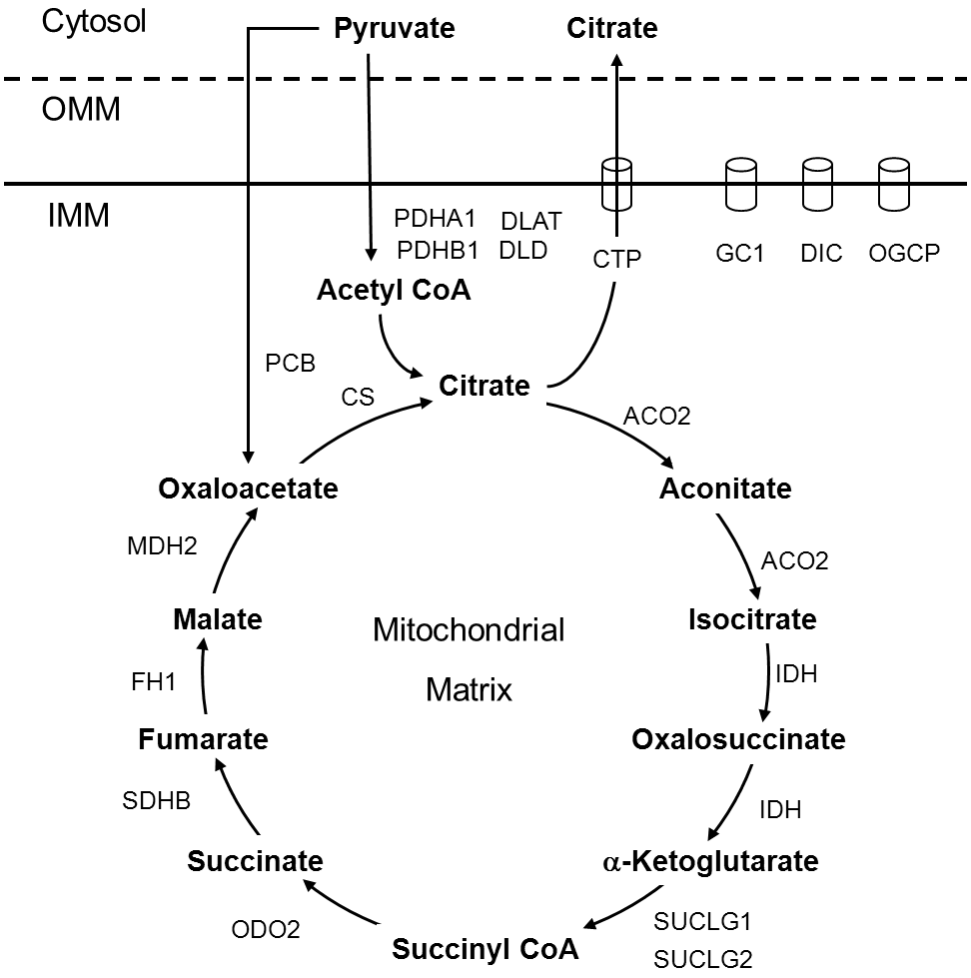

Figure 2.4. The citric acid cycle.

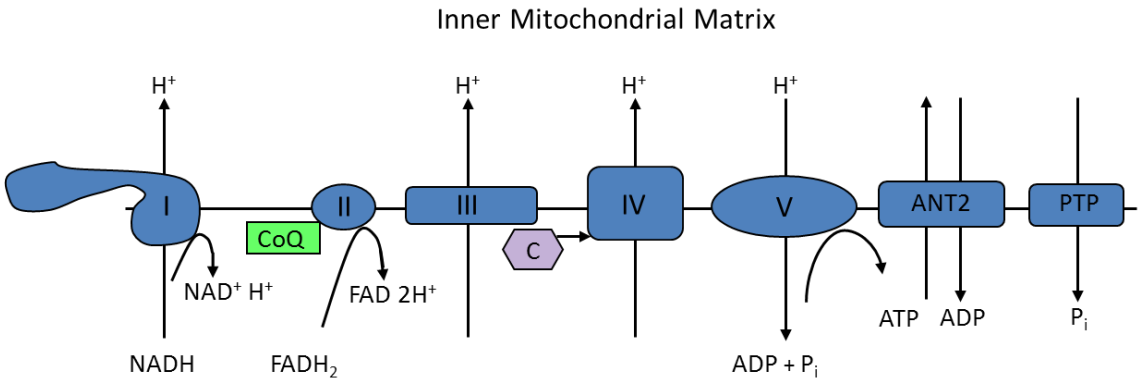

Figure 2.5. The electrons transport chain.

ROS, such as superoxide (119, 120). The FMN group where NADH binds and the ubiquinone binding site mentioned above are two sites are recognized as being the most likely sources electron leakage and superoxide generation, primarily due to the fact they allow closest physical distance between oxygen and electrons extracted from NADH (120, 121). It is believed that superoxide production by ETC complex I is not constant but depends on the metabolic state of the cell. Murphy has summarized three particular metabolic modes that are likely to affect the rate of ROS production (120):

- Mode 1: $NADH/NAD^+$ ratio is high, ΔH^+ gradient is high or low, ATP production is low, and O_2 consumption is low. ROS generation is high
- Mode 2: $CoQH_2/CoQ$ ratio is high, ΔH^+ gradient is high, ATP production is low, and O_2 consumption is low. ROS generation is high
- Mode 3: $NADH/NAD^+$ ratio is low, ΔH^+ gradient is low, ATP production is high, and O_2 consumption is high. ROS generation is low

Mode 1 is a situation where low ATP demand has likely caused the $NADH/NAD^+$ ratio to increase; this ratio leads to more reduced FMN, and allows for easier transfer of electron to O_2. Mode 2 occurs when an excess of reduced electron carriers leads to a highly reduced CoQ pool. This high $CoQH_2/CoQ$ ratio in the presence of high ΔH^+ gradient leads to reverse electron transport (RET) back onto complex I at the CoQ binding site. The mechanisms underlying the subsequent generation of superoxide is not well understood but may be the result of electrons backing up to FMN site (120). Mode 3 is thought as the most normal operating mode, where the cell is consuming oxygen and

generating ATP. This may also be the most significant source of superoxide over time because it is presumed the cell will be predominantly in mode 3, and it is not generally known how often or how much time is spent in modes 1 and 2 (120).

ETC complex II (succinate dehydrogenase) is much smaller in comparison and couples the oxidation of succinate to fumarate with the reduction of ubiquinone to ubiquinol. As mentioned this enzyme also participates in the TCA cycle.

ETC complex III (cytochrome C reductase) reduces cytochrome C by oxidizing ubiquinol ($CoQH_2$) back to ubiquinone (CoQ). This is coupled to moving H^+ ions from the matrix to the intermembrane space. This process, referred to as the Q cycle (122, 123), is a complex cycle that ultimately binds 2 ubiquinol molecules at site Q_0 and ubiquinone molecule at site Q_1 along with 2 molecules of oxidizer cytochrome C. The net result of the complex III cycle is the oxidation of two ubiquinol molecules to ubiquinone, the reduction of the ubiquinone and two cytochrome C units along with moving two H^+ ions to the inter membrane space. There is evidence that ETC Complex III is a significant source of ROS production, especially when cell is operating in what Murphy referred to as "mode 2" (120), where there is an excess of reduced electron carriers leading to highly reduced CoQ pool (124, 125). Murphy states ETC complex 1 likely still produces more ROS than complex 3 in mode 2, but in the "normal" operating mode the amount of ROS produced by complex 3 may be significant (120). There are auxiliary electron carriers that make significant contributions to the reduced CoQ pool

besides ETC complex II (succinate dehydrogenase), such as the electron transferring flavoprotein (ETF). Electron transferring flavoproteins contain an FAD co-factor reduced during fatty acid beta oxidation. They then transfer their electrons to the CoQ pool via ETF:CoQ oxidoreductase (126).

ETC complex IV (cytochrome C oxidase) receives a total of 4 cytochrome C units, removes 4 electrons from them and transfers them to an O_2 molecule to form two molecules of water along with moving 4 H^+ ions to the inter-membrane space. Complex IV is critical to operation of the entire ETC and is the terminal electron acceptor where molecular oxygen is reduced. It is inhibited by cyanide and carbon monoxide.

ETC complex V (ATP synthase) is the final enzyme in the oxidative phosphorylation pathway (31). This enzyme is ubiquitous to all forms of life and functions the same way, by using potential energy from the protein gradient generated by the rest of the ETC. Three to four protons are estimated to be required to form one molecule of ATP.

2.6. REACTIVE OXYGEN SPECIES, LIPID PEROXIDATION AND PROTEIN MODIFICATION

The biological formation of reactive oxygen species (ROS) and their subsequent effect on biological systems has garnered much interest. A state of oxidative stress exists when effects of ROS begin to overwhelm cellular antioxidant and repair mechanisms. Almost all organisms rely on the use of oxygen as final electron acceptor to drive the energetic

processes necessary for life, but doing so efficiently is not simple. Biological systems typically use oxygen by binding it to a metal atom such as iron. The iron is complexed in an organic prosthetic group, such as heme, which in turn, is part of a larger protein, i.e., hemoglobin (31). The oxygen can only bind to iron when it is in the +2 state, and after binding iron, it is considered to be in the +3 state. More importantly, the bound oxygen is considered to be in the superoxide (O_2^-) form (31, 127). Because of the unpaired electron, this bound superoxide has inherent degree of instability (99), and a certain fraction of this bound superoxide can decouple from the iron (as shown in the P450 catalytic cycle in the previous section Fig. 2.3) (99, 128, 129). The superoxide ion is considered to be the most abundant ROS in biological systems, even though precise measurement of concentrations *in vivo* remains difficult (99, 119, 120, 130). Evidence for the toxicity of superoxide is given by the fact that in most cells there are three forms of the enzyme superoxide dismutase (90), which catalyze the reaction of superoxide to hydrogen peroxide and oxygen.

$$2(O_2^-) + 2H^+ \xrightarrow{\text{Superoxide dismutase}} H_2O_2 + O_2 \qquad (2)$$

The largest source of superoxide ion is considered to be ETC complex I (NADH dehydrogenase) in the mitochondria (99, 119, 120, 130). ETC complex III (cytochrome c reductase) is also a source for superoxide ions and the relative amounts produced at each site is likely dependent on the metabolic and redox state of the cell (120, 124). Complex III is also considered important because it can produce superoxide on both sides of the inner mitochondrial membrane (124). Complexes I and III do not bind

oxygen as part of their catalytic function; superoxide is believed to formed by electron leakage occurring at certain sites and directly reducing a nearby oxygen molecule to form the superoxide ion (120).

Other major sources of superoxide ions include members of the cytochrome P450 mono-oxygenase family such as CYP2E1 that has been discussed in the previous section. Up to now sources of superoxide have been categorized as more or less accidental byproducts of catalytic processes. However, the specific purpose of NADPH oxidase is to produce superoxide, and it is primarily expressed by white blood cells as part of immune defense. The purpose of this superoxide is to attack and kill bacteria, this is known as the respiratory burst (131). However, infiltration and accumulation of white blood cells is implicated in several chronic disease such as arthrosclerosis (132) and alcoholic steatohepatitis (77), and the ROS produced by NADPH oxidase from white blood cells is significant in these conditions.

While superoxide itself is toxic and found to deactivate iron-sulfur centers of some proteins like acconitase (130), it also is catalyzed into other ROS. Superoxide is also catalyzed into H_2O_2 by superoxide dismutase, and H_2O_2 is detoxified by catalase, as shown below.

$$2H_2O_2 \xrightarrow{\text{Catalase}} 2H_2O + O_2 \quad (3)$$

When hydrogen peroxide encounters a metal ion such as iron it can participate in Fenton chemistry, to form the extremely reactive hydroxyl radical (HO*), as shown below.

$$Fe^{2+} + H_2O_2 \rightarrow Fe^{3+} + OH\cdot + OH^- \quad (4)$$
$$Fe^{3+} + H_2O_2 \rightarrow Fe^{2+} + OOH\cdot + H^+ \quad (5)$$

The hydroxyl radical has an oxidation potential of 2.9 V, second only to fluorine, and an estimated half-life of 10^{-9} seconds (119), essentially reacting with any molecule it encounters. Catalase contains a heme center has been found vulnerable to modification by ROS (133). In addition to forming the hydroxyl radical, superoxide has been shown to form other ROS (90), hypochlorous acid (HOCl) (134), and peroxynitrite ($ONOO^-$) (135). ROS can damage all classes of biomolecules: fatty acids, proteins, and nucleic acids (129).

Because ROS has short half-lives and rapid turnover, accurate measurement of them is difficult if not impossible (119, 120, 130); therefore, many researchers have chosen to study the effects of ROS on biomolecules. Measurement of the type and extent of ROS-mediated modifications have been used as markers for oxidative stress (1, 11). DNA is

vulnerable to ROS, and amount of oxidized deoxyguanosine (8-Oxo-2'-deoxyguanosine) has been used as measure of oxidative stress in a mouse model (136). Lipids are subject to oxidative attack by ROS and this can initiate systematic chemical deterioration of unsaturated fatty acids known as lipid peroxidation (137, 138). The chemical mechanism of lipid peroxidation and the formation of the peroxidation end product 4-hydroxynenal are shown in Figures 2.6 and 2.7. Proteins are subject to oxidative modifications by ROS and types of modification fall into two broad categories: reversible and irreversible (1, 89). Reversible oxidative protein modifications can occur spontaneously when ROS contact a vulnerable site of protein, or can be enzyme mediated. In either case they can be reversed by enzymatic action (1), and reversible oxidative protein modifications are shown in Table 2.2. Nitrosylation and sulfination occur spontaneously, but glutathiolation and disulfide cross-linking are enzymatically mediated (1). In many cases reversible modifications are involved in cell signaling, or may actually protect residues from a permanent modification (1, 139).

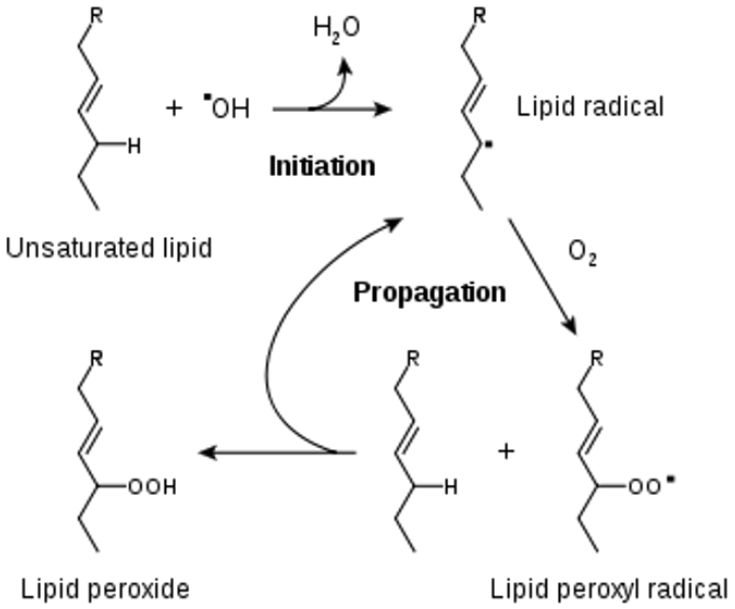

Figure 2.6. The chain reaction of lipid peroxidation (138).

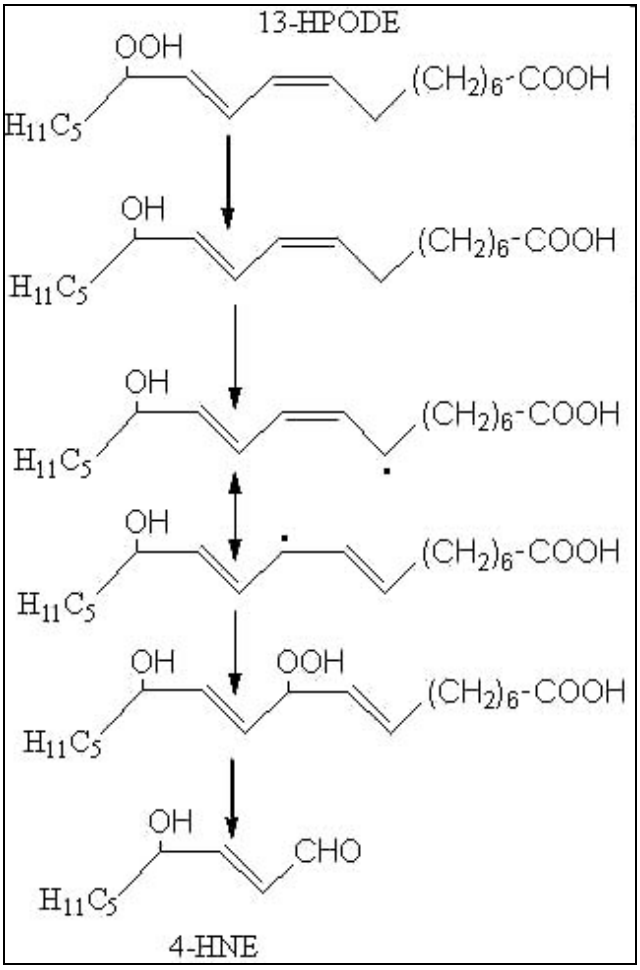

Figure 2.7. Formation of 4-HNE (138).

Table 2.2. Reversible and irreversible protein modifications.

Reversible Modifications	
Glutathiolation	R-SH + GSH → -RS-SG
Nitrosylation	R-SH + NO → -RS-NO
Disulfide cross-linking	R-SH + R-SH → -RS-SR-
Sulfination	-SH + (ROS) → (-SOH)
Irreversible Modifications	
Nitration	R-SH + ($ONOO^-$) → ($R-NO_2$)
Sulfonation	–SH + (ROS) → ($-SO_3H$)
Carbonylation	Direct oxidation of amino acid side chains (Lys, Arg, Pro, and Thr)
	Cleavage of polypeptide backbone by a-amidation or oxidation of Glu residues
	Addition of oxidized sugars to free amine of lysine residues (AGE's)
	Addition of lipid peroxidation products, such as 4-hydroxy nonenal (4-HNE) to Lys, Cys or His residues

Irreversible protein modification results in permanent damage to a protein (Table 2.2, lower) , and if it causes change in conformation or loss of function, these proteins are degraded and re-synthesized, as these modifications are highly disruptive to cells (1, 89). Nitration and sulfonation tend to disrupt active sites because they modify tyrosine or sulfur containing residues (140, 141). The last major class of irreversible class of protein modification is protein carbonylation, which is encompasses a variety of spontaneous chemical reactions the result in the non-enzymatic covalent addition of a carbonyl group to a protein (1, 89). Protein carbonylation has been used a biomarker for oxidative stress in numerous studies (10, 113, 142, 143). Four major classes of reactions have been described that result in the covalent addition of a carbonyl group to a protein (1). Direct oxidation of amino acid side chains (Lys, Arg, Pro, and Thr) by hydroxyl radical mediated reactions has been detailed by Stadtman (144). In addition, cleavage of the polypeptide back-bone by α-amidation or oxidation of Glu residues has also been studied (139, 144, 145). In either of these cases the end of reaction process results in the creation of aldehyde groups. Sugars such as glucose or mannose can be oxidized so that they form an aldehyde group. This sugar-aldehyde can bind to a primary amine, forming a Schiff base (146). When this reaction involves the primary amine of a lysine, this is referred to as the Maillard reaction and these products are referred to as advanced glycation end products (AGE) (147, 148). A fourth method of carbonylated protein occurs by the addition of lipid peroxidation products, such as 4-hydroxynonenal (4-HNE) to Lys, Cys or His residues (1, 10, 128), as shown in Figure 2.8, and currently, 4-HNE is a highly studied carbonylation source.

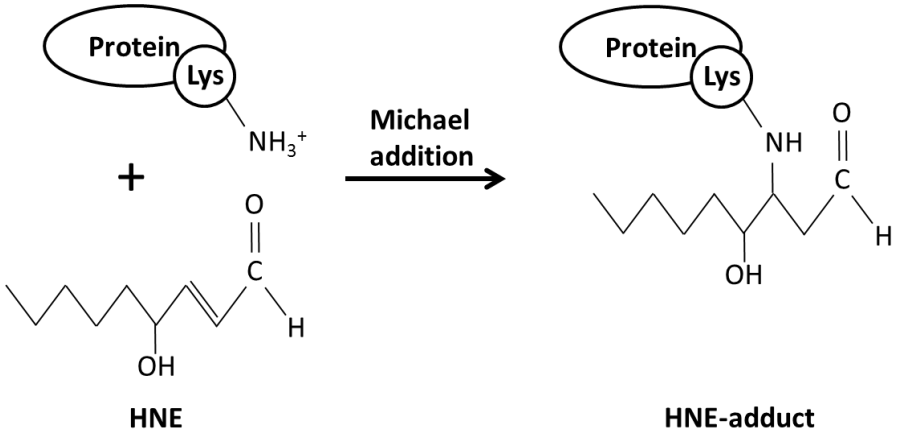

Figure 2.8. The Michael addition of 4-HNE.

CHAPTER III

PROTEOMIC ANALYSIS OF 3T3-L1 ADIPOCYTE MITOCHONDRIA DURING DIFFERENTIATION, MATURATION, AND ENLARGEMENT

3.1. OVERVIEW

The increase in adipose tissue mass arises in part due to progressive lipid loading and triglyceride accumulation in adipocytes. Enlarged adipocytes produce the highest levels of pro-inflammatory molecules and reactive oxygen species (ROS). Since mitochondria are the site for major metabolic processes (e.g., TCA cycle) that govern the extent of triglyceride accumulation as well as the primary site of ROS generation, we quantitatively investigated changes in the adipocyte mitochondrial proteome during different stages of differentiation and enlargement. Mitochondrial proteins from 3T3-L1 adipocytes at different stages of lipid accumulation (days 4 through 18) were digested and labeled using the iTRAQ 8-plex kit. The labeled peptides were fractionated using a liquid phase isoelectric fractionation system (MSWIFT) to increase the depth of proteome coverage, and analyzed using LC-MS/MS. A total of 398 mitochondrial proteins, including endoplasmic reticulum-associated mitochondrial proteins, were identified and classified into 12 functional categories. The identified proteins included enzymes and transporters involved in the TCA cycle, fatty acid oxidation, and ATP synthesis. Our results indicate that cultured adipocytes enter a state of metabolic-overdrive where increased flux through the TCA cycle and increased fatty acid oxidation occur simultaneously. The proteomic data also suggest that accumulation of reduced

electron carriers and the resultant oxidative stress may be attractive targets for modulating adipocyte function in metabolic disorders.

3.2. INTRODUCTION

Obesity is a risk factor in the development of cardiovascular disease, stroke, cancer and type II diabetes (41). Obesity arises from an imbalance in energy metabolism, wherein the intake of energy exceeds the energy expenditure for extended periods of time (41, 149). The excess energy is stored in adipocytes, which are the main constituents of white adipose tissue (150), as triglycerides, and as a result, there is a significant expansion in the mass of white adipose tissue. The increase in adipose tissue mass can occur through either an increase in the number of adipocytes (hyperplasia) or an increase in the size of existing individual adipocytes (hypertrophy). While hyperplasia involves the recruitment of recruitment, proliferation and differentiation of precursor preadipocytes, hypertrophic enlargement, arises due to the increase in the lipid content in adipocytes. A number of in vivo studies (151-153) support a “critical fat cell size” hypothesis, where recruitment of new fat cells occurs when adipocytes reach a threshold critical size (154). This hypothesis is also consistent with observations that suggest that an increase in the size of the mature adipocytes usually precedes the proliferation of precursor cells, and adipocytes do not have an unlimited capacity for expansion in size (44, 155). The presence of hypertrophic adipocytes has been correlated with type II diabetes (156) as well as abnormal levels of pro-inflammatory molecules such as cytokines (interleukin-6,

interleukin-8) and leptin (44). Together, these studies underscore the importance of hypertrophic enlargement of adipocytes in obesity and its associated disorders.

Obesity has also been strongly correlated with increased oxidative stress. Furukawa et al., found elevated levels of the oxidative stress marker malondialdehyde in the plasma and white adipose tissue of obese mice (12). Kobayashi et al., reported that activity of the anti-oxidant enzyme glutathione peroxidase was reduced 40 percent in obese mice, with a corresponding increase in gamma glutamylcysteine which is used in de novo synthesis of glutathione (51). These authors also reported that 3T3-L1 adipocytes demonstrated reduced insulin signaling after exposure to hydrogen peroxide or GPX inhibitor. 3T3-L1 adipocytes were also shown to have increased reactive oxygen species (ROS) generation during the differentiation process and through 8 days of culture (12) and 8-day old 3T3-L1 adipocytes had higher ROS levels and lower GPX activity when compared to pre-adipocytes (51). These studies illustrate the correlation between lipid accumulation and oxidative stress.

Mitochondria are the major source of ROS in the cell (157). It has been suggested that mitochondrial dysfunction caused by oxidative damage contributes to insulin resistance (158, 159). An increase in glucose levels and free fatty acids (FFA) increases mitochondrial ROS levels. While low levels of ROS are important in several cellular processes, including signaling and gene expression (157, 158) elevated levels of ROS due to increased production or incomplete removal by the cellular anti-oxidant

machinery, can damage DNA, protein, and lipids. Numerous studies have correlated oxidative stress with the etiology of insulin resistance (160, 161), diabetes (162, 163), and cardiovascular disease. Indeed, levels of enzymes and anti-oxidants involved in ROS scavenging (superoxide dismutase and catalase, the enzymes involved in superoxide radical removal, vitamin E) are all reduced during diabetes (164, 165).

Because mitochondria are the site of metabolic processes that govern the extent of triglyceride accumulation, such as the TCA cycle and fatty acid oxidation, as well as a major source for ROS generation, we investigated the changes in adipocyte mitochondrial proteome during adipocyte differentiation and lipid loading-driven enlargement. While Molina et al. (15) characterized the 3T3-L1 adipocyte nuclear proteome and secreted proteome during differentiation (through day 7) using SILAC, and Cho et al. (26) studied changes in the mitochondrial proteome in isoproternol-treated adipocytes at a single time point, a quantitative study of the temporal dynamics of the 3T3-L1 adipocyte mitochondrial proteome during differentiation and lipid loading-driven enlargement has not been previously reported. Here, we report the quantitative profiling of the mitochondrial proteome at different stages of differentiation and enlargement – from undifferentiated adipocytes to young and mature adipocytes to enlarged adipocytes. A multiplex strategy using iTRAQ labeling was coupled with mitochondrial protein isolation and liquid-phase isoelectric focusing to quantitatively monitor proteome changes underlying increased lipid loading and oxidative stress in 3T3-L1 adipocytes.

3.3. MATERIALS AND METHODS

3.3.1. Reagents and Supplies

Cell culture media and reagents were purchased from Hyclone (Logan, UT). All reagents for mitochondrial protein extraction were purchased from Fisher Scientific (Hampton, NH). Mammalian protease inhibitor cocktail was purchased from Sigma-Aldrich (St. Louis, MO). The iTRAQ kit and reagents were purchased from Applied Biosystems (Foster City, CA).

3.3.2. Adipocyte Cell Culture

3T3-L1 preadipocytes (166) were routinely cultured to confluence in DMEM growth medium supplemented with calf serum (10%, v/v), penicillin (200 U/ml), and streptomycin (200 μg/ml). During this period, medium was replenished every other day. Preadipocytes were subcultured in 10 cm dishes for mitochondrial protein extraction and 12-well plates for biochemical assays as previously described (167). Cells were cultured for an additional 24 h after reaching confluence, and this time point was designated as day 0 (i.e., prior to differentiation). Differentiation of preadipocytes to adipocytes was induced as described earlier (167, 168). After the induction of differentiation, media was replenished every other day for the duration of the experiment.

3.3.3. Mitochondrial Protein Isolation

Mitochondrial proteins were isolated from three 100 mm dishes at each time point - days 0 (i.e. undifferentiated preadipocytes), 4, 7, 10, 14, and 18 days post-differentiation – by

differential centrifugation (169). Briefly, cells were washed twice with phosphate buffered saline, and 3 mL of 0.1X isolation buffer (3.5 mM Tris-HCl, pH 7.8, 2.5 mM NaCl, 0.5 mM MgCl2 with 0.3% v/v mammalian protease inhibitor (PI) cocktail) was added to each 10 cm dish. After 10 min incubation at room temperature, cells were scraped off the dish and centrifuged at 300 × g for 10 min at 4^{o}C. This resulted in any undifferentiated (heavier) preadipocytes settling at the bottom, while the adipocytes (lighter) were in the supernatant. The supernatant was then lysed by passing through a 27.5 gauge needle. Three ml of 10X hypertonic buffer (0.35 M Tris-HCl, pH 7.8, 0.25 M NaCl, 0.05 M $MgCl_2$) was added to the lysed cells and the lysate was centrifuged at 200 × g for 3 min at 4°C to pellet the nucleus. The supernatant was transferred to another tube and centrifuged again at 200 × g for 3 min to remove any residual nuclear material or cellular debris. The supernatant was centrifuged at 13000 × g for 10 min at 4ºC and the pellet was washed with 100 µl 1X hypertonic buffer (0.035 M Tris-HCl, pH 7.8, 0.025 M NaCl, 0.005 M $MgCl_2$, supplemented with 0.3% v/v PI cocktail and 1 mM tris-(2-carboxyethyl)-phosphine, TCEP).

Supernatants containing mitochondrial proteins from the triplicate dishes were pooled, and the sample was centrifuged at 13000 × g for 10 min and the pellet was resuspended in 250 µl homogenization buffer A (320 mM sucrose, 1 mM EDTA, 10 mM Tris-HCl, pH 7.4) supplemented with PI (0.3% v/v) and TCEP (1 mM). The sample was centrifuged at 13000 × g for 1 min and the pellet resuspended in 250 µl homogenization buffer B (25 mM sucrose, 95 mM sorbitol, 100 mM KCl, 0.05 mM EDTA, 5 mM

$MgCl_2$, 10 mM H_3PO4, 10 mM Tris-HCl, pH 7.4) supplemented with PI (0.3% v/v) and TCEP (1 mM). The sample was then centrifuged at 1600 × *g* for 2 min to pellet down any residual debris, and the supernatant centrifuged at 13000 × *g* for 1 min to collect the mitochondrial pellet. The pellet was resuspended in 100 µl homogenation buffer B supplemented with PI (0.3% v/v) and TCEP (1 mM) and heated at 95ºC for 20 minutes to lyse the mitochondria. Mitochondrial samples were stored at -80ºC until further use.

3.3.4. iTRAQ Labeling of Mitochondrial Proteins

Mitochondrial proteins were quantified using Pierce 660 nm Protein Assay Reagent (Pierce, Rockford, IL) and precipitated with cold acetone to remove tris, salts, and protease inhibitors, as described in the iTRAQ kit protocol. The protein pellet was then resuspended in solubilization buffer (1M 1-(3-Sulfopropyl) pyridinium betain (NDSB-201), 0.05 wt% SDS, 25 mM HEPES, pH 8.0) supplemented with TCEP (1 mM). The NDSB-201 was used as it yielded best protein solubilization and was fully compatible with downstream fractionation steps (not shown). The resuspended mixture was placed on ice and sonicated twice with a Model 60 sonic dismembrator (Fisher Scientific) at a setting of 4 W for 15 sec. The sample was then incubated at 60ºC for 45 minutes. Protein concentrations were again determined using the Pierce 660 nm Protein Assay Reagent. Typical protein recovery yields were between 70 and 90 percent.

Equal amounts of mitochondrial proteins were digested with trypsin prior to labeling with the iTRAQ reagents. One µl of cysteine blocking reagent, methyl methane-

thiosulfonate (MMTS) (supplied with the iTRAQ kit, Applied Biosystems, Foster City, CA) was added to 100 μg of protein, and incubated 10 minutes at room temperature. The cysteine blocked sample was combined with 1.2 μg of sequencing grade trypsin (K/R cleavage) (Promega Corp., Madison, WI) and $CaCl_2$ (5mM). Protein digestion was conducted by placing the sample containing tube in a shaker at 37ºC for 8 hours, followed by addition of another 1.2 μg of trypsin and incubation for another 8 hours.

Trypsin-digested mitochondrial proteins were labeled with iTRAQ reagents from the iTRAQ 8plex Kit (Applied Biosystems) according to the manufacturer's instructions. Reagents 113, 115, 117, 118, 119, and 121 were added to samples T0, T4, T7, T10, T14, and T18 respectively, which correspond to mitochondrial protein samples from days 0, 4, 7, 10, 14, and 18 days post-differentiation. Sample T0 corresponds to undifferentiated pre-adipocytes. Labeled samples were stored at -80ºC until further use.

3.3.5. Liquid Phase Isoelectric Point Fractionation

The design, assembly and operation of the in-house isoelectric trapping device called "membrane separated wells for isoelectric focusing and trapping" (MSWIFT) have been previously described (170, 171). Prior to separation, alumina separation wells were assembled serially to contain six separation wells. The anode solution was 3 mM methanesulfonic acid and 3 mM sodium hydroxide was used as the cathode buffer. Compartment solutions were pH biased using ampholytic buffers (172) and tunable pH buffering membranes were synthesized in-house, as previously described (173-176).

The pH values of the buffering membranes were as follows: 2.9, 4.2, 5.4, 6.8, 7.5, 9.5 and 11.0. The digested sample was loaded in the fourth separation well (pH 6.8-7.5) and separated at 5 W constant power (upon reaching constant current) for one hour. Solutions obtained from each fraction were stored at -80°C until further use.

3.3.6. Liquid Chromatography (LC) and Tandem Mass Spectrometry (MS/MS)

A 40 µL aliquot from each MSWIFT fraction was acidified with trifluoroacetic acid to pH ~ 2 and concentrated two-fold. The concentrated sample was then injected (10 µL) onto an 150-µm x 15 cm column (Vydac) using an LC-Packings autosampler and pumps (LC Packings, Sunnyvale, CA) equipped with robotic spotting (ProBot, Dionex, Sunnyvale, CA), as previously reported (177). The LC gradient used for all samples spanned 2-60% (solvent B, 85% ACN, 5% IPA, 0.1% TFA) over 90 minutes. The effluent was mixed with the matrix-assisted laser desorption/ionization (MALDI) matrix (7 mg mL-1 α-cyano-4-hydroxycinnamic acid, 60% ACN, 10% IPA, 10 mM dihydrogen ammonium phosphate) and a total of 840 spots were obtained per sample. Positive ion MALDI-MS data was acquired using a model 4800 Proteomics Analyzer (Applied Biosystems, Foster City, CA). The 30 highest intensity peaks (S/N >50) per spot were fragmented using collision induced dissociation and resulting tandem MS data were searched against the mouse genome database integrated in the Celera Discovery System (CDS, KBMS5.0, release date 03/02/2005, 115660 sequences) (178) using ProteinPilot software version 3.0 (Revision 114732) with the ParagonTM algorithm version 3.0.0.0 37 (Applied Biosystems, Foster City, CA). Peak lists were generated via the ProGroup

Algorithm built into the ProteinPilot software. The following modifications were included in the "thorough" database search: iTRAQ label (8-plex, peptides N-terminus and lysine), MMTS modification on cysteine residues and trypsin cleavage. Details regarding cleavage specificity, modifications and mass tolerance threshold were as previously described for the Paragon Algorithm (179).

Protein quantitation values were calculated by taking the ratio of peak area of the iTRAQ labeled signal to the baseline label peak area. Protein quantitation values are an average value of the highest confidence peptides as selected by the ProteinPilot Software. Bias correction was performed using the ProGroup AlgorithmTM to correct for bias associated with systematic error. Peptides with quantitation data that was blank, zero or 9999 were excluded as these were classified as discordant by the ProteinPilot software and p-values could not be calculated. Proteins satisfying three criteria – (i) a ProtScore of at least 1.3 (corresponding to a $\geq$ 95% CI), (ii) two peptides with unique sequences that were not discordant and in which one had a minimum confidence interval $\geq$ 95% (180), and (iii) a measurable quantitation peak from the associated iTRAQ label across all 6 time point samples (i.e., present at all time points) - were chosen for analysis. The global false discovery rate (FDR) was calculated using the PSPEP tool and a decoy database in the ProteinPilot Software package. The initial 398 protein identifications correspond to an estimated FDR of ~8 percent at the protein level using a standard q-value approach as previously described (181). However, the lowest ranked

protein discussed in the text and presented in the figures on pages 60 and 62 and the tables on pages 64 and 68 has a rank of 314, which corresponds to a FDR of < 5 percent.

Data generated from two independent iTRAQ labeling and MS runs were used as follows. Fold-change in protein expression at each time point was calculated relative to the corresponding expression value in preadipocytes (T0). Proteins that demonstrated a statistically-significant ($p \leq 0.05$) change in expression (i.e., a change that has a 95 percent probability of not being the result of chance) on both MS data sets were identified as being differentially expressed. Peptides from proteins that were identified as differentially expressed in replicate iTRAQ and MS experiments were used for determining the average fold-change in expression. The fold-change was calculated only using peptides that were common to each protein in the two data sets. In other words, although multiple peptides may have been used in the replicate runs for protein identification, fold-change quantitation was based only on common peptides between the two datasets. This data was presented in the figures on pages 60 and 62 and the tables on pages 64 and 68. The identified proteins, their quantitation ratios and the number of peptides as calculated by ProteinPilot are found in Supplemental Table S1.

3.3.7. Adipocyte Triglyceride Assay

Adipocyte triglyceride content was determined using the Adipored ™ assay reagent (Lonza, Walkersville, MD) according to the manufacturer's instructions. Measurements

were made in triplicate and the readings normalized to the corresponding cellular protein levels, which was determined using the Bradford assay (BioRad, Hercules, CA).

3.3.8. ROS Production in 3T3-L1 Adipocytes

Adipocyte ROS generation was measured by the reduction of nitro blue tetrazolium according to the method of Rook et al. (182). The NBT assay indicates presence of the superoxide ($O_2^{\bullet -}$) ion by the reduction of yellow nitroblue tetrazolium to a dark blue formazan compound. Cells were incubated for 90 minutes followed by rinsing and fixing with 10% v/v formalin in PBS. Formazan levels were normalized to the cellular protein content, as determined using the Bradford assay (BioRad).

3.3.9. ATP Assay

Cellular ATP was measured using a luminescence assay kit (Promega, Madison, WI) that is based on the ATP-dependent activity of luciferase. ATP levels were normalized to the corresponding sample protein content, which was determined using the Bradford assay (BioRad).

3.4. RESULTS

We report changes in the adipocyte mitochondrial proteome during differentiation, post-differentiation maturation, and lipid loading-driven enlargement. In order to decrease sample complexity and observe organelle-specific changes in protein expression, mitochondria were isolated from adipocytes and used for proteome analysis. Tryptic

peptides from the mitochondrial proteins were also fractionated using a liquid phase isoelectric point separating device, MSWIFT (170) to increase the depth of proteome coverage. The proteomics strategy used is shown in Figure 3.1.

The hallmark of adipocyte differentiation and hypertrophy are the formation and enlargement of intracellular lipid droplets. Figure 3.2*A*-*F* shows transmitted light micrographs of adipocytes at different stages of differentiation, from undifferentiated preadipocytes with no lipid droplet (Fig. 3.2*A*) to mature adipocytes with normal sized droplets (Fig. 3.2*D*) and enlarged adipocytes with lipid droplets occupying on average ~ 70 percent of the cell volume (Fig. 3.2*F*). Quantification of TG accumulation (Fig. 3.2*G*) shows that TG levels increase rapidly in adipocytes from day 4 though day 10, with a slower rate of increase observed beyond 10 days post-differentiation.

A total of 398 mitochondrial proteins, including endoplasmic reticulum-associated mitochondrial proteins, were identified and quantified using the identification criteria described in Materials & Methods, and represented ~60 percent of the total identified proteins (Figure 3.3*A*) and ~ 69 percent of identified peptides. The 398 proteins were also sorted into 12 functional categories (Figure 3.3*B*) using the protein ontology information in the UniprotKB / Swiss-Prot database (http://www.uniprot.org/uniprot/) and scientific literature available at PubMed (http://www.ncbi.nlm.nih.gov/protein/). Broadly, these categories reflected changes that represent enhanced metabolic flux through the TCA cycle and fatty acid oxidation pathway. The TCA cycle (8%), fatty

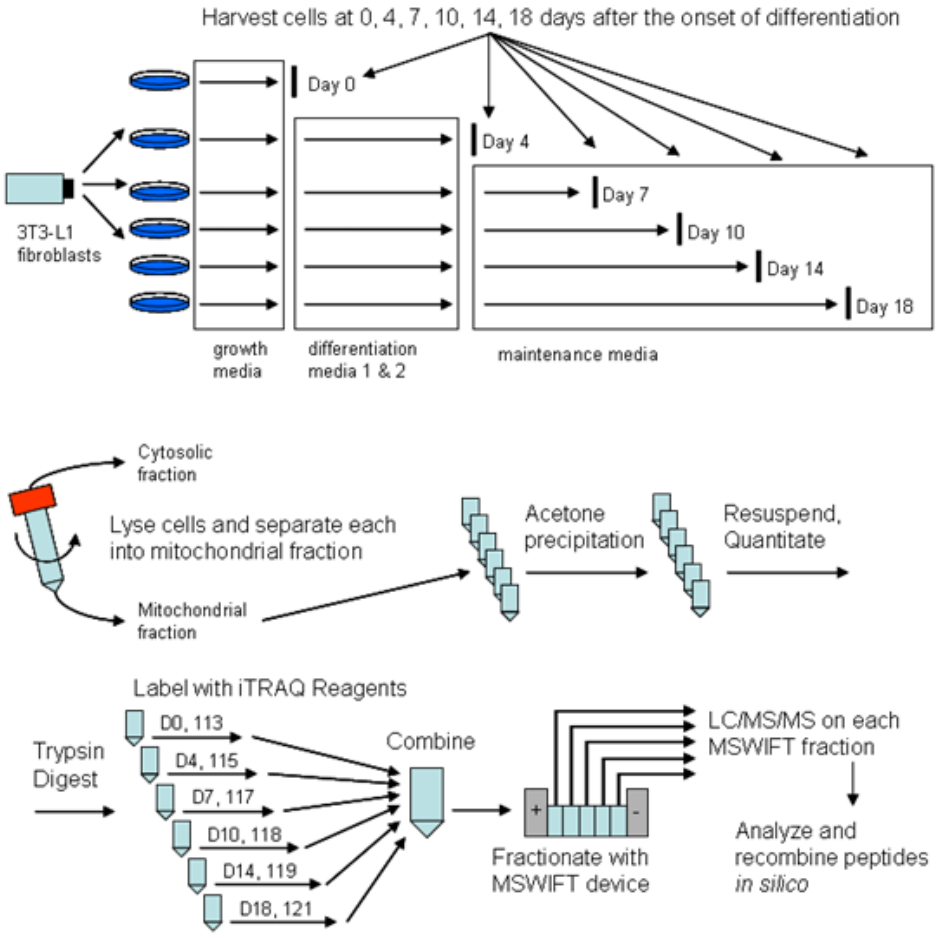

Figure 3.1. Flowchart for quantitative characterization of the mitochondrial proteome during adipocyte differentiation and lipid loading-driven enlargement. Mitochondria from three independent culture dishes were pooled for each time point. Two independent iTRAQ labeling and MS identification runs were performed.

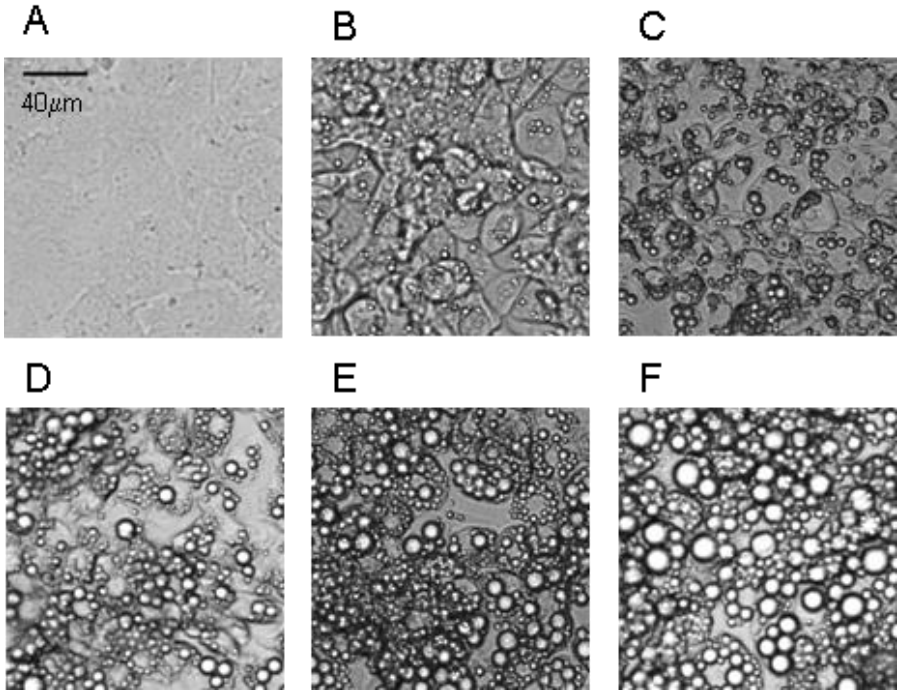

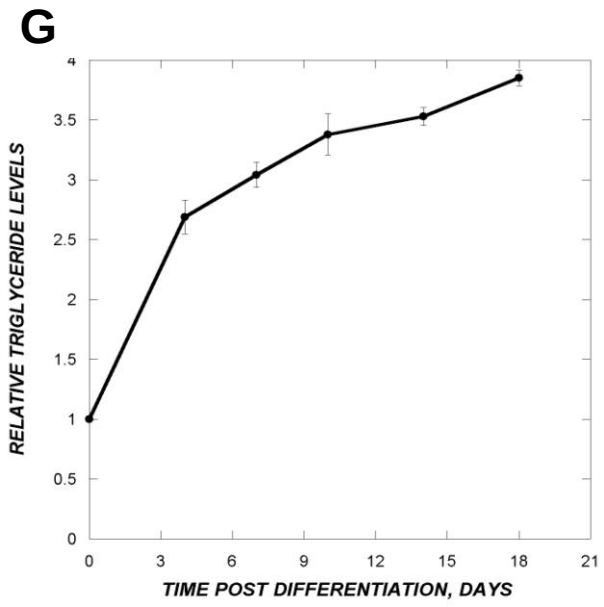

Figure 3.2. Lipid accumulation in adipocytes. Representative transmitted light images of *A*) preadipocytes, and *B*) adipocytes at different stages of differentiation and enlargement – day 4, *C*) day 7, *D*) day 10, *E*) day 14, *F*) and day 18 – are shown. The lipid levels at the different time points were also quantified using the *G*) AdipoRed assay and normalized to the preadipocyte lipid levels. Data shown are mean ± standard deviation from three independent experiments.

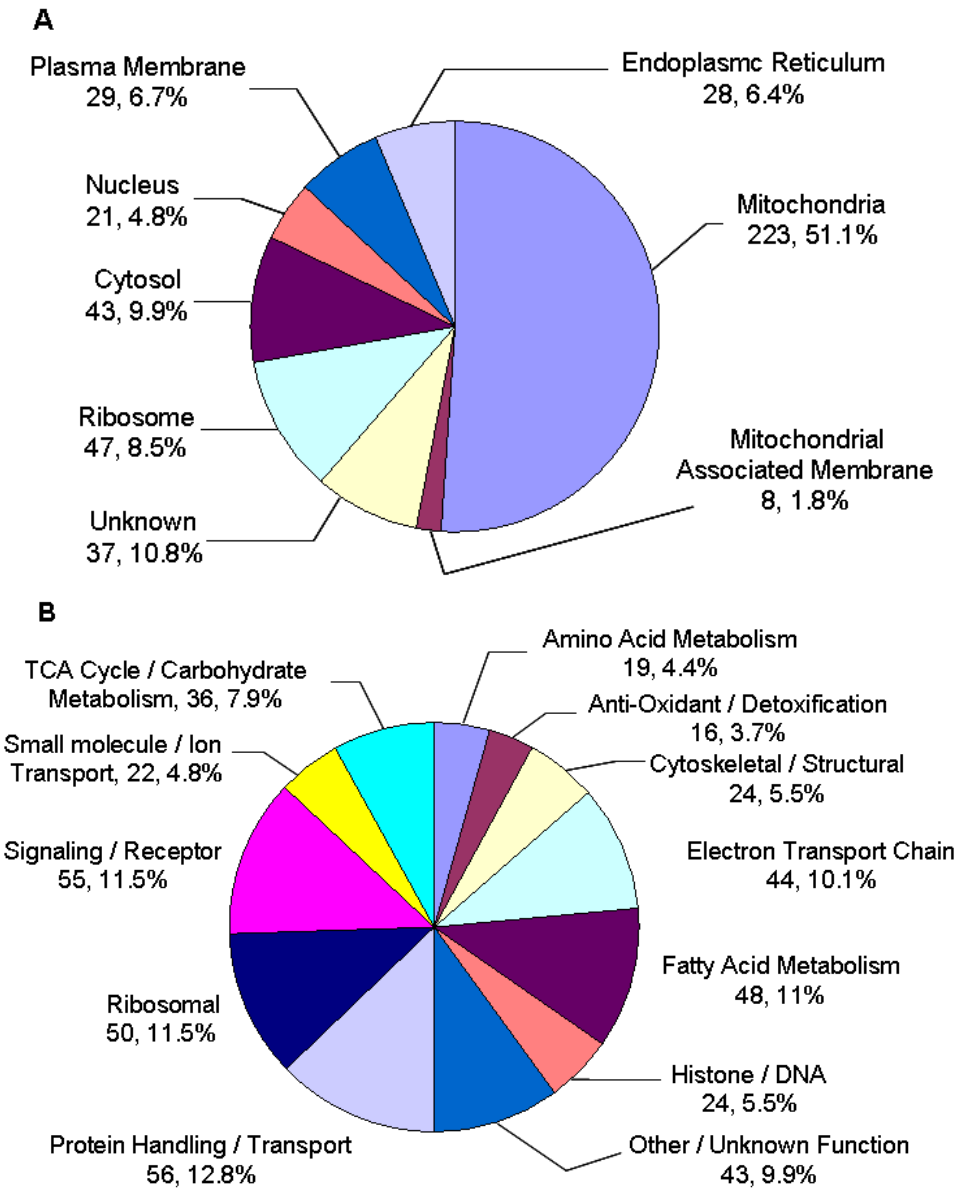

Figure 3.3. Classification of proteins by cellular location *A*) and function *B*). Mitochondrial proteins identified using the scheme described in Materials & Methods were classified using the protein ontology information provided in the UniprotKB/Swiss-Prot database (www.uniprot.org/uniprot), and scientific literature available at PubMed (www.ncbi.nlm.nih.gov/protein).

acid metabolism (11%), electron transport and ATP synthase complexes (10%), and antioxidant and detoxification (4%) categories accounted for 33 percent of the proteins that were identified (Fig. 3*B*). Changes in these major pathways are described below.

3.4.1. The Citric Acid Cycle

Sixteen enzymes involved in the TCA cycle were significantly up-regulated at different time points post-differentiation. Figures 3.4*A & B* show changes in the expression of enzymes involved in the TCA cycle and pyruvate handling. Pyruvate dehydrogenase (PDHA1) and pyruvate carboxylase (PCB), which allows pyruvate to enter the TCA cycle as acetyl-CoA, and extends it by one carbon and allows its entry into the cycle as oxaloacetate, respectively, were two of the enzymes that were significantly up-regulated by 2.7 to 2.9-fold from days 7 through 18. These two enzymes allow proper balance of the substrates for citrate synthase (CS), which combines oxaloacetate and acetyl-CoA into citrate and is considered the overall rate limiting step for the TCA cycle (183). Our data show that the expression of CS was also progressively up-regulated from days 4 to 18 by 1.8 to 2.9-fold. Aconitase (ACO2) and isocitrate dehydrogenase (IDH) catalyze the next several cycle steps, converting citrate to aconitate, then to isocitrate and oxalosuccinate, and finally to α-ketoglutarate. The levels of ACO2 increased by 2.6 to 3.4-fold from days 10 through 18 while IDH demonstrated a moderate (45 – 56%), but constant, increase in expression from day 7 to day 18.

TCA cycle enzymes downstream of ACO2 and IDH, including succinyl CoA lygase alpha (SUCLG1), that catalyzes the conversion of α-ketoglutarate to succinyl CoA, was also significantly up-regulated on days 14 (1.5-fold) and 18 (1.7-fold). The oxoglutarate dehydrogenase complex E2 (ODO2), succinate dehydrogenase (SDHA and SDHB), which catalyzes the formation of fumarate from succinate, fumarate hydratase, which converts fumarate to malate, and malate dehydrogenase (MDH2), which catalyzes the final conversion of malate to oxaloacetate, all demonstrated statistically significant increases in expression at different time points (Figs. 3.4*A* &*B* and Supplemental Table S1), which suggests increased flux through the TCA cycle. In addition to the TCA enzymes, the citrate transporter (CTP) and the mitochondrial dicarboxylate transporter (DIC) also were increased in expression on day 10 (2.8-fold) and day 7 (3.1-fold), respectively, and were consistently up-regulated at a high expression level until day 18 (maximum fold change of 3.3-fold and 4.2-fold, respectively for CTP and DIC).

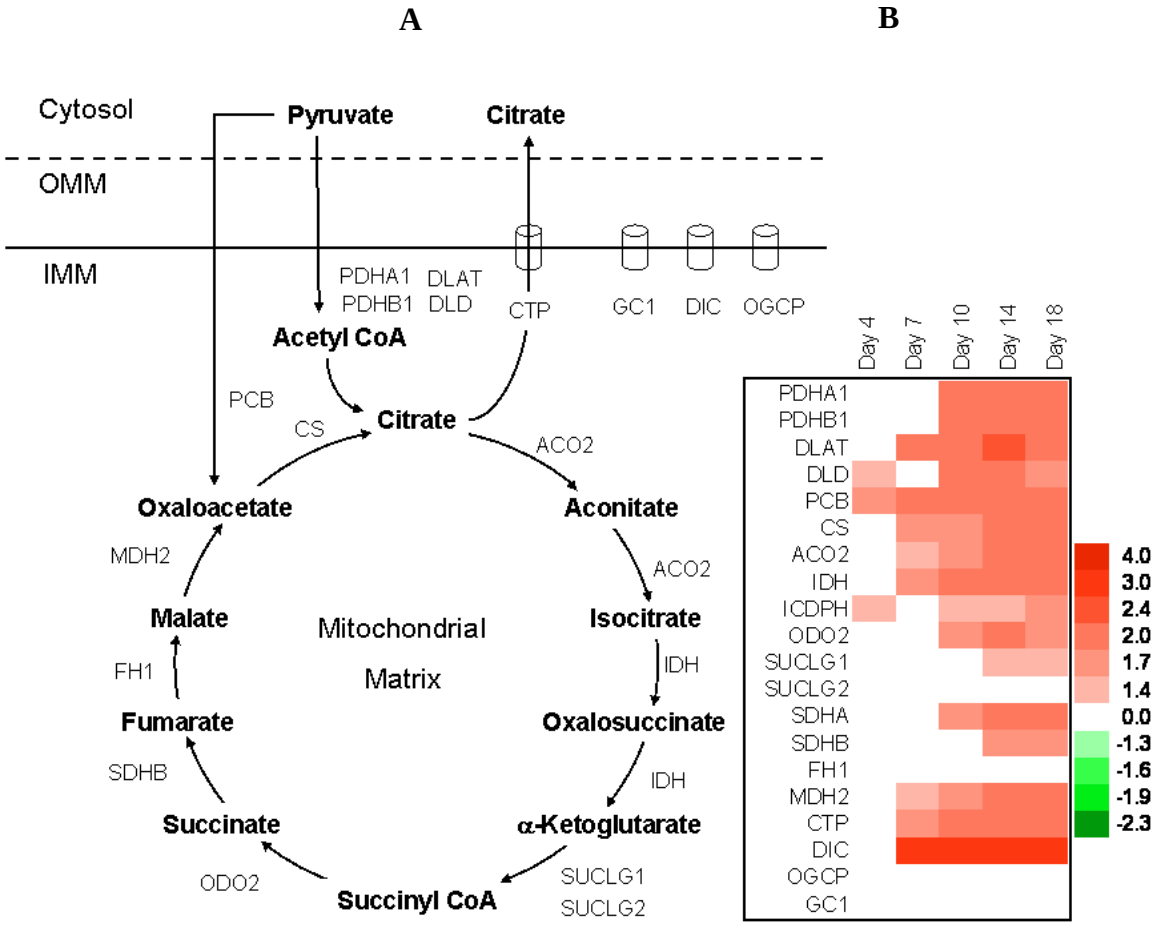

Figure 3.4. Changes in the expression of enzymes involved in the TCA cycle. *A*) Proteins whose expression was significantly altered ($p \leq 0.05$) at any one of the time points, are indicated on the TCA cycle schematic. The schematic was drawn based on Lehninger Principles of Biochemistry (31). *B*) The protein expression at different time points is represented as a heat map. Statistically significant quantitative changes are based on the ratio of the average iTRAQ label peak area between duplicate experiments for each day relative to day 0 (undifferentiated pre-adipocytes). Fold increase is represented as red, while fold-decreases are in green as indicated by the vertical color vs. fold change legend. Values appearing colorless were not determined to have a statistically-significant fold change. Data shown are average values from duplicate iTRAQ experiments.

3.4.2. Fatty Acid Metabolism

Figures 3.5*A & B* schematically show changes in the enzymes involved in the mitochondrial import of fatty acids and their subsequent breakdown via beta-oxidation. Seven enzymes involved fatty acid metabolism were up-regulated in adipocytes during differentiation and enlargement. Acyl-CoA synthetase (ACSL1), the mitochondrial membrane protein that catalyzes activation of free fatty acids by combining them with CoA and preparing them for import by sterol carrier protein 2 (SCP2), was up-regulated at all time points during differentiation and enlargement, with the maximal up-regulation (6.9-fold) being observed at day 7 post-differentiation followed by a slight decrease to 5.5-fold increase in expression at day 18. The expression of cartinine acyltransferase (CAT), which attaches cartinine to the acyl molecule in the inter membrane space, increases to a maximal level of 3.2-fold on day 14, and was slightly decreased (3.2-fold) at days 18.

Enzymes that convert the *trans*-2-Enoyl CoA to hydroxyl CoA, the hydroxyl short chain enoyl-CoA hydratase (ECHS1) was also significantly up-regulated in expression (3.1 to 4.3-fold) from day 10 to day 18. The enzyme that dehydrogenates the hydroxyl group to

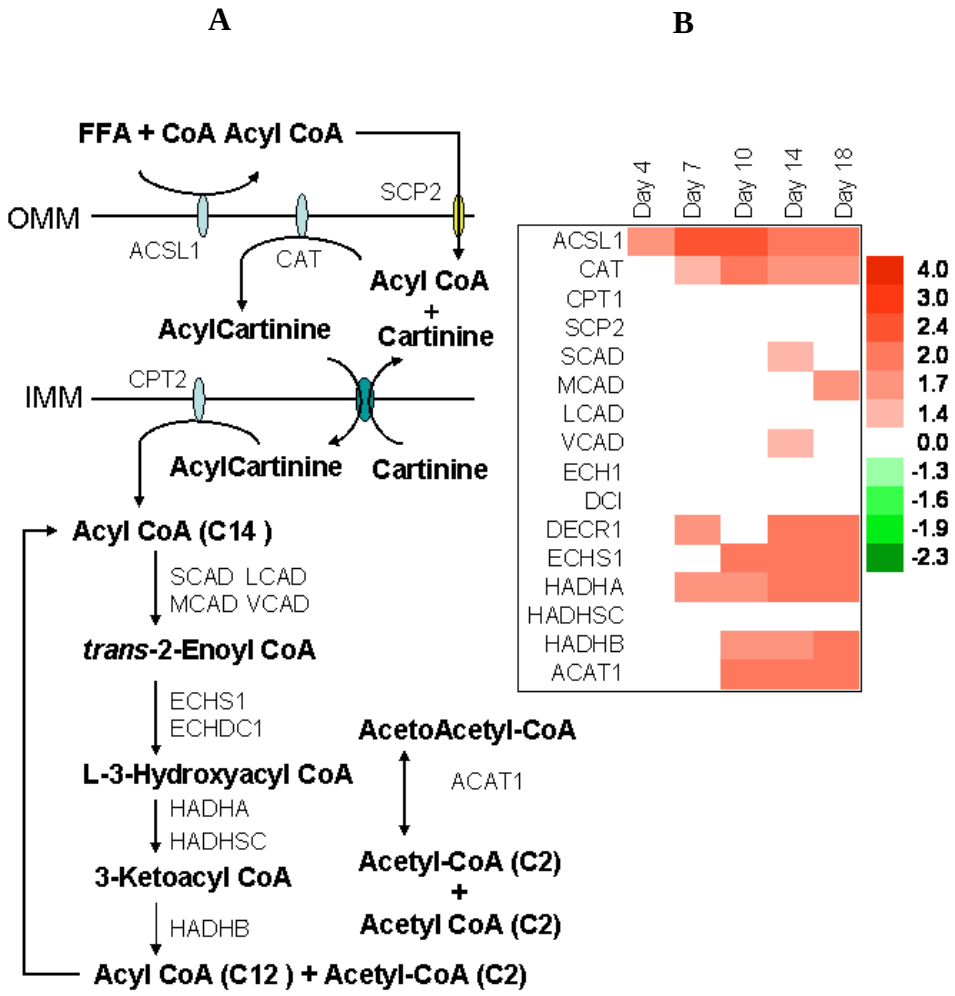

Figure 3.5. Changes in the expression of enzymes involved in the fatty acid metabolism. *A*) Proteins whose expression was significantly altered ($p \leq 0.05$) at any one of the time points, are indicated on the fatty acid import and beta-oxidation pathway schematic. Intermediates are denoted in bold. The schematic was drawn based on Lehninger Principles of Biochemistry (31). *B*) The protein expression at different time points is represented as a heat map Statistically significant quantitative changes are based on the ratio of the average iTRAQ label peak area between duplicate experiments for each day relative to day 0 (undifferentiated pre-adipocytes). Fold increase is represented as red, while fold-decreases are in green as indicated by vertical color vs. fold change legend. Values appearing colorless were not determined to have a statistically-significant fold change. Data shown are average values from duplicate iTRAQ experiments.

a keto group, hydroxyacyl-coenzyme A dehydrogenase (HADHA), was increased 1.9-fold at day 7 and increased to 2.9-fold by day 18. Similarly, beta-ketothiolase (HADHB), which catalyzes the removal of an acetyl group from acyl chain, was also increased in expression from 2.3-fold on day 10 to 3.0-fold on day 18. The acetyl-CoA generated during beta oxidation primarily enters the TCA cycle, but is also available as a substrate for acetyl-CoA acetyltransferase (ACAT1), which is the first step in the formation of acetoacetone and other ketone bodies (134). The expression of this enzyme increased 3.3-fold on day 10 and increased to 3.8-fold by day 18.

3.4.3. Electron Transport Chain and ATP Synthase

Proteins that are part of electron transport chain complexes II, and IV and V were differentially expressed (Table 3.1). Two proteins in complex II, which transfers electrons from succinate to CoQ via FADH2 and is not explicitly linked to transfer of protons across the inner membrane, were up-regulated during differentiation and enlargement. The expression of succinate dehydrogenase A (SDHA) was significantly increased by 2.4-fold at day 10 and increased to 2.5-fold by day 18. The expression of

Table 3.1. Temporal profile of mitochondrial electron transport chain and auxiliary electron carrier enzymes during 3T3-L1 adipocyte differentiation and enlargement[a].

Protein Name	Accession	iTRAQ Label Quantitation Ratios				
		Day 4	Day 7	Day 10	Day 14	Day 18
NADH-ubiquinone oxidoreductase 51	Q91YT0				1.4	
Electron transferring flavoprotein, alpha	Q99LC5			2.5	3.0	3.1
Electron transferring flavoprotein, beta	Q810V3				2.4	2.7
ETF-ubiquinone oxidoreductase	Q921G7			2.4	2.3	2.8
Succinate dehydrogenase, alpha	Q921P5			2.4	2.6	2.5
Succinate dehydrogenase, beta	Q9CQA3					1.8
cytochrome C oxidase unit 6	Q9CPQ1	1.5				
cytochrome C (somatic)	P62897				3.3	
ATP synthase alpha chain	Q03265	1.5	1.9	2.3	2.2	2.2
ATP synthase beta chain	Q8CI65		1.8	2.3	2.1	2.3
ATP synthase oligomycin sensitivity protein	Q9DB20			2.3	2.3	
ADP,ATP carrier protein 2	P51881		3.2	4.3	4.0	3.8
Phosphate carrier protein	Q8VEM8			1.9		

[a] Statistically significant fold increase is represented as red while fold-decreases are in green. White indicates that the change in expression was not statistically-significant. Other electron transport chain proteins (See Supplemental Table 1) were identified in the samples but the fold-changes in expression were not statistically-significant.

SDHB was significantly increased only on day 18 (1.8-fold). Two proteins in Complex IV, which catalyzes the oxidation of reduced cytochrome C with oxygen, also were increased in expression during adipocyte differentiation and enlargement. The cytochrome C oxidase subunit 6 (COX6C) was up-regulated 1.49-fold on day 4 and cytochrome C (somatic) was up-regulated 3.3-fold on day 14 post-differentiation. Complex V (ATP synthase) forms ATP by using energy stored in the proton gradient created by the other 4 complexes. The expression levels of three key enzymes (ATP5A1, ATP5B, ATP5O) increased in expression at different time points (Tab. 3.1). The expression of ATP5A1 was significantly increased from 1.5 on day 4 and remained significantly up-regulated (maximum value of 2.3-fold on day 10) throughout the duration of the experiment. Similarly, the expression of ATP5B was increased in expression from days 7-18 by 1.9 to 2.3-fold. Interestingly, none of the proteins in complex I, also known as NADH ubiquinone oxidoreductase that is the largest of the ETC complexes and transfers electrons from NADH to CoQ with a concomitant transfer of protons across the inner mitochondrial membrane, were differentially expressed.

Two important transporters, adenine nucleotide translocator two (ANT2) and phosphate carrier protein (PCP), were also increased in expression at all time points. These transporters exchange ATP for ADP and import phosphate with H^+, respectively. ANT2 increased 3.2-fold at day 7 and remained up-regulated until day 18 (3.8-fold), while PCP increased 1.9-fold at day 10. These data suggest increased ATP generation from the mitochondria. Two other proteins, the electron transferring flavoproteins alpha and beta

(ETFA, ETFB) that are auxiliary proteins involved in recycling FAD from the electron transport chain, for use as a coenzyme by acyl CoA dehydrogenase (184), were also increased in expression during differentiation and enlargement. The expression of ETFA was significantly increased 3.0-fold on day 10 and progressively increased to 3.4-fold by day 18. ETFB increased by 2.4-fold on day 14 and 2.7-fold on day 18. The ETF-ubiquinone oxidoreductase protein was also up-regulated 2.4-fold on day 10 and reached 2.8-fold increase by day 18.

Since the electron transport chain is critical for ATP synthesis, we also determined the ATP levels at different stages of adipocyte lipid accumulation. Figure 3.6 shows that the ATP level in differentiating adipocytes (i.e., day 3 after addition of the differentiation cocktail) was nearly 17-fold greater than undifferentiated pre-adipocytes. However, ATP levels rapidly decreased as adipocytes matured (days 4 through 9), and was slightly less than undifferentiated pre-adipocytes beyond day 10.

3.4.4. Antioxidant and Detoxification Proteins

Table 3.2 lists the changes in the expression of different antioxidant and detoxification proteins altered during adipocyte differentiation and enlargement. Lung carbonyl reductase (adipocyte protein p27), involved in reducing endogenous carbonyls derived from lipid peroxidation and 3-ketoacyls was up-regulated by 2.7-fold at day 10 post-differentiation and increased to a maximum of 3.7-fold on day 18. Peroxiredoxin-3 and -5 are both thioredoxin peroxidases and serve important roles in reducing alkyl hydro-

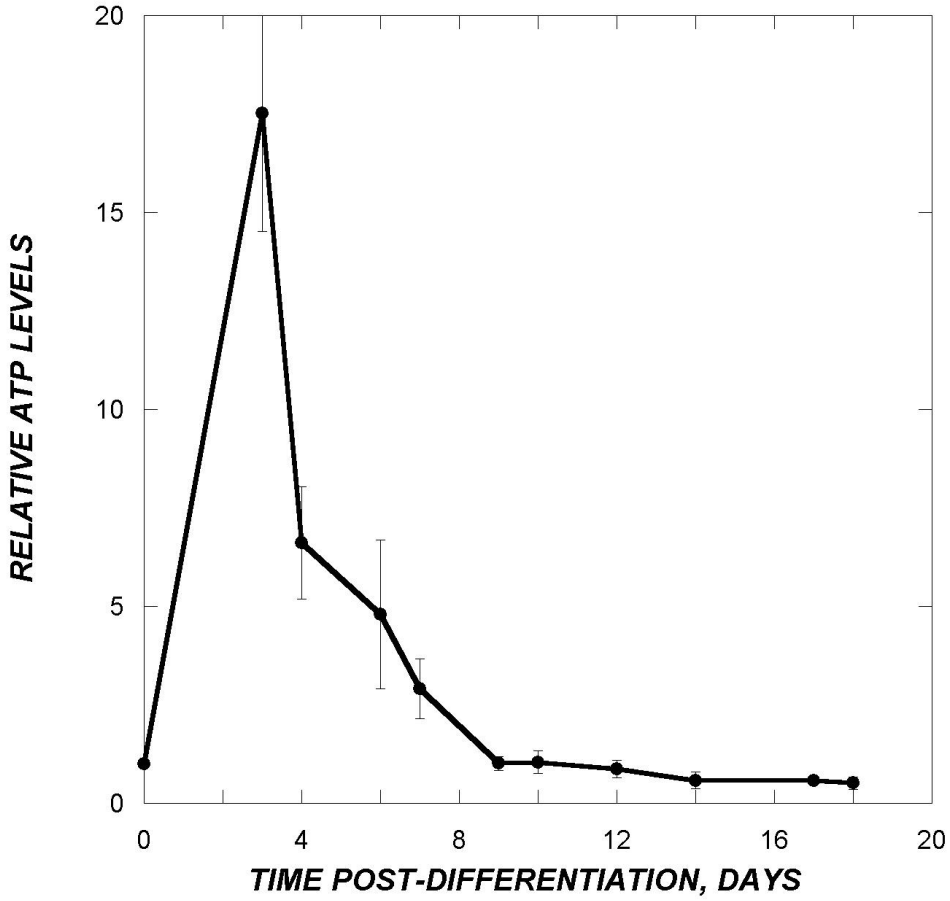

Figure 3.6. ATP level in adipocytes during differentiation and enlargement at different time points relative to undifferentiated 3T3-L1 fibroblasts. The ATP levels were determined using a commercially available assay as describe in the Materials and Methods. Data shown are mean ± standard deviation from three independent experiments.

Table 3.2. Temporal profile of mitochondrial antioxidant and detoxification enzymes during 3T3-L1 adipocyte differentiation and enlargement[a].

Protein Name	Accession Number	iTRAQ Label Quantitation Ratios				
		Day 4	Day 7	Day 10	Day 14	Day 18
Lung carbonyl reductase	P08074			2.7	3.5	3.7
Thiosulfate sulfurtransferase	P52196		1.3	1.6	2.4	2.3
Superoxide dismutase, mitochondrial	P09671	0.60	0.70			

[a] Statistically significant fold increase is represented as red while fold-decreases are in green. White indicates that the change in expression was not statistically-significant. Seven other anti-oxidant proteins (See Supplemental Table 1) were identified in the samples but the fold-changes in expression were not statistically-significant.

peroxides formed during lipid peroxidation (185). Thiosulfate sulfurtransferase which maintains mitochondrial iron-sulfur subunits and functions as a ROS scavenger in concert with thioredoxin (186), was up-regulated by 1.3-fold at day 7, and its expression progressively increased to 2.3-fold over baseline at day 18. Surprisingly, superoxide dismutase (MnSOD), the enzyme that catalyzes removal of superoxide ion (187), was reduced in expression by 1.5 to 1.8-fold on days 4 and 7, but was unchanged in expression beyond day 7.

We also determined the levels of ROS using the NBT assay (Figure 3.7). ROS levels were increased initially (5.2-fold more than undifferentiated preadipocytes on day 3), decreased marginally (3.9-fold more than undifferentiated preadipocytes on day 7), and again increased to 5.5-fold more than baseline by day 10. However, as adipocytes further increased in size, cellular ROS levels continually decreased and was only 2.7-fold more than undifferentiated preadipocytes on day 18.

3.5. DISCUSSION

Based on a quantitative proteomic study of mitochondrial proteins during adipocyte differentiation and enlargement, we found a broad increase in the expression of proteins involved in the TCA cycle, fatty acid beta-oxidation, ATP generation, and anti-oxidant functions. Our conclusions are supported by the fact that multiple proteins in each

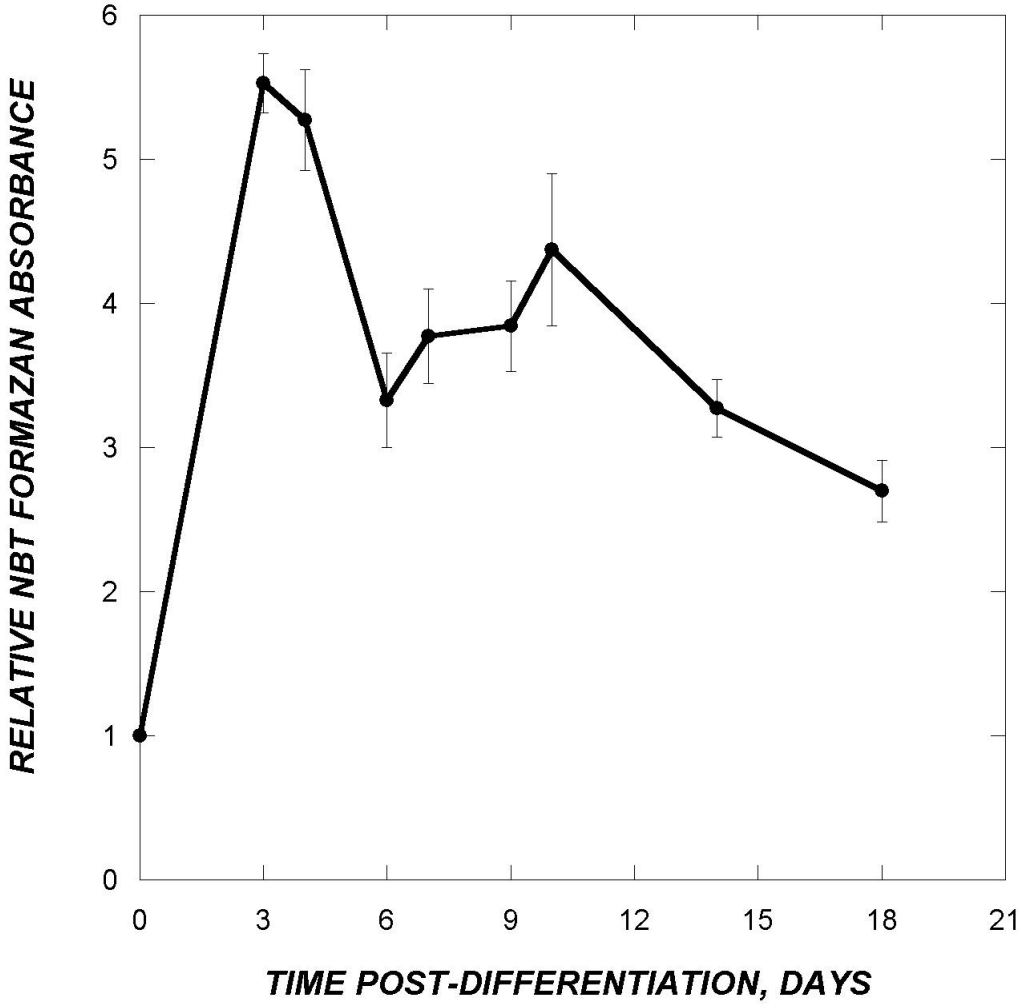

Figure 3.7. Reactive Oxygen Species (ROS) levels in 3T3-L1 adipocytes during differentiation and enlargement. Cellular ROS levels were determined using the NBT assay. Data shown are mean ± standard deviation from three independent experiments.

pathway (e.g., TCA cycle, fatty acid oxidation) were coordinately increased in expression across multiple time points and replicate measurements, with good across multiple time points and replicate measurements, with good concordance between changes in protein expression and metabolite levels.

All major proteins of the TCA cycle (except SUCLG1 and SUCLG2) were found to be up-regulated throughout the time course. The increase in the expression of these enzymes is indicative of overall increased metabolism during adipocyte lipid accumulation and enlargement. In addition to providing reducing equivalents for oxidative phosphorylation, one of the major reasons for up-regulation of TCA cycle proteins could be for the generation of citrate for fatty acid synthesis in the cytoplasm. The sustained up-regulation of the citrate transporter (CTP) also suggests increased flux of citrate towards fatty acid synthesis. Similarly, the increase in the dicarboxylate carrier (DIC) suggests channeling of cytosolic malate into the mitochondria for use in the TCA cycle, as DIC translocates malate, malonate and succinate in exchange for phosphate, sulfate, sulfite or thiosulfate across the mitochondrial inner membrane. Thus, the increase in expression of DIC is consistent with the need to bring in more substrate from the cytosol (188) to fuel the TCA cycle.

Enzymes involved in fatty acid import and beta-oxidation were found to be increased in expression throughout the time course. Fatty acids that are being synthesized from citrate formed in the TCA cycle are, in part, consumed and converted into acetyl-CoA

that will re-enter the TCA cycle. This pattern may represent metabolic flexibility in adipocytes necessary to maintain intracellular homeostasis, as the ability to generate acetyl-CoA and TCA intermediates from lipids would be necessary during times of fasting. However, excess production of acetyl CoA (as is likely to be the case in high-glucose growth medium) may be detrimental, as it can lead to excess reduced electron carriers that contribute to ROS formation in the electron transport complexes (4, 119, 120). This putative increased demand for recycling electron carriers is supported by an increase in the expression of electron transport flavins (ETFA, ETFB). ETFA experiences a large increase (2.4 fold) at 10 days post-differentiation, and this may correlate with the second peak of ROS production observed at day 10. The up-regulation of acetyl-CoA acetyltransferase (ACAT1) also may be indicative of a fraction of the acetyl-CoA being shuttled into ketone body formation. It should be noted that adipocytes are not known for export of ketone bodies, but instead it is believed that ketone bodies are used by adipocytes as an additional pathway to make lipids (189).

Other than complex II (which also participates in the TCA cycle) and complex V, the expression of proteins in the remaining ETC complexes was not observed. The simplest explanations for this observation are that the basal expression level of the other ETC complexes is still sufficient to meet increased demand or proteins in the different ETC complexes have additional levels of regulation. Complex I has been reported as not being the rate limiting step in the normal functioning mitochondrial respiratory chain

(119, 190), and thus likely has reserve capacity, which explains the lack of increase in expression of proteins in complex I.

The 5-fold increase in ROS with young adipocytes (day 3 post-differentiation) compared to undifferentiated preadipocytes is likely due to an increase in the overall metabolic activity of the cell that is required for lipid accumulation. Even though on an oxygen basis cellular metabolic activity produces the lowest $O_2^{\bullet -}$ (120), there is likely still a significant amount produced due to the large quantities of O_2 consumed. Interestingly, there is a transient, yet statistically-significant, ~ 30 percent decrease in the fold-increase in ROS levels on day 7 (relative to day 4) after differentiation. This may be due to alterations in cellular metabolism or up-regulation of the cellular anti-oxidant systems; however, we did not observe statistically-significant changes in the expression of antioxidant proteins.

Although lipid accumulation has been linked to oxidative stress (12, 44), it was surprising that ROS levels between day 10 through day 18 were lower than that on day 10 (i.e., lower ROS with higher lipid accumulation). This observation is likely due to the interplay between changes in ATP demand and levels of reduced electron carriers in the mitochondrion. A recent review by Murphy (120) suggests that cells exist in three metabolic states with different levels of mitochondrial ROS. When the cellular ATP demand is high, the levels of reduced electron carriers (e.g., NADH/NAD^+ ratio) are low due to continuous regeneration, and although high levels of ROS are produced, they are

efficiently scavenged by the cellular anti-oxidant system. On the other hand, when the production/consumption of ATP is low, the levels of reduced electron carriers are high as there is "backflow" of reduced electron carriers (120) which can lead to accumulation of ROS. For example, a high NADH/NAD^+ ratio leads to the production of $O_2^{\bullet -}$ at the ETC complex I (*state 1*) (120) or results in high levels of reduced CoQ10 and ΔpH across the mitochondrial membrane (and therefore, $O_2^{\bullet -}$ production from $CoQ10H_2$) (*state 2*) (120).

Our proteomic and metabolic data suggest that cultured 3T3-L1 adipocytes develop metabolic conditions (accumulation of reduced electron carriers) similar to the mitochondrial *state 1* and/or *state 2* described by Murphy (120), which may be responsible for the high ROS levels detected at day 10 (Fig. 3.7). The increase in the expression of (i) different TCA cycle enzymes which generates high NADH/NAD+ levels, (ii) enzymes involved in fatty acid oxidation (which leads to reduction of FAD^+), (iii) ETFA and ETFB which transfers the reduced $FADH_2$ to the ETC, and (iv) ETF-ubiquinone oxidoreductase which transfers electrons from ETFA/ETFB to CoQ10, all support this hypothesis. The fact that ROS levels decrease beyond day 10 is not surprising as levels of electron carriers will eventually level off if overall cellular metabolism is sufficiently reduced (i.e., slowdown in lipid accumulation). It remains to be seen if the mitochondrial states attributed to this cultured adipocyte model can be identified in adipose tissue *in vivo*.

It was interesting that the major anti-oxidant protein superoxide dismutase (SOD2) was not up-regulated at any time point throughout the experiment (in fact, decreased in expression at days 4 and 7). One possible explanation for this could be aberrant calcium signaling. Calcium homeostasis is a major mitochondrial function (119, 191-193) and our data presents evidence that calcium flux is increased during adipocyte differentiation and enlargement. The proteins VDAC1 and GRP 75 (statistically significant changes in expression on days 7-18 and days 10-18, respectively; Supplemental Table S.1), along with IP3R (not increased in expression), form a junction between the mitochondria and the endoplasmic reticulum that primarily serves as channel to transport Ca^{2+} into the mitochondria from the ER to help support oxidative phosporylation (192, 193). The large increase in ATP levels during differentiation may suggest depleted mitochondrial calcium stores, and a compensatory increase in the VDAC1-GRP75 junction to normalize mitochondrial calcium levels. Since mitochondrial Ca^{2+} levels have also been reported to be critical as for SOD2 activation (191), it is possible that the drop in mitochondrial calcium leads to the decrease in SOD2 expression.

Since oxidative stress primarily originates in the mitochondria (119), adipocyte mitochondrial proteins may be more sensitive to the effects of ROS, and such effects have been proposed to be a main cause of adipocyte dysfunction (12, 41, 194). An intriguing question arising from our data is whether adipocytes in *states 1 and 2* described by Murphy (120) (i.e., high ROS due to low ATP demand and high reduced electron carriers) are more susceptible to loss of function. Recently, Hoehn et al. (195)

reported that insulin resistance may be part of a cellular defense against mitochondrial oxidative stress, as mitochondrial superoxide stress precedes insulin resistance and exposure to antioxidants or over-expression of SOD2 ameliorates insulin resistance in cell culture and animal models. Although preliminary, our proteomic data strongly suggest that control of mitochondrial superoxide production (especially sources linked to excess reduced electron carriers arising from enhanced TCA cycle activity and/or fatty acid oxidation), and the resultant oxidative stress may be attractive targets for modulating adipocyte function and for the development of novel approaches against metabolic disorders.

CHAPTER IV

DEVELOPMENT AND CHARACTERIZATION OF A DOXYCLINE INDUCIBLE CYP2E1 EXPRESSING HEPATOCYTE CELL LINE

4.1. OVERVIEW

We investigated if ROS produced from controlled expression of cytochrome P450 2E1 leads to enhanced sensitivity to oxidative stress. The ethanol inducible mono-oxygenase CYP2E1 is responsible for increased ROS production and oxidative stress in hepatocytes during chronic ethanol ingestion. We developed an inducible CYP2E1 expressing HepG2 cell line to investigate CYP2E1 mediated oxidative stress with greater control and sensitivity. Use of the pTet-On/pRevTRE inducible expression system, retroviral transduction, and single colony screening resulted in the isolation of a sub-clone (RD12) that shows minimal CYP2E1 activity in the absence of induction with doxycycline (i.e., tight control) and fast kinetics of induction (75 percent of maximal activity is obtained after 12 hours induction). RD12 cells demonstrated 30 percent higher CYP2E1 activity as measured by p-nitrophenol oxidation than the established HepG2 E47 cell line that constitutively expressed CYP2E1. RD12 cells also demonstrated higher susceptibility to oxidative stress induced by CYP2E1-metabolism of acetaminophen, as cells exposed to 20 mM acetaminophen for 24 hours had 30 percent lower viability than E47 cells. RD12 cell incubated with acetaminophen for 2 hours also had 25 percent lower glutathione than E47 cells, which further corroborates the increased oxidative stress. The control over CYP2E1 induction and increased sensitivity to oxidative stress makes this cell line

a powerful tool for analyzing the effect of fatty acids, cytokines, and antioxidants on cellular metabolism and function.

4.2. INTRODUCTION

Experimental approaches for inducing oxidative stress in different cell types utilize exogenous addition of an oxidant (e.g., hydrogen peroxide, *tert*-butyl hydroperoxide) (196) to increase oxidative stress for observing its effects on cell viability and/or expression of marker proteins. While such approaches are likely to give an population-wide, averaged response to a step-change in oxidative stress, the resultant general increase in concentration of reactive oxygen species (ROS) throughout the cell and the cellular response do not accurately represent what is encountered *in vivo*. First, the production of ROS and the resultant oxidative stress occurs gradually inside cells due to accumulation of ROS (as compared to a step-change arising from external addition of pro-oxidants). Moreover, oxidative stress and ROS are typically highly localized in organelles such as the mitochondrion and endoplasmic reticulum (ER). Therefore, widespread and general oxidative damage to all cellular components resulting from exogenous addition of pro-oxidants does not represent effects of physiological profiles of ROS production.

Attempts have been made to create model systems that more accurately represent biologically relevant induction of oxidative stress (27, 197). The most notable of these is the HepG2 E47 cell line constitutively expresses the CYP2E1 enzyme (27). CYP2E1

is an ethanol-inducible member of the cytochrome p450 family and is involved in the metabolism of ethanol and other small molecules (84, 198, 199). However, the increase in metabolic activity due to the breakdown of small molecules results in the generation of ROS and possibly toxic intermediates (84, 198, 199). The E47 cell line has been used extensively since its development (27, 28, 93, 112, 113), and has contributed to a fundamental understanding of oxidative stress mechanisms at the molecular level. However, a drawback with this cell line is that CYP2E1 expression is constitutive, which leads to a higher basal level of oxidative stress in these cells. More importantly, constitutive generation of ROS and oxidative stress also leads to higher baseline activity of anti-oxidant systems (e.g., catalase, gamma-glutamyl cysteine synthetase) (28) As a result of the increased anti-oxidant activity, elaborate treatment regimes, such as time dependent, sequential exposure to different compounds, is required to generate a significant increase in oxidative stress. One such regimen used to generate oxidative stress in E47 cells involves a three-step sequential treatment process, as cells are first treated with chelated iron, followed by loading with polyunsaturated fatty acids, and then exposure to ethanol to induce oxidative stress (113). Other approaches that have been used to overcome this problem include reducing cellular capacity to produce glutathione either by serum starvation (200) or by direct inhibition of glutathione synthetase (27); however, these have also only proved to be moderately successful.

Consideration of the biological imprecision of direct addition of an exogenous oxidant and complex strategies to induce oxidative stress is the motivation for development of a

cell line with inducible expression of CYP2E1. There are two main advantages in developing an inducible CYP2E1 expression system. First, an inducible CYP2E1 expression system will enable presenting cells with any pharmacological agent or molecule that may enhance or mitigate the effects of oxidative stress, prior to the induction of oxidative stress, as investigation of pre-treatment cannot be conducted using a constitutive CYP2E1 expression system. In addition, this also allows utilizing some of the powerful new tools in proteomics, such as isotopic labeling (15) and chemical tracers (144), prior to the induction of CYP2E1, which enables dynamic studies to measure changes in metabolite or protein expression levels due to CYP2E1 expression. It is also likely that an inducible system will have lower levels of basal anti-oxidant systems and be more sensitive to CYP2E1 induced oxidative stress, which would allow determining the toxicity of a particular compound or its metabolic intermediates, since the activation of molecules through the CYP450 enzymes often leads to the production of more toxic intermediates as well as high levels of oxidative stress.

In this chapter, we describe the development of an inducible CYP2E1 expression system in HepG2 cells that is a well-established model cell line for toxicity studies. We further demonstrate the utility of this cell system by applying it to investigate the sensitivity and oxidative stress of HepG2 cells with acetaminophen treatment.

4.3. MATERIALS AND METHODS

4.3.1. Reagents and Supplies

All cell and bacterial culture media and reagents were purchased from Thermo Fisher Scientific (Waltham, MA). Tetracycline-free fetal bovine serum was purchased from HyClone (Logan, UT). Ampicillin, G418, hygromycin-B, doxycycline, and oleic acid were purchased from MP Bio (Solon, OH). Cell culture dishes (10 cm), 6-well, 12-well, and 24-well cell culture plates, cloning cylinders (6 × 8 mm) were purchased from Corning (Lowell, MA). Silicone vacuum grease was purchased from Thermo Fisher Scientific. Para-nitrophenol and Triton-X100 were purchased from Sigma-Aldrich (St. Louis, MO).

4.3.2. HepG2 Culture

HepG2 E47 cells (referred to as E47 cells henceforth) were a kind gift from Prof. A. I. Cederbaum (Mount Sinai School of Medicine, New York). HepG2 cells were purchased from ATCC. Both HepG2 and E47 cells were cultured in MEM-EBSS, supplemented with 10% fetal calf serum, 100 units of penicillin per milliliter, 100 mg/ml of streptomycin, and 2 mM glutamine in a humidified atmosphere in 5% CO_2 at 37°. Experiments with the inducible CYP2E1 cells used the same media formulation, except that tetracycline-free FBS was used. PBS (8 g/l NaCl, 0.2 g/l KCl, 1.44 g/l Na_2HPO_4, 0.24 g/l KH_2PO, pH 7.3) was used for rinsing cells. Dulbecco's PBS consists of PBS supplemented with 0.41 g/l $MgSO_4 \cdot 6H_2O$, 0.37 $CaCl_2 \cdot 2H_2O$, 50 mg/l sodium pyruvate, pH 7.3.

4.3.3. Cloning of Full Length CYP2E1 cDNA into pRevTre-MCS Expression Vector

The pRevTRE / pTet-On inducible plasmid expression system (Clontech, Mountainview, CA) was used to create an inducible CYP2E1 expression system. In this system, plasmid pTet-On expresses the tTA (Tet-transactivator) protein that, when bound with a ligand such as doxycycline, binds to the Tet response element DNA sequence and initiates transcription from a minimal promoter. In the absence of a ligand, tTA does not bind to the target DNA sequence; thereby, providing an On/Off switch for controlling expression of a target gene cloned downstream of the Tet response element. Plasmid p91023 containing full length human CYP2E1 cDNA was a kind gift from Dr. F. J. Gonzalez at the National Cancer Institute, Bethesda, MD.

PCR was used to add a Kozak consensus sequence (to initiate translation) (201), and appropriate restriction sites (*Hind*III, and *Hpa*1) to plasmid p91023 prior to cloning CYP2E1 into the pRevTRE plasmid. The forward primer containing a 5' *Hind*III restriction site and a Kozak sequence (underlined) was TTATGAGTGAAAGCT-TGCCACCATGTCTGCCCTC. The reverse primer containing a 3' *Hpa*I restriction site was ATACGATATGCTGTTAACTCATGAGCGGGG. The Primer extension reaction was performed with Phusion DNA Polymerase (New England Biolabs, Ipswich, MA) according to the manufacturer's instructions. Briefly, a total reaction volume of 25 µl containing 10 ng of template DNA, 0.2 µl Phusion DNA Polymerase, and 1 µM forward and reverse primers was placed in a Bio-Rad Icycler (Bio-Rad, Hercules, CA) for 0.5 min at 98°C

followed by 35 cycles of 0.2 min at 98°C, 0.3 min at 71°C, 0.35 min at 72°C, and a 5-min final step at 72°C. The PCR product was purified with the Wizard PCR clean-up system (Promega, Madison, WI) using the provided protocol.

Approximately 2.5 μg of amplified DNA containing the CYP2E1 gene was sequentially digested with *Hpa*I and *Hind*III according to standard protocols for 2 h each (202). The pRevTRE-MCS plasmid was also sequentially digested with *Hpa*I and *Hind*III using 7.5 μg of plasmid DNA. The digested vector (6.5 kb) and CYP2E1 insert (1.45 kb) were gel-purified a 1% low melting point agarose gel, followed by purification with Wizard PCR clean-up system (Promega, Madison, WI).

The purified pRevTRE-MCS vector was phosphatase treated according to the protocol provided by NEB. The CYP2E1 insert was ligated into pRevTRE-MCS using T4 DNA ligase (NEB) with a 3:1 molar ratio of insert to vector DNA for 4 h at 16^{o}C. Ligation reactions were heat inactivated at 65°C for 15 minutes prior to electroporation

Two μL (~ 20 ng) of the ligation reaction was electroporated into ~ 10^{11} electrocompetent *E. coli* XL1-Blue cells (Stratagene, La Jolla, CA) in 2 mm gap electroporation cuvettes (Bio-Rad) according to the standard Bio-Rad protocol. Immediately following electroporation, cells were incubated at 37ºC for 1 hour with agitation (203).

Plasmid DNA was extracted from 12 colonies and the insert verified by restriction digests. Inserts were sequenced to verify the fidelity of the CYP2E1 gene using the Big Dye Terminator v3.1 sequencing kit with a 3130xl Genetic Analyzer, both from Applied Biosystems (Foster City, CA) according to manufacturer's instructions.

4.3.4. Generation of Retroviral Particles

Retroviral particles containing the genes of interest (pTet-On and pRevTRE-CYP2E1) were generated by co-transfecting the CYP2E1 expression plasmid with *POL, GAG* and *VSVG* plasmids that code for reverse transcriptase, capsid, and envelope proteins, respectively, created by standard protocols (204). Briefly, 12 μg of the target expression plasmid (pTet-On or pRevTRE-CYP2E1), 1.0 μg of plasmid pGAG, 1.0 μg pPOL, and 1.2 μg pVSV-G were gently mixed in 100 μl of DMEM complete media. The pooled plasmids were complexed with FuGene 6 transfection reagent (Roche, Basel, Switzerland) for 15 min at 20^{o}C as per the manufacturer's protocol and added dropwise to 293T cells cultured in a 100 mm dish at 60% confluency. The medium was replenished after 48 hours and the supernatant collected after 96 hours. Cell debris was removed by filtering through a 0.45 μm syringe filter and the virus concentrated to a viral titer of 2.0×10^5 TU/ml using a 500 kDa Centricon centrifugal filter (Millipore, MA) according to the manufacturer's instructions. Viral stocks were aliquoted and stored at -80°C until further use.

4.3.5. Generation of the Inducible CYP2E1 HepG2 Cell Line

HepG2 cells were seeded in 10 cm dishes and allowed to reach reaching 40% confluency. Polybrene (Millipore) was added to HepG2 media at a final concentration of 8 ng/ml, and then 125 µl of the pTet-On virus stock was added to each ml media. This dilution corresponded to a multiplicity of infection of 0.01-0.015 and gave the largest number of viable, single colonies. Cells were exposed to virus-like particle containing media for 24 h and then the media was replaced with normal growth media supplemented with 880 µg/mL of G418 and replenished every 48 h. After 96 h, the media was switched to a mixture of 50% fresh growth medium and 50% cell-free spent medium from HepG2 cells, with G418 supplementation. The addition of spent media was found to greatly increase the viability of the HepG2 clones. The media was changed every two days for approximately two weeks until the majority of cells were dead and single colonies of surviving cells were evident. Single colonies were isolated as described by Wieder et. al. (205), and each colony was transferred to a single well of a 24-well culture plate. The sub-clones were maintained in the fresh/spent medium mixture supplemented with 550 µg/mL G418.

A two-step strategy was adopted for generating the inducible CYP2E1 line. HepG2 cells were first transduced with pTet-On virus to express the tTA protein. Clonal populations of HepG2 pTet-On cells were collected and propagated in a 12-well plate as described above. At ~ 40% confluency, cells were transiently transfected with a reporter plasmid pRevTRE-d2EGFP (206) using the GenJet Transfection Reagent for HepG2 (Signagen,

Ijamsville, MD) according to the manufacturer's instructions. After 24 hours, 10 ng/ml of doxycycline was added to induce GFP expression from the reporter plasmid. The extent of GFP induction in each clone was quantified with an Axiovert 500M fluorescent microscope (Zeiss, Thornwood, NY). Clones with highest induction of fluorescence signal with low background fluorescence in the absence of doxycycline were identified (6 out of approximately 50) and used for introducing the CYP2E1 expression plasmid.

HepG2 clones stably integrated with the pTet-On plasmid were subsequently transduced with pRevTRE-CYP2E1 virus particles as described above for the pTet-On virus, except that cells were maintained in 0.55 mg/ml G418 until viral transduction and sub-clones were selected for stable integration of the CYP2E1 virus particle using 280 µg/mL Hygromycin-B and 0.55 mg/ml G418.

Clonal populations containing both the pTet-On and pRevTRE-CYP2E1 plasmids were propagated in phenol red-free media in a 12 well plate. After reaching 60% confluency, CYP2E1 expression was induced through addition of 20 ng/ml doxycycline to each clone in triplicate. After 24 hours, the media was replaced with fresh media containing 20 ng/ml doxycycline and 0.2 mM p-nitrophenol and incubated for 18 hours to assess the CYP2E1 mediated conversion of p-nitrophenol to p-nitrochatecol (91, 207). This assay is non-destructive and no harm was observed in cells. After incubation, 100 µl of the yellow supernatant was mixed with 10 µl of 0.1 M EDTA and 10 µl of 10 M NaOH to convert the p-nitrochatecol to a pink chromophore (91). The levels of the pink

chromophore were quantified by measuring absorbance at 510 nm in triplicate. The three sub-clones that produced the highest absorbance at 510 nm while maintaining very low CYP2E1 activity in the absence of doxycycline were selected for further propagation.

4.3.6. Comparison of p-Nitrophenol Oxidation in Inducible CYP2E1 Expressing Cells and E47 Cells

The CYP2E1 activity of the doxycycline inducible clones was compared to the established constitutive CYP2E1 expressing E47 cell line (27, 112). E47 cells were cultured according to recommended protocols (112), except that the E47 media contained 0.55 mg/ml G418. E47 cells (passage 3-5) and the doxycycline inducible clone were plated into 12 well plates at 1.0×10^5 cells per well in phenol red-free media. Expression of CYP2E1 was induced as described above. The cells were processed in manner as the previously described section to measure absorbance of p-nitrocatechol. The molar extinction coefficient of p-nitrocatechol is 1.3×10^4 (208). Instead of returning fresh media to cells, they were rinsed with PBS, and then 200 μl of 1% v/v Triton X-100 was added to each well followed by incubation at 20°C for 15 minutes. The lysed cells were collected in micro-centrifuge tubes, vortexed, and centrifuged 13000 × g for 30 seconds at 20°C. The supernatant protein concentration was measured for normalization, using the 660 nm Protein Assay (Thermo Fisher Scientific) according to the manufacturer's instructions.

4.3.7. Comparison of Cytotoxicty in Paracetamol Treated Inducible CYP2E1 Expressing Cells and E47 Cells

E47 cells and the doxycycline inducible clone were plated into 24 well plates at 0.50 × 10^5 cells per well. After 2 days, 20 ng/ml doxycycline was added to the inducible cell line alone to induce CYP2E1 expression. After 24 hours, all cells received fresh media containing paracetamol concentrations of: 0, 2.5, 5, 10, and 20 mM, with 20 ng/ml doxycycline added to the inducible line. After an incubation of 12 and 24 hours, 200 µl samples of the supernatant media were collected. Cell toxicity was determined using the CytoTox-One LDH membrane integrity assay (Promega, Madison, WI) according to manufacturer's instructions.

4.3.8. Comparison of Glutathione in Paracetamol Treated Inducible CYP2E1 Expressing Cells and E47 Cells

E47 cells and the doxycycline inducible clone were plated into 24 well plates at 0.50 × 10^5 cells per well and CYP2E1 expression induced as described above. After 24 hour induction, all cells received fresh media with 20 mM paracetamol; in addition, the inducible line (except for negative control) received 20 ng/ml doxycycline. After an incubation of two hours, the cells were incubated with ThiolTracker fluorescent glutathione dye (Invitrogen, Carlsbad, CA) according to the manufacturer's instruction to determine relative levels of glutathione. The ThioTracker was then rinsed once and fluorescence read at 410/530 nm in a SpectraMax GeminiEM (Molecular Devices, Sunnyvale, CA). All conditions were tested in triplicate.

4.4. RESULTS

4.4.1. Development of an Inducible CYP2E1 Expressing Cell Line

Here we report the development of a doxycycline inducible CYP2E1 expressing HepG2 cell line, hence referred to as RD12. This cell line is based on the pTet-On/pRevTRE two-plasmid system (46, 209) that utilizes an artificial transcription factor (tTA)and its affinity to the tetracycline response element (TRE) for regulating target gene expression, and has been used in multiple studies (167, 210, 211). The inducible system offers two advantages over a cell line that constitutively over-expresses CYP2E1. First, the expression of CYP2E1 can be induced at any time point through addition of tetracycline or doxycycline. Second, the extent of induction can also be controlled by varying the concentration of the inducer (212). These advantages are especially important as it enables investigating the cellular response to varying effect of oxidative stress. Different levels of oxidative stress produce different effects; high levels are associated with apoptosis and loss of function (11, 12, 29), and lower levels have been shown to actually induce anti-oxidant effects (28, 30). Precise control allows pre-treatment of cells with fatty acids or cytokines, such as TNFα, which has been implicated in the progression of alcoholic steatohepatitis (106).

4.4.2. Verification of CYP2E1 Activity

Cytochrome P450 2E1 activity was measured by determining the rate of oxidation of p-nitrophenol to p-nitrocatechol (PNP) (91, 207). We are certain PNP oxidation is the result of CYP2E1 activity because in the absence of doxycline, RD12 cells and regular HepG2 cells show negligible PNP oxidation. Traditional assays for CYP2E1 activity have been based on collecting the microsomal fraction from hepatocytes and conducting the oxidation reaction in a tube with NADPH as the required co-factor (27, 112). The PNP oxidation product, p-nitrocatechol forms a bright pink chromophore at high pH, and allows spectrophotometric determination of the conversion rate. The disadvantages of the microsomal method are that it is labor intensive and requires ultracentrifugation, many cells per assay (~10^7), and the addition of NADPH to the reaction mixture. We used and adapted a method of measuring CYP2E1 activity based on the direct addition of PNP to the cell culture media, collecting the media, and measuring the concentration of p-nitrocatechol (85, 92). We found the highest rates of rates of CYP2E1 activity in inducible cells occurs at 24 hours after the addition of doxycycline, but significant activity occurs in 12 hours. In both RD12 and E47 cells, maximal PNP oxidation was greater in fresh media than in spent media, and this may be related to the metabolic requirement for pyruvate or other source for cellular NADPH production previously mentioned (85). We observed no ill effects to cells upon adding PNP to culture media, and this was an advantage in the screening process, as clones were screened after single colonies expanded to several wells of 12 well plate, and cells used to perform the first CYP2E1 screening test were further propagated to become the stable clone.

The newly created RD12 line CYP2E1 activity was compared to that of E47 cells, and showed 33 percent greater PNP oxidation activity (Figure 4.1). The measured activity of 0.121 nm/mg protein/min correlates very well to the PNP oxidation of 0.130 nm/mg protein/min found in primary hepatocytes exposed to 100 mM ethanol (92). While an exact conversion is not possible, it has been noted that activity from microsomal protein can be approximated using 5 times as much total cellular protein (112), and thus gives an equivalent activity of 0.65 nm/mg microsomal protein/min, which is in line with published results (27). CYP2E1 activity was not detected in the absence of doxycycline, as RD12 cells without doxycycline had identical activity to normal HepG2 cells.

4.4.3. CYP2E1 Mediated Acetaminophen Toxicity in RD12 and E47 Cells

Acetaminophen (APAP) is converted to the toxic intermediate NAPQI by CYP2E1 and has been shown to be toxic to CYP2E1 expressing cells (87, 114, 213, 214). We sought to determine if RD12 were more sensitive than E47 cells to APAP, by determining if APAP exposure caused more cellular lactate dehydrogenase LDH leakage. A common way to characterize the cytotoxicity of compound is measurement of LDH released from damaged cells (215, 216).

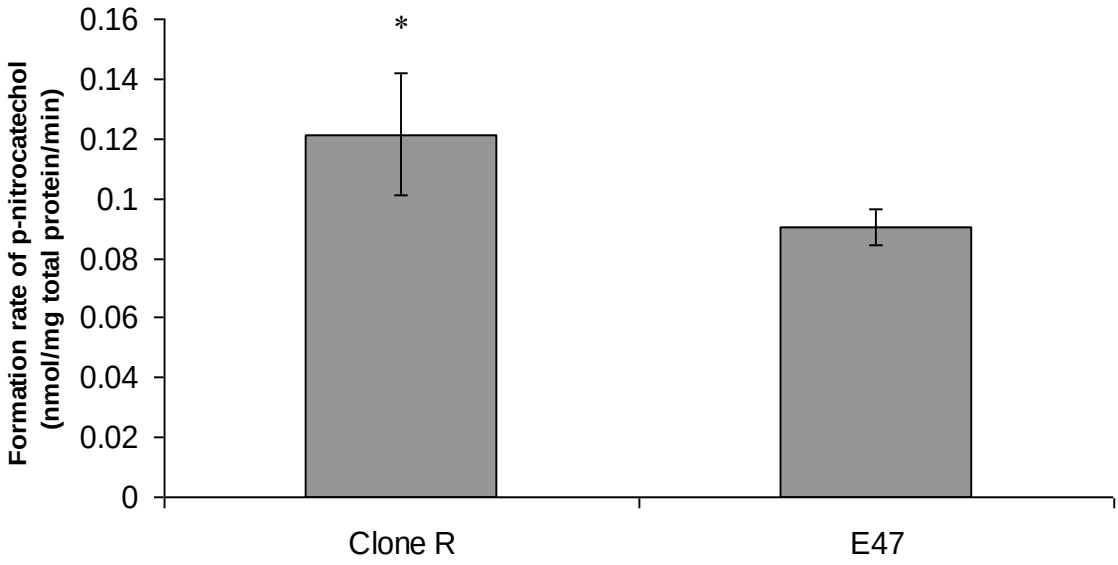

Figure 4.1. Comparison of CYP2E1 activity in clone RD12 to that of E47 cell line. Cells were exposed to doxycycline (20 ng/ml) for 24 hours and then media was changed to 1000 µl of media containing doxycycline and 0.2 mM p-nitrophenol. 100 µl of this supernatant was collected after 18 hour exposure and read for absorbance at 510 nm as described in Materials and Methods. * indicates statistical significance at $p < 0.05$.

We exposed cells to increasing doses of APAP for 12 and 24 hours and then collected supernatants to measure LDH activity. In most cases, the nominal value of the LDH fluorescence for RD12 cells was higher than that of E47 cells, however the data appear noisy, and only the 24 incubation produced a statistically significant increase of 30 percent more LDH fluorescence than E47 cells (Figure 4.2).

It is interesting that the RD12 cells treated with doxycycline (to induce CYP2E1) did not experience significant increases in LDH fluorescence over RD12 cells not treated with doxycycline. This was unexpected, as the CYP2E1 mediated metabolism of APAP was expected to induce cellular damage. In a related trend in the E47 cells treated with APAP for both 12 and 24 hours experienced less LDH release with increasing APAP concentration. This inverse correlation was roughly linear, and E47 cells exposed to 20 mM APAP had 35 percent and 40 percent lower rates of LDH release after 12 and 24 hours of exposure when compared to cells not receiving APAP, respectively.

It has been reported that E47 cells have enhanced glutathione production compared to non-CYP2E1 expressing cells (28). In order to determine if RD12 cells are more sensitive to oxidative stress than E47 cells, we determined if relative glutathione levels were lower in RD12 cells after the induction of CYP2E1. Because the CYP2E1 activated APAP metabolite NAPQI is detoxified with glutathione (214, 217), we also

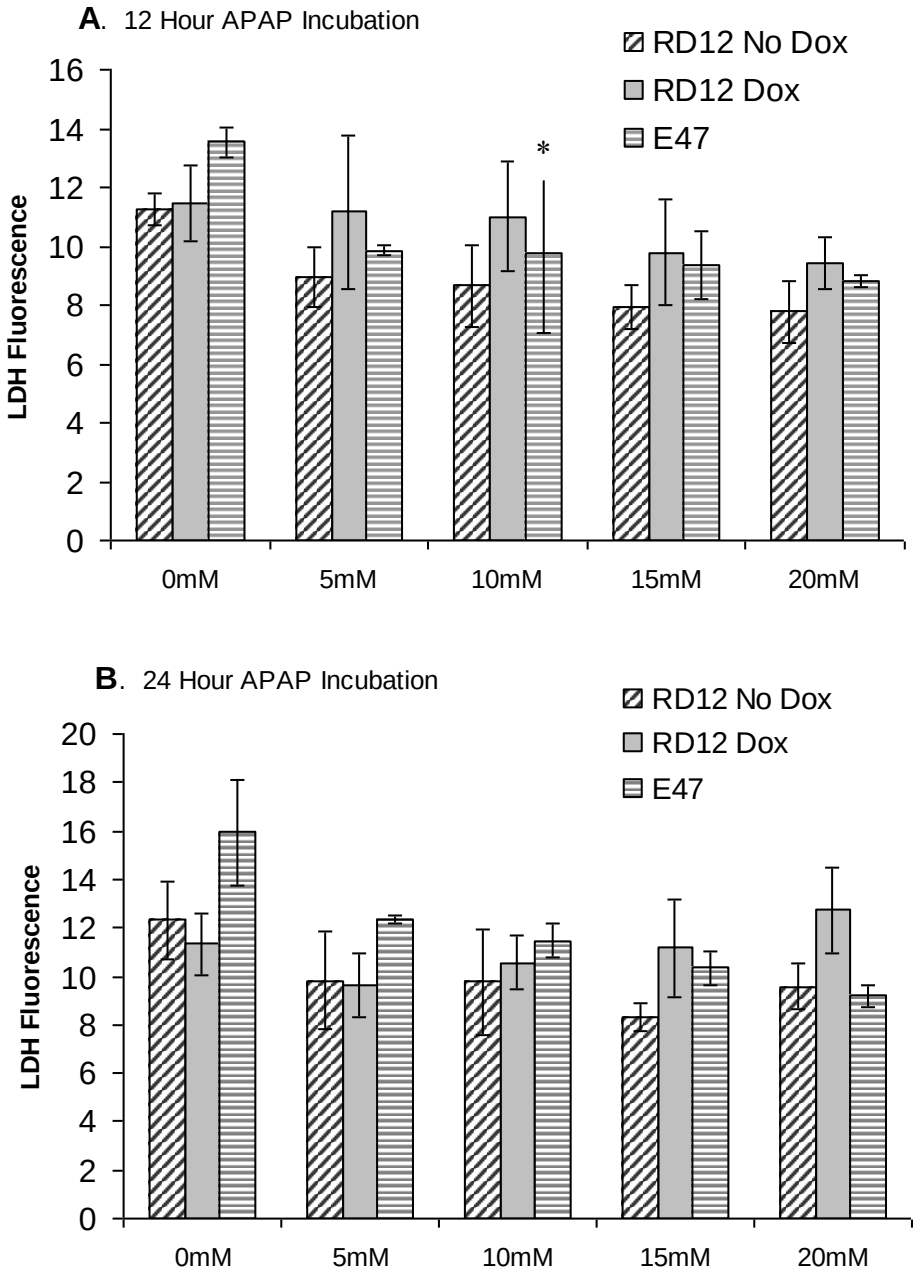

Figure 4.2. Cytotoxicity as measured by LDH fluorescence for CYP2E1 expressing HepG2 cells exposed to acetaminophen (APAP) for 12 (A) and 24 (B) hour exposure. Clone RD12 cells were incubated for 24 hours with 20 nM Doxycycline prior to APAP exposure to induce.

sought to determine if APAP treated RD12 cells had lower glutathione than E47 cells. Relative reduced glutathione levels were determined by using the ThiolTracker dye from Invitrogen. This binds to free thiols to form a fluorophore, and can be measured with a fluorescent plate reader at 530/590 nm. The RD12 cells treated with doxycycline had glutathione levels 20 percent higher than non-doxycycline treated cells and levels essentially equivalent to E47 cells (Figure 4.3). This counter-intuitive effect reinforces that CYP2E1 expression itself is correlated to an increase in glutathione levels. Doxycycline treated RD12 cells incubated with APAP did show 25 percent lower glutathione levels than cells treated with doxycycline alone, and happened to be equivalent to untreated RD12 cells, likely indicating full metabolism of APAP was consuming significant glutathione (Fig. 4.3).

Cells not treated with doxycycline but treated with APAP showed the same glutathione as untreated RD12 cells, thus confirming the CYP2E1 activation of APAP. Somewhat surprisingly, E47 cells treated with APAP did not show lower glutathione levels than non-APAP treated E47 cells. This finding along with results from the LDH assay may provide further evidence of the ability E47 cells to up-regulate its glutathione production or turnover capabilities.

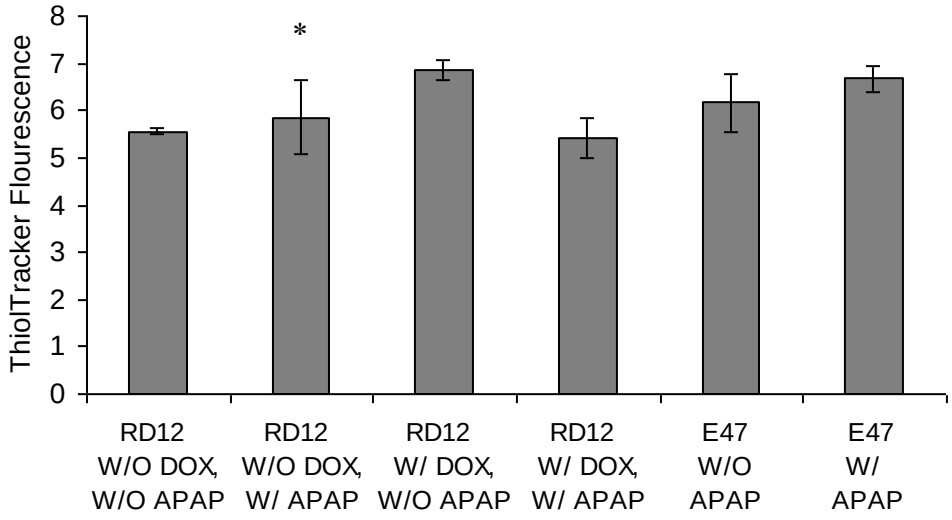

Figure 4.3. Cytotoxicity as measured by LDH fluorescence for CYP2E1 expressing HepG2 cells exposed to acetaminophen (APAP) for 12 (A) and 24 (B) hour exposure. Clone RD12 cells were incubated for 24 hours with 20 nM doxycycline prior to APAP exposure to induce CYP2E1.

4.5. DISCUSSION

The goal of this project was to create a cell line with an inducible CYP2E1 expression that would enable greater control and sensitivity to CYP2E1 mediated oxidative stress. This allows for more precise measurement and determination of the effects of biologically relevant sources of oxidative stress, and to our knowledge a stable, inducible CYP2E1 expressing hepatocyte line has not been reported. The development of a double stable clone, here dubbed RD12, required development and refinement of molecular cloning techniques and meticulous screening and propagation of candidate cell populations. The result is a cell line that after induction has a higher CYP2E1 activity (as measured by PNP oxidation) than previously developed constitutive cell lines (27). To evaluate CYP2E1 activity on a large scale, PNP was added directly to cell culture media, and this proved successful and is likely a better representation of the CYPE1 activity that occurs in experiments conducted in cell culture.

We chose to use the well characterized APAP-CYP2E1-NAPQI metabolic pathway to demonstrate sensitivity to oxidative stress because it places stress on antioxidant systems by ROS generated from the CYP2E1 catalytic cycle (99) and the reactive intermediate can be conjugated to glutathione for detoxification (87, 114). RD12 cells showed are more sensitive to CYP2E1 mediated oxidative stress by showing a direct increase in cytotoxicity (Fig. 4.2) and with lower glutathione levels (Fig. 4.3). These results indicate a modest, but notable increase in sensitivity, especially considering RD12 cells had a 30 percent increase in CYP2E1 activity. However, E47 cells demonstrated a

remarkable ability to adapt to conditions designed to increase oxidative stress. The E47 line has been report as having up-regulated glutathione and expression of gamma glutamyl-cysteine synthetase, the first enzyme in glutathione synthesis (28). It is likely that creation of the E47 cell line selected for traits in the underlying HepG2 line leading to this adaptation (i.e. high CYP2E1 activity required attenuation of oxidative stress). Because RD12 cell share the same base HepG2 line, it may share a degree of adaptability. Considering that RD12 cells have shown 30 percent greater CYP2E1 activity, it is not surprising that RD12 cells have a modest but not radical increase in sensitivity to oxidative stress.

Given the high oxygen demand, mitochondrial number, and metabolic demand of hepatocytes, it is expected that hepatocytes have the ability to deal with elevated levels of oxidative stress. Numerous studies have shown an acute adaptability of hepatocytes to mutagenic, toxic, or pro-oxidant compounds. The pretreatment of H4 hepatoma cells with low non-toxic doses of the alkylating agent N-methyl-N'-nitro-N-nitrosoguanidine (MNNG) renders the cells more resistant to future toxic and mutagenic doses when compared to non-pretreated controls (218). HepG2 cells treated with wastewater concentrate containing chlorine dioxide and peracetic acid experienced reduced glutathione levels after a two hour exposure, but after 24 hours experienced an increase over control levels (219). Pretreatment of HepG2 cells with oleic acid induced a cyto-protective effect that made cells more resistant to a subsequent exposure to *t*-butyl hydro-peroxide (30). Taken together this reinforces the notion that when studying

oxidative stress, especially in hepatocytes, it should not be viewed as a binary phenomenon where a cell has or does not have oxidative stress, but rather what systems are activated or deactivated by the overall re-dox state of the cell.

In summary the inducible cell line RD12 has demonstrated good CYP2E1 activity and increased sensitivity. Future studies will take advantage of the inducible nature of the RD12 cells line and allow for pretreatment of cells with compounds that enhance or mitigate oxidative stress. This could be important in modeling certain conditions such as alcoholic liver disease where progression of the disease requires fat accumulation and oxidative stress, in the so called “two hit” hypothesis (21), or inflammation, where cells could be pre-stimulated with cytokines. The control in an inducible system allows experiments of a dynamic nature to determine the precise roll metabolite availability on CYP2E1 activity, or the rate and magnitude of protein expression in response to CYP2E1 related oxidative stress.

CHAPTER V

EFFECT OF DIETARY FATTY ACIDS AND PRO-OXIDANT CHALLENGE ON PROTEIN CARBONYLATION IN HEPG2 HEPATOCYTES

5.1. OVERVIEW

The effects of dietary fatty acids on the accumulation of fat in the liver (steatosis) are not fully understood. Results from many steatotic models suggest that different fatty acids may exert time and concentration dependent effects on hepatocytes. For example, studies with palmitic and linoleic acid loading in hepatocytes found an increase in certain markers of oxidative stress and cytotoxicity in hepatocytes; however, low doses of oleic acid were found to reduce cytotoxicity to subsequent pro-oxidant challenge. We hypothesized that the ability of hepatocytes to respond to pro-oxidant challenge depends on the level to which different fatty acids induce oxidative stress, which would result in different levels and patterns of protein carbonylation. HepG2 cells were exposed to different doses (0 - 0.5 μM) of oleic, linoleic, and palmitic acid, followed by challenge with a pro-oxidant molecule *t*-butyl hydroperoxide. Cells pre-loaded with 0.2 mM oleic acid for 48 hours demonstrated a statistically-significant 20 % reduced cytotoxicity after treatment with 0.5 mM *t*-butyl hydroperoxide for 8 hours. This protective effect was not observed at other concentrations of oleic acid or with any concentration of palmitic acid and linoleic acid. Affinity chromatography was used to purify carbonylated proteins from oleic acid-treated HepG2 cells and SDS-PAGE analysis indicated that the protein carbonylation pattern was different upon oleic acid pre-treatment; however, only a few

proteins demonstrated a clear change in expression. Subsequent experiments suggested that the non-specific binding of proteins to the affinity column and sub-optimal degree of separation of carbonylated proteins were issues of concern. Current recommendations to improve the affinity chromatography separation are to enhance the specificity of the affinity separation through pre-blocking of the column with ovalbumin, optimizing the protein loaded, and using detergents to reduce protein aggregation.

5.2. INTRODUCTION

The accumulation of fat in the liver, or steatosis, occurs due to a variety of reasons including those that are dietary (220), viral (e.g. hepatitis C (221)), and/or behavioral (e.g., alcohol consumption (6, 21)). The degree of fat accumulation correlates to the general susceptibility of the liver to further damage, but it is believed that fat accumulation alone is not sufficient to trigger development of more serious pathologies such as steatohepatitis (56). According to this "two-hit" hypothesis (21), additional stressors such as oxidative stress and cytokine action are likely involved in the progression of steatosis to steatohepatitis (6, 21, 56). The cellular accumulation of fat is linked to increased lipid peroxidation in both non-alcoholic steatohepatitis (77, 222) and alcoholic related oxidative stress (21, 92, 94, 222). Lipid peroxidation products have been found to form protein adducts (6, 223), and are a major cause of protein carbonylation (1, 10, 224, 225), the most permanent and deleterious oxidative protein modification (1, 225).

Several groups have developed in-vitro models of steatosis (29, 30, 226, 227); and a survey of recent findings reveals that individual fatty acids have dissimilar effects on steatosis that are time and concentration dependent. Moderate to high concentrations of palmitic acid has been found to be toxic to HepG2 cells and shown to activate pro-apoptotic pathways (29, 226), and are linked to increased hydrogen peroxide production (29). On the other hand, Damelin et al. have recently shown that low to moderate doses of oleic acid actually bolsters cellular resistance to subsequent pro-oxidant challenge (30). Low doses of linoleic acid have been found to produce greater cell death and more lipid peroxidation than palmitic or oleic acid (227). These results suggest that cells treated with different dietary fatty acids undergo different levels of basal oxidative stress, and therefore, different susceptibility to subsequent pro-oxidant challenge. Furthermore, because these fatty acids have different effects and susceptibility to lipid peroxidation it is expected that they produce different amounts and patterns of protein carbonylation. It would be expected that linoleic acid treated cells would likely have the highest degree of carbonylation. Based on the cytoprotective effect of low levels of oleic acid (30), it may be expected to have the lowest level of carbonylated protein. However, the protein modifications at high doses of palmitate cannot be easily predicted because even though saturated fatty acids are not susceptible to lipid peroxidation on the scale of unsaturated fatty acids (137), palmitate does induce H_2O_2 production (29). Because of the permanent and deleterious nature of protein carbonylation, linking it to fatty acid loading may provide mechanistic information on how steatotic cells are vulnerable to oxidative stress induced damage.

In this study, we exposed HepG2 cells to different concentrations of three dietary fatty acids – oleic, linoleic, and palmitic acid – and investigated its effect on the cellular response to challenge with a pro-oxidant molecule. We also isolated carbonylated proteins to determine whether the extent of carbonylation correlates with the effect of the different fatty acids on HpeG2 cells.

5.3. MATERIALS AND METHODS

5.3.1. Reagents and Supplies

All cell culture media and reagents were purchased from Thermo Fisher Scientific (Waltham, MA). Mammalian protease inhibitor cocktail was purchased from Sigma (St. Louis, MO). Disposable 5 ml spin columns, monomeric avidin agarose beads, and Tween20 were purchased from Thermo Fisher Scientific. Palmitic, linoleic and oleic acid were purchased from MP Bio (Solon, OH). Cytotox-One LDH cytotoxicity assay was purchased from Promega (Madison, WI).

5.3.2. Cell Culture

HepG2 cells were cultured in MEM-EBSS without phenol red, supplemented with 10% fetal calf serum, 100 units of penicillin per milliliter, 100 mg/ml of streptomycin, and 2 mM glutamine in a humidified atmosphere in 5% CO_2 at 37°. All the experiments were carried out while the cells were in exponential growth phase. The cells were passed from the culture flasks at 70-80% confluence with 0.25% trypsin in PBS with 0.02% EDTA, and resuspended in media containing 10% FBS.

5.3.3. Preparation of Fatty Acid Stock Solution

Linoleic and oleic acid stock solution (75 mM) were each prepared by dissolving 0.375 mmol fatty acid in 4.5 ml of 4 g/l bovine serum albumin (Thermo Fisher) in dd H_2O, pH 8.5. The fatty acid mixture was heated to 37°C, vortexed vigorously, and then titrated with 2M NaOH, with vortexing between additions until the fatty acid dissolved to form a clear solution. Water was added to the clear fatty acid solution for a final volume of 5.0 ml and then passed through a 0.22 μm syringe filter for sterilization and stored at -80°C. Palmitic acid stock solution (2.0 mM) was prepared by dissolving pure, molten palmitic acid in 100 ml of complete media pH 8.5, with stirring on a hot plate at 37°C. The palmitic acid containing media was readjusted to pH 7.3, and then passed through a 0.22 μm syringe filter for sterilization and was stored at 4°C.

5.3.4. Fatty Acid Pre-Loading and Pro-Oxidant Challenge with *tert*-Butyl Hydroperoxide

HepG2 cells were seeded in a 24-well plate (1×10^5 cells/well). Upon reaching 60 – 70 % confluency, fatty acid (oleic, palmitic, or linoleic) were diluted into fresh growth media at concentrations ranging from 0.1 – 1.0 mM and used to pre-treat cells for 48 hours. Following fatty acid exposure, fresh growth media containing 0.50 mM *tert*-butyl Hydroperoxide (*t*-BHP) was added to the cells, followed by incubation for 8 hours. Culture supernatants were collected before and after *t*-BHP addition and stored at -80°C.

5.3.5. LDH Cytotoxicity Assay

Culture supernatants collected after fatty acid exposure and *t*-BHP challenge were assayed in triplicate for release of the intracellular enzyme LDH using the Cytotox-One LDH cytotoxicity assay (Promega). The supernatants were assayed using the 100 µl micro plate format with a 15 minute exposure period, according to manufacturer's instructions.

5.3.6. Carbonylated Protein Isolation

After fatty acid and *t*-BHP exposure, approximately 3.0×10^7 cells (cells from two 10 cm dishes) were harvested using trypsin, resuspended in 800 µl PBS and stored at -80 °C until further use. Carbonylated proteins were isolated from the frozen cell suspension as previously described (142, 228) with minor modifications. Specifically, affinity columns were sequentially loaded and used in batch-mode instead of high performance liquid chromatography, protease inhibitor cocktail was added to a final concentration of 0.3% v/v, biotin hydrazide (Thermo Fisher) was used at a concentration of 8 mM, and SDS was added at a concentration of 0.5% wt/v. Each cell solution was sonicated using a Model 60 sonic dismembrator (Fisher Scientific) at a power setting of 4 watts for 15 seconds on ice. The mixture was incubated for 30 min and then sodium cyanoborohydride was added to a concentration of 10 mM to reduce hydrazone bonds (146). The samples were dialyzed to remove excess reagents using 3 ml Slide-A-Lyzer Cassettes (7.5 k MWCO, Thermo Fisher). The samples were dialyzed for 24 hours at 4 °C in 300 ml dialysis buffer (PBS with 4 mg/ml BSA, pH 7.3), with the

dialysis buffer changed every 8 hours. The protein content of the dialyzed sample was assayed using the 660 nm Protein Assay dye (Thermo Fisher) according to the manufacturer's instructions.

Affinity purification of biotinylated carbonylated proteins was performed in disposable 5ml chromatography spin columns. Each column was filled with 1.2 ml of 50% wt. supported monomeric avidin slurry to obtain approximately 0.6 ml of settled monomeric avidin beads in the column. The avidin beads were prepared and equilibrated according to the manufacturer's instructions. Briefly, 1 ml of eluting and blocking buffer (2 mM D-Biotin in 25 mM ammonium bicarbonate (ABC) pH 7.6) was added to each column and centrifuged in order to bind non-reversible sites. Biotin was removed by adding 1 ml of stripping buffer (100 mM glycine pH 2.8) to the column, followed by centrifugation. Each of the samples were added to a column and incubated on rocker for 30 minutes to capture biotinylated carbonylated proteins. The samples were centrifuged and the supernatants were discarded. The avidin beads were washed and centrifuged 4 times with 4 ml PBS with 0.05% v/v Tween to remove non-specifically bound protein and then washed and centrifuged with 25 mM ABC to remove salt and detergent. Biotinylated carbonylated proteins were eluted by adding 300 µl eluting and blocking buffer to the column and eluting four times for each sample. The elute samples were lyophilized and stored at -80°C.

5.3.7. SDS-PAGE

Lyophilized carbonylated protein samples were rehydrated using SDS-PAGE buffer with 0.8% v/v BME and 0.05% v/v bromophenol blue and were resolved on a pre-cast 4-20% gel at 100 V until the dye front reached 2-3 mm from the bottom of the gel. The gel was carefully removed from the cassette, rinsed with DI water and then fixed by incubating in a solution containing 20% v/v methanol and 7% v/v acetic acid for 20 minutes. After incubating with DI H2O for 20 minutes, the gel was stained with GelCode Blue Stain Reagent (Thermo Fisher) overnight and then destained in DI water, according to manufacturing instructions. Gels were imaged with a Versa Doc 3000 imaging system (Bio-Rad, Hercules, CA).

5.4. RESULTS

5.4.1. The Effects of Fatty Acid Loading on HepG2 Cells

The effects of fatty acid loading on hepatocytes have been reported to be concentration and dose dependent. Palmitic acid has been shown to increase H_2O_2 production (29) and induce pro-apoptotic pathways (29, 226), linoleic acid has increased lipid peroxidation products (227, 229), and low doses of oleic acid bolstered cellular defenses against pro-oxidant challenge (30). We decided to focus on the three most common dietary fatty acids - oleic, linoleic, and palmitic acid – and investigated their effect on hepatocyte cytotoxicity based on LDH levels in culture supernatants. The effect of different concentrations of the three fatty acids on HepG2 cells is shown in Figure 5.1. Cells exposed to only oleic acid demonstrated a 14 - 20 percent statistically significant

decrease in cytotoxicity at concentrations of 0.15 and 0.2 mM compared to untreated cells. This trend was reversed at concentrations above 0.2 mM as exposure to 0.3 mM oleic acid showed no difference over control, and concentrations greater than 0.3 mM eliciting 16 (0.4 mM) and 40% (0.5 mM) increase in cytotoxicity compared to untreated controls. (Fig. 5.1*A*). On the other hand, cells exposed to linoleic acid did not demonstrate any statistically significant change over control at 0.15, 0.2, and 0.3 mM. At 0.4 and 0.5 mM, the cytotoxicity was 19 and 33 percent higher than untreated controls (Fig. 5.1*B*).

Palmitic acid increased LDH values at all concentrations (Fig. 5.1*C*), with concentrations of 0.15 mM resulting in a 12 percent increase in toxicity than the control. Loadings of 0.2 and 0.3 mM produced LDH values 100 and 300 percent fold higher untreated control. Palmitic acid loadings of 0.4 and 0.5 mM resulted in significant cell death as with more than 600 percent increase in cytotoxicity.

5.4.2. Effect of Fatty Acid Pre-Loading on Subsequent Pro-Oxidant Challenge

The accumulation of fat in the liver is correlated to the onset of potential disorders alcoholic and non-alcoholic fatty liver disease (20); therefore, we investigated if pre-loading with dietary fatty acids would affect the subsequent response of HepG2 cells to the pro-oxidant molecule *t*-BHP. HepG2 cells were pre-loaded with different concentrations of oleic, linoleic, and palmitic acid for 48 hours, and exposed to 0.5 mM *t*-BHP for 8 hours.

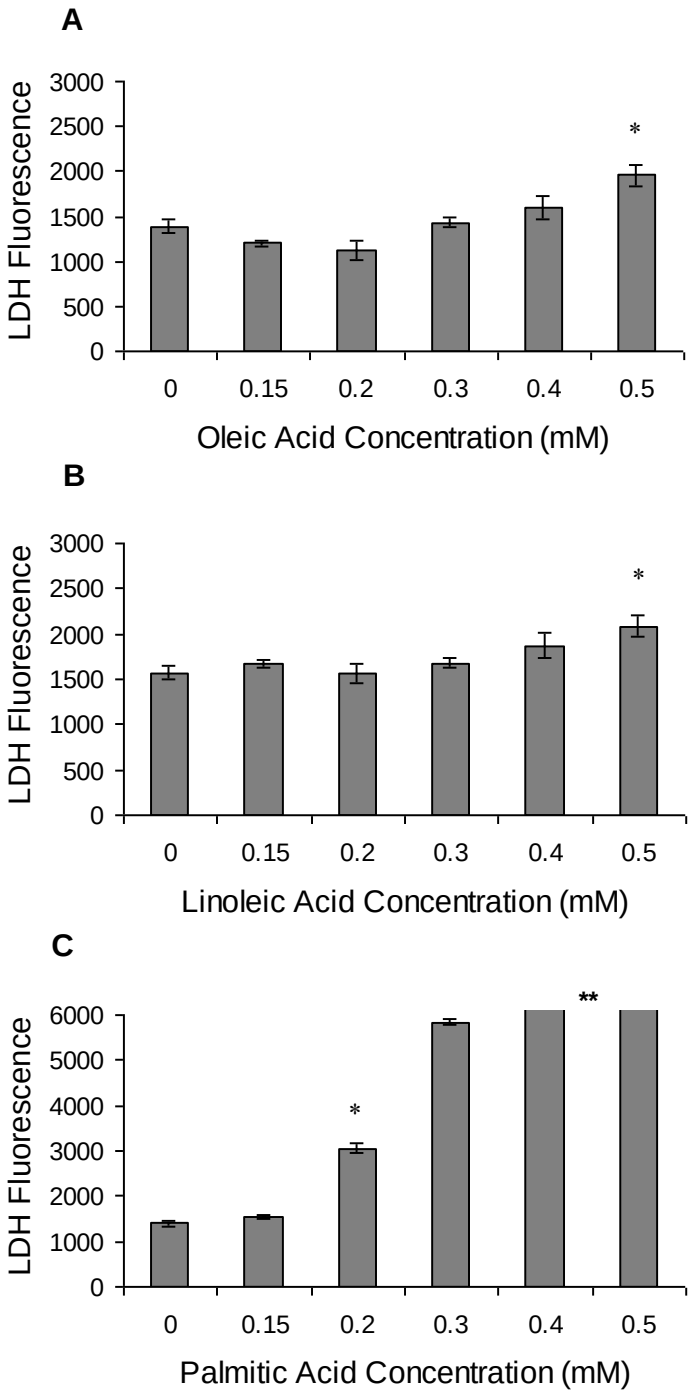

Figure 5.1. LDH fluorescence of culture supernatant of HepG2 cells incubated with varying (A) oleic, (B) linoleic, or (C) palmitic acid concentrations for 48 hours. Note ** Palmitic acid concentrations of 0.4 mM and 0.5 mM result in LDH fluorescence values of 10100 and 12600, respectively.

Figure 5.2 shows that oleic acid pre-treatment affected the response of HepG2 cells to *t*-BHP in a dose-dependent manner. Cells exposed to 0.15 mM and 0.2 mM oleic acid, followed by *t*-BHP demonstrated 10 and 20 percent lower cytotoxicity, respectively, than HepG2 cells treated with *t*-BHP alone (Fig. 5.2*A*). However, HepG2 cells pretreated with 0.3 and 0.4 mM oleic acid demonstrated a 40 and 80 percent increase in cytotoxicity, while cells treated with 0.5 mM oleic demonstrated a 500 percent increase in cytotoxicity. Linoleic acid treated cells also demonstrated a similar response, with cells pretreated with 0.15 mM and 0.2 mM fatty acid having no statistically significant change over cells treated with *t*-BHP alone (Fig. 5.2*B*). Cells treated with 0.3, 0.4 and 0.5 mM linoleic acid had 30, 60, and 100 percent, respectively, more cytotoxicity than cells treated only with *t*-BHP. Cells pretreated with 0.15 mM palmitic acid resulted in 80 percent more LDH activity than *t*-BHP treatment only (Fig. 5.2*C*). Since pre-treatment with concentrations above 0.15 mM palmitic acid led to significant cell death, subsequent *t*-BHP exposure could not be carried out.

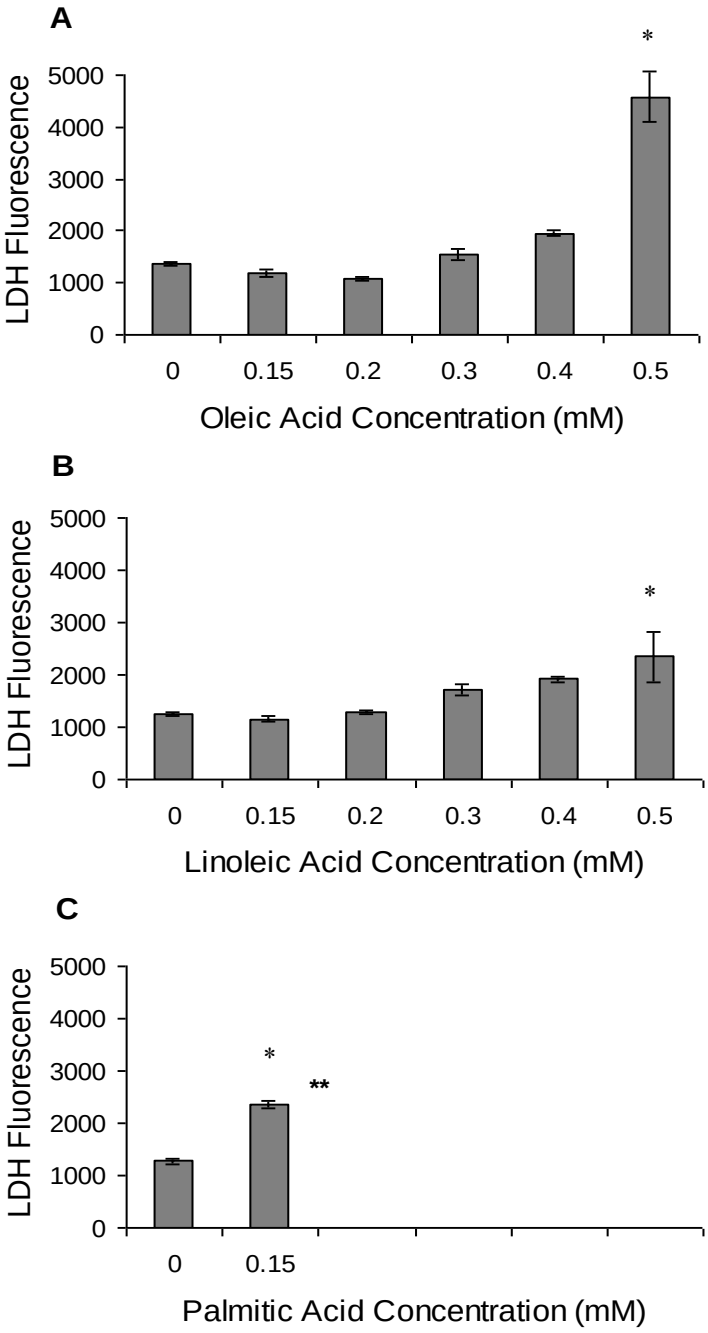

Figure 5.2. LDH fluorescence of culture supernatant of HepG2 cells incubated with 0.5 mM *t*-BHP for 8 hours, after 48 hours incubation with varying (A) oleic, (B) linoleic, or (C) palmitic acid concentrations. Note** Palmitic acid concentrations 0.2 mM and above result in massive cell death, so LDH values cannot be accurately be reported.

5.4.3. Resolution of Carbonylated Proteins in HepG2 Cells Treated with Fatty Acids and *t*-BHP

Biotinylated carbonylated proteins isolated as described in the Materials and Methods were resolved on a gel and stained with Coomassie Blue (Figure 5.3). Carbonylated proteins from cells treated with only 0.2 mM oleic acid and 0.2 mM palmitic acid appear to have the most protein in them due to the overall intensity of bands in lanes C and D. In these samples, a protein just below 100 kDa also appears to be over-expressed (short arrows) as compared to the other samples. Similarly, treatment with *t*-BHP appears to correlate with disappearance of a band between 75 and 50 kDa (see long arrows on lanes B, D, F, and H), as this protein band is present in all samples not treated with *t*-BHP (lanes A, C, E, G) and disappears on samples that were exposed to *t*-BHP (lanes B, D, F, H).

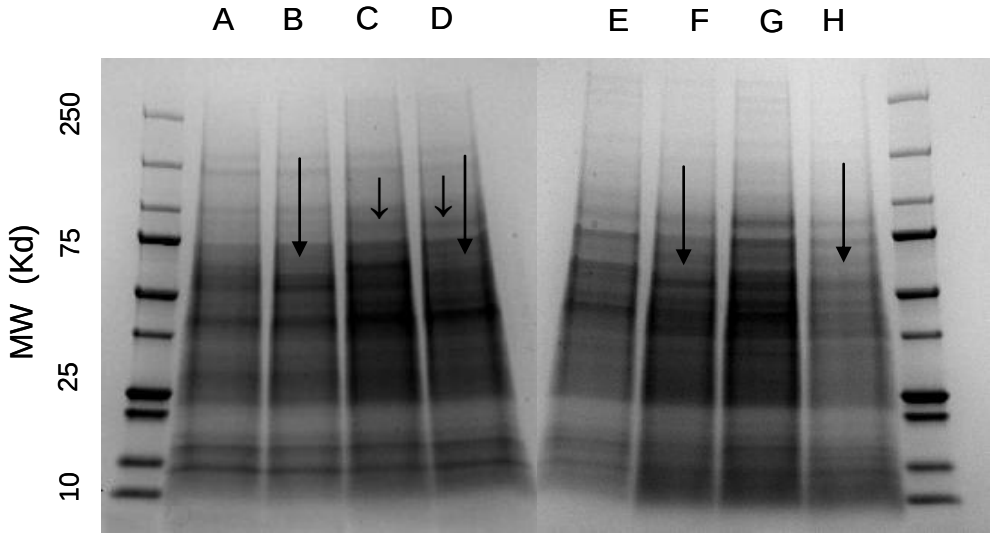

Figure 5.3. Carbonylated proteins isolated from oleic acid (left side) and palmitic acid (right side) treated HepG2 cells, according to procedure described in the materials and methods. A) Control, no fatty acid or *t*-BHP treatment, B) Cells treated with 0.50 mM *t*-BHP for 8 hours, C) Cells treated with 0.2 mM oleic acid for 48 hours, D) Cells treated with 0.2 mM oleic acid for 48 hours, followed by 8 hour exposure to 0.50 mM *t*-BHP. E) Control, no fatty acid or *t*-BHP treatment, F) Cells treated with 0.50 mM *t*-BHP for 8 hours G) Cells treated with 0.2 mM palmitic acid for 48 hours, H) Cells treated with 0.2 mM palmitic acid for 48 hours, followed by 8 hour exposure to 0.50 mM *t*-BHP.

5.5. DISCUSSION

We sought to investigate the effect of fatty acid exposure on the ability of HepG2 cells to withstand subsequent insult or inflammation. Our data show that all fatty acids tested are toxic and cause cell death at concentrations greater than 0.3 mM. However, HepG2 cells treated 0.2 mM oleic acid alone demonstrated decreased cytotoxicity, as seen from the decrease in LDH activity in the supernatant. This result is especially interesting as accumulation of fatty acids and lipids are thought to increase cell death through an increase in oxidative stress brought about by the increase in breakdown of these fatty acids. However, it is possible that exposure to low concentrations of oleic acid leads only to a basal level of reactive oxygen species and oxidative stress that HepG2 cells are capable of withstanding. In addition, it is also possible that the level of oxidative stress induced by fatty acids with a higher degree of saturation such as palmitic acid is high enough to cause cell death. Thus, there appears to be a narrow optimal range where exposure to fatty acids reduces cell death.

We also investigated if pre-exposure to fatty acids impacted the subsequent effect of exposure to a pro-oxidant molecule. This is a realistic model of what has been described as the "Two-Hit" hypothesis; where a second insult such as oxidative stress is required in addition to fat accumulation to damage hepatocytes in liver disease (21, 52). Interestingly, only pre-exposure to oleic acid protected cells from subsequent exposure to *t*-BHP. These results are consistent with those observed by Damelin et al. (30), who reported that exposure to 0.15 mM oleic acid for 48 hours followed by a 0.5 mM *t*-BHP

challenge for 18 hours produced nearly a two-fold reduction in LDH based toxicity, compared to non-fat loaded cells.

It is intriguing to speculate that exposure to low concentrations of oleic acid activates the cellular anti-oxidant machinery that confers resistance to subsequent pro-oxidant challenge. At higher concentrations, the induced oxidative stress could be too large for the cell's anti-oxidant machinery to handle; thereby, leading to cell death. In other words, we propose that exposure to moderate concentrations of fatty acid "primes" the cellular defense machinery to resist subsequent insults. While we have demonstrated this effect only with oleic acid, it is possible that other dietary fatty acids, either individually or in combination, can also induce a similar phenomenon.

One of the characteristics of oxidative stress is the modification of cellular proteins (1, 139, 144). Of these modifications, protein carbonylation is an important modification as it is considered irreversible (1, 139), and requires degradation and re-synthesis of affected proteins (1, 225). Carbonylated proteins are also capable of cross-linking and forming aggregates that can inhibit proteasomes (113). Lipid peroxidation products, especially MDA and 4-HNE (10, 223, 225) are also associated with increased protein carbonylation. Therefore, it was of interest to determine the extent of protein carbonylation under conditions presented here. Investigating the extent of carbonylation with 0.15 mM oleic acid loading was of highest interest, as HepG2 cells loaded with this concentration of oleic acid were more resistant to subsequent oxidative challenge, as was reported earlier (30). While it might be expected that such pretreatment would then lead

to lower levels of protein carbonylation, the same study (30) revealed lower levels of free glutathione in oleic acid treated cells, suggest the cellular response to oleic acid may be related to an oxidative stress marker such as protein modification. Protein modifications such methione oxidation (139) or binding of 4-HNE (10, 225) have been proposed to be involved in cell signaling. Thus, the observed cytoprotective effect may be cellular adaptation to increased oxidative stress, and we sought to determine if protein carbonylation played a role in this process. In addition, since double bonds of unsaturated fatty acids are subject to oxidation more than saturated fatty acids (229), we also expected to find more carbonylation in linoleic acid-loaded cells than in cells exposed to oleic acid. It was also of interest to determine the relative levels of protein carbonylation in palmitic acid loaded cells relative to oleic and linoleic acid-loaded cells as palmitic acid was shown to have the highest cytotoxicity and results in greater production of ROS, such as hydrogen peroxide (29). But in an in vivo study, saturated fatty acids also ameliorated alcohol based damage (230), indicating that the cellular response to palmitic acid may be more complex. But, inspection of the carbonylated protein gel (Figure 5.3) shows a similar degree of carbonylation between the different fatty acid pre-treatments, including the control samples. While it is expected that the untreated controls contain some carbonylated protein, as even newborn rat tissue was found to have almost 50 percent of the total protein carbonylation of 24 month old rats (231). However, this does not rule out technical difficulties in the biotin/avidin affinity chromatography used for isolating carbonylated proteins. To test the degree of separation between biotinylated carbonylated and non-carbonylated proteins, we repeated the affinity purification scheme described in Materials and Methods, except that

the biotin hydrazide was omitted. Without the biotin tagging, eluates are expected to have minimal proteins; however, we observed that samples even without biotin hydrazide contained proteins comparable to those obtained with biotin tagging. This surprising result suggested that non-specifically bound proteins are a problem that overwhelms the detection of carbonylated proteins. Therefore, it could not be conclusively determined if the differentially expressed protein bands are a result of changes in protein carbonylation or a change in protein expression. The problem of non-specific binding is known to be a problem in any protein detection technique such as Western blotting or ELISA. But, it is especially a problem in affinity chromatography that is not only compounded by the high surface area of the agarose bead packing material, but also the fact that these surfaces are covered with biological ligands (232, 233). There are several strategies that are recommended to improve the experimental protocol and reduce non-specific binding. The first is the use of a blocking agent to pre-block the surface of the agarose beads. Bovine serum albumin or powdered milk are traditional choices, but using BSA as a blocker would interfere with the use of biotinylated BSA as a positive control for testing avidin/biotin binding and release. Powdered milk is poor choice as well because it may contain traces of free biotin, and the casein in dry milk is actually a set of several proteins and further contributes to sample complexity. Therefore, we suggest use of the egg white protein, ovalbumin. Ovalbumin is a 45 kDa monomer in size, compared to 67 kDa for BSA, and therefore the appearance of an ovalbumin band on a gel will be readily identified and not interfere with a biotinylated BSA band. The second strategy is to dilute the load sample protein concentration and add detergent to the sample buffer and to the wash buffer. This

should reduce protein-protein, and protein-surface interaction and minimize nonspecific binding. Of course the buffer conditions have to be tested so that they do not interfere with the target binding of the biotin to avidin. Thirdly, strepavidin-linked agarose beads may be used over the monomeric avidin-linked beads currently described in the protocol. Monomeric avidin beads were used because they possess far milder eluting conditions (2 mM free biotin via competitive binding or 150 mM Glycine, pH 2.5), are reusable, and because they were referenced in recent papers describing the isolation of carbonylated protein (142, 228). The streptavidin-biotin interaction is among the strongest non-covalent interaction known, and elution is done with guanidine or by boiling with SDS-PAGE buffer, and renders the beads unusable afterwards. Rather than seen as weakness, the stronger binding characteristics of the streptavidin could be exploited in order to allow for harsher sample buffer and washing conditions. In fact, we have inadvertently proven the stripping buffer (150 mM glycine, pH 2.5) used to regenerate the monomeric avidin beads is capable of removing non-specifically bound proteins. But, even this stripping buffer is not able to disrupt the full streptavidin-biotin interaction. In some methodologies SDS could interfere with downstream procedures, but because in our procedure the eluted proteins are intended for resolution by SDS-PAGE, then elution by SDS-PAGE buffer should not be problematic. And, finally pre-clearing the sample by passing it over blank agarose beads is possible, and this is recommended for co-immunoprecipitation techniques. It is expected that these suggested improvements will lead to better purification and recovery of carbonylated proteins.

CHAPTER VI

CONCLUSIONS AND RECOMMENDATIONS

6.1. CONCLUSIONS

In this work, we have successful profiled the mitochondrial proteome of 3T3-L1 pre-adipocytes and 4, 7, 10, 14, and 18 day old adipocytes using the iTRAQ 8-plex peptide amine labeling kit. As part of the protein profiling experiment, we used the MSWIFT liquid phase isoelectric trapping device to increase proteome coverage and reduce sample complexity. Concurrent biochemical assays were conducted to measure lipid loading, ROS production, and ATP levels. We found citric acid cycle proteins such as pyruvate carboxylase, citrate synthase, and citrate transporter, as well as beta-oxidation enzymes; cartinine acyl transferase and long-chain enoyl-CoA hydratase up-regulated from 7 through 18 days post differentiation onset. These data indicate TCA cycle up-regulation for enhanced metabolic and citrate output necessary for lipid synthesis in aging and growing adipocytes. The data also show the simultaneous increase in the fatty acid beta oxidation pathway. Biochemical assays showing peaks in ATP and ROS generation in 3 day old adipocytes indicate a peak in metabolic output during the differentiation. A second peak in ROS generation was observed in 10 day old adipocytes. Concurrently at day 10, ATP generation reduced to near pre-adipocyte

levels, and this may indicate a metabolic shift to a state that results in increased production of mitochondrial ROS. This metabolic mode is characterized by excess of reduced electron carriers (High NADH/NAD^+ and $CoQH_2$/CoQ ratios), high ΔH^+, low ATP levels, and low O_2 consumption). Shift to this mode is supported by increases in expression of ETFA, ETFB, and ETF-ubiquinone oxidoreductase, which together shuttle electrons from fatty acid oxidation to the electron transport chain. This metabolic shift likely results in the observed increase in ROS in 10 day old adipocytes and this may be general mechanism for increased oxidative stress in hypertrophic adipocytes.

We developed a doxycycline inducible CYP2E1 expressing HepG2 cell line using the pTet-On/pRevTRE expression system to allow greater control and sensitivity in the generation CYP2E1 mediated oxidative stress. A thorough clone-screening process resulted in the isolation of the cell line (RD12), which demonstrated stability and tight expression control. After exposure to doxycycline for 12 hours, RD12 cells showed 75 percent of the CYP2E1 activity of the established constitutive CYP2E1 expressing E47 (112) cell line, and after a 24 hour exposure, RD12 cells showed 30 percent greater CYP2E1 activity based the oxidation p-nitrophenol per mg of protein. In the absence of doxycycline RD12 cells showed essentially no activity. RD12 cells showed 30 percent

greater toxicity than E47 cells when exposed to 20 mM acetaminophen for 24 hours, indicating RD12 cells are more sensitive to the effects reactive intermediates generated by CYP2E1. RD12 cells also showed 25 percent less free glutathione than E47 cells after a two hour exposure to acetaminophen. These results indicate the successful development of an inducible CYP2E1 expressing hepatocyte line with increased sensitivity to CYP2E1 mediated oxidative stress.

We investigated the toxicity of dietary fatty acids (oleic, linoleic, and palmitic) on HepG2 hepatocytes in order to determine fatty acid doses that induced metabolic changes, but not excessive cell death. The dose of 0.20 mM linoleic for 48 hours produced very little toxicity, and palmitic acid produced toxicity that increased rapidly with increasing concentration. Oleic acid at 0.20 mM actually produced lower toxicity than untreated cells, indicating an adaptive response. After fatty acid exposure cells were treated with a pro-oxidant to determine which fatty acid increased the susceptibility to protein carbonylation.

Our results and other published studies (29, 30, 226, 227) demonstrate that treating hepatocytes with different fatty acids produces different levels of cytotoxicity. We hypothesized that the cytotoxicity produced by fatty acids would correlate with the level of carbonylation induced after a pro-oxidant challenge. We therefore expected palmitic and linoleic acid treatment to produce greater carbonylation than oleic acid. The result of

the carbonylated protein isolation procedure indicated the palmitic acid may induce more carbonylation than oleic acid. The resolution of carbonylated protein on an SDS-PAGE gel revealed a small number of differentially-expressed protein bands may be present in palmitic acid treated cells, however the protein pattern of all samples were extremely similar. These results indicate greater efficiency in the isolation procedure is required for a confidant determination of carbonylated protein in fatty acid loaded hepatocytes.

6.2. RECOMMENDATIONS

The results of the proteomic and biochemical profiling presented in the current 3T3-L1 adipocyte study present many interesting targets for further research. Overall the data appear to provide an *in vitro* cell culture base example of mitochondrial metabolic operating modes described by Murphy, with the peaks in ROS generation in 3 and 10 day old adipocytes corresponding closely to the metabolic states 3 and 2, respectively (120). By, operating in mode 2 one might expect Day 10 adipocytes to have higher ROS generation than 3 day old adipocytes, but our data show day 3 adipocytes have the highest level of ROS. In this instance, it appears the metabolic burst necessary for protein and lipid synthesis in newly differentiating adipocytes is so great, that even though ATP level is high, ROS generation is very high. Further biochemical measurements such as O_2 consumption, $NADH/NAD^+$, $CoQH_2/CoQ$ ratios may provide greater elucidation of this subject. Perhaps oxygen consumption is so great in day 3 adipocytes, that even though they presumably operate in the "normal" mode (*mode 3* (120)), ROS generation is still relatively high. Considering this makes the second ROS

peak observed in 10 day old adipocytes even more interesting. If oxygen consumption is proportional to ATP levels, then Day 10 adipocytes would be consuming 15-20 times less oxygen than day 3 adipocytes, even though they only produce approximately 20 percent less ROS. This would indicate that on an oxygen basis, day 10 adipocytes produce far more ROS than day 3 adipocytes, which would coincide with metabolic modes outlined by Murphy (120). We have implicated the up-regulation of ETFA, ETFB, and ETF-ubiquinone oxidoreductase in the increased ROS observed in day 10 adipocytes, verification of the activity of these enzymes in this process is warranted.

The current study reflected conditions experienced by 3T3-L1 adipocytes cultured according to standard protocols for 18 days. It would be very interesting to determine if conditions exist that allow cells to re-enter the mode 2 and produce the high ROS demonstrated in 10 day old adipocytes. In other words, is metabolic cycling possible that allows adipocytes to continually re-enter high ROS producing states. And for further relevance, it would be necessary to verify potential adipocyte metabolic modes in an animal study.

In addition, to increase sensitivity to CYP2E1 generated ROS, we were motivated to develop the RD12 inducible cell line in order to gain control of CYP2E1 expression. Such control allows cells to be pretreated with agents such as fatty acids, antioxidants or those who may form toxic intermediates prior to CYP2E1 induction. This control also

allows pre-labeling of cells with radioactive isotopes or SILAC reagents, so that profiling or degradation experiments can be conducted upon the induction of CYP2E1.

We wanted to determine which of the dietary fatty acids (oleic, linoleic, palmitic) induced greater amounts of protein carbonylation upon challenge with pro-oxidant *t*-BHP. The affinity chromatography experiment designed to isolate carbonylated protein was overwhelmed by a large amount of non-specifically bound protein. Several methods to reduce the problem of non-specifically bound protein include: pre-blocking with a protein such as ovalbumin, diluting the protein concentration and including detergent in the load sample, and increasing salt and detergent concentration in wash buffer.

REFERENCES

1. Dalle-Donne, I., Aldini, G., Carini, M., Colombo, R., Rossi, R., and Milzani, A. (2006) Protein carbonylation, cellular dysfunction, and disease progression. *J. Cell. Mol. Med.* **10**, 389-406
2. Galasko, D. (2005) Biomarkers for Alzheimer's disease--clinical needs and application. *J. Alzheimers Dis.* **8**, 339-346
3. Curtiss, L. K. (2009) Reversing atherosclerosis? *N. Engl. J. Med.* **360**, 1144-1146
4. Green, K., Brand, M. D., and Murphy, M. P. (2004) Prevention of mitochondrial oxidative damage as a therapeutic strategy in diabetes. *Diabetes* **53 Suppl 1**, S110-118
5. Farrell, G. C., and Larter, C. Z. (2006) Nonalcoholic fatty liver disease: from steatosis to cirrhosis. *Hepatology* **43**, S99-S112
6. Ramaiah, S., Rivera, C., and Arteel, G. (2004) Early-phase alcoholic liver disease: an update on animal models, pathology, and pathogenesis. *Int. J. Toxicol.* **23**, 217-231
7. Muller, F. L., Lustgarten, M. S., Jang, Y., Richardson, A., and Van Remmen, H. (2007) Trends in oxidative aging theories. *Free Radic. Biol. Med.* **43**, 477-503
8. Reiter, R. J., Tan, D. X., Osuna, C., and Gitto, E. (2000) Actions of melatonin in the reduction of oxidative stress. A review. *J. Biomed. Sci.* **7**, 444-458
9. Reed, T. T., Pierce, W. M., Markesbery, W. R., and Butterfield, D. A. (2009) Proteomic identification of HNE-bound proteins in early Alzheimer disease:

Insights into the role of lipid peroxidation in the progression of AD. *Brain Res.* **1274**, 66-76

10. Grimsrud, P. A., Picklo, M. J., Sr., Griffin, T. J., and Bernlohr, D. A. (2007) Carbonylation of adipose proteins in obesity and insulin resistance: identification of adipocyte fatty acid-binding protein as a cellular target of 4-hydroxynonenal. *Mol. Cell. Proteomics* **6**, 624-637
11. Moon, K. H., Hood, B. L., Kim, B. J., Hardwick, J. P., Conrads, T. P., Veenstra, T. D., and Song, B. J. (2006) Inactivation of oxidized and S-nitrosylated mitochondrial proteins in alcoholic fatty liver of rats. *Hepatology* **44**, 1218-1230
12. Furukawa, S., Fujita, T., Shimabukuro, M., Iwaki, M., Yamada, Y., Nakajima, Y., Nakayama, O., Makishima, M., Matsuda, M., and Shimomura, I. (2004) Increased oxidative stress in obesity and its impact on metabolic syndrome. *J. Clin. Invest.* **114**, 1752-1761
13. Newton, B. W., Russell, W. K., Russell, D. H., Ramaiah, S. K., and Jayaraman, A. (2009) Liver proteome analysis in a rodent model of alcoholic steatosis. *J Proteome Res* **8**, 1663-1671
14. Meany, D. L., Xie, H., Thompson, L. V., Arriaga, E. A., and Griffin, T. J. (2007) Identification of carbonylated proteins from enriched rat skeletal muscle mitochondria using affinity chromatography-stable isotope labeling and tandem mass spectrometry. *Proteomics* **7**, 1150-1163
15. Molina, H., Yang, Y., Ruch, T., Kim, J. W., Mortensen, P., Otto, T., Nalli, A., Tang, Q. Q., Lane, M. D., Chaerkady, R., and Pandey, A. (2009) Temporal

profiling of the adipocyte proteome during differentiation using a five-plex SILAC based strategy. *J. Proteome Res.* **8**, 48-58

16. Maher, J. J. (2002) Alcoholic steatosis and steatohepatitis. *Semin. Gastrointest. Dis.* **13**, 31-39

17. Blonde, L. (2007) State of diabetes care in the United States. *Am. J. Manag. Care* **13 Suppl 2**, S36-40

18. Inzucchi, S. E., and Sherwin, R. S. (2005) The prevention of type 2 diabetes mellitus. *Endocrinol. Metab. Clin. North. Am.* **34**, 199-219

19. Lin, Y., Berg, A. H., Iyengar, P., Lam, T. K., Giacca, A., Combs, T. P., Rajala, M. W., Du, X., Rollman, B., Li, W., Hawkins, M., Barzilai, N., Rhodes, C. J., Fantus, I. G., Brownlee, M., and Scherer, P. E. (2005) The hyperglycemia-induced inflammatory response in adipocytes: the role of reactive oxygen species. *J. Biol. Chem.* **280**, 4617-4626

20. Day, C. P. (2006) Genes or environment to determine alcoholic liver disease and non-alcoholic fatty liver disease. *Liver Int* **26**, 1021-1028

21. Day, C. P., and James, O. F. (1998) Hepatic steatosis: innocent bystander or guilty party? *Hepatology* **27**, 1463-1466

22. Burt, A. D., Mutton, A., and Day, C. P. (1998) Diagnosis and interpretation of steatosis and steatohepatitis. *Semin. Diagn. Pathol.* **15**, 246-258

23. Rice, D. P. (1999) Economic costs of substance abuse, 1995. *Proc. Assoc. Am. Physicians* **111**, 119-125

24. Schreuder, T. C., Verwer, B. J., van Nieuwkerk, C. M., and Mulder, C. J. (2008) Nonalcoholic fatty liver disease: an overview of current insights in pathogenesis, diagnosis and treatment. *World J. Gastroenterol.* **14**, 2474-2486

25. Caldwell, S., and Argo, C. (2010) The natural history of non-alcoholic fatty liver disease. *Dig. Dis.* **28**, 162-168

26. Cho, S. Y., Park, P. J., Shin, E. S., Lee, J. H., Chang, H. K., and Lee, T. R. (2009) Proteomic analysis of mitochondrial proteins of basal and lipolytically (isoproterenol and TNF-alpha)-stimulated adipocytes. *J. Cell. Biochem.* **106**, 257-266

27. Chen, Q., Galleano, M., and Cederbaum, A. I. (1997) Cytotoxicity and apoptosis produced by arachidonic acid in Hep G2 cells overexpressing human cytochrome P4502E1. *J. Biol. Chem.* **272**, 14532-14541

28. Cederbaum, A. I. (2006) Cytochrome P450 2E1-dependent oxidant stress and upregulation of anti-oxidant defense in liver cells. *J. Gastroenterol. Hepatol.* **21 Suppl 3**, S22-25

29. Srivastava, S., and Chan, C. (2007) Hydrogen peroxide and hydroxyl radicals mediate palmitate-induced cytotoxicity to hepatoma cells: relation to mitochondrial permeability transition. *Free Radic. Res.* **41**, 38-49

30. Damelin, L. H., Coward, S., Kirwan, M., Collins, P., Selden, C., and Hodgson, H. J. (2007) Fat-loaded HepG2 spheroids exhibit enhanced protection from Pro-oxidant and cytokine induced damage. *J. Cell. Biochem.* **101**, 723-734

31. Nelson, D. L., and Cox, M. M. (2004) *Lehninger Principles of Biochemistry*, W. H. Freeman, New York

32. Suckale, J., and Solimena, M. (2008) Pancreas islets in metabolic signaling - focus on the beta-cell. *Frontiers in Bioscience* **13**, 7156-7171

33. Cotran, R. S., Kumar, V., and Collins, T. (1999) *Robbins Pathologic Basis of Disease*, 1425, Saunders, Philadelphia

34. Abu-Lebdeh, H. S., and Nair, K. S. (1996) Protein metabolism in diabetes mellitus. *Baillieres Clin Endocrinol Metab* **10**, 589-601

35. Kieffer, T. J., and Habener, J. F. (1999) The glucagon-like peptides. *Endocr Rev* **20**, 876-913

36. Hyttinen, V., Kaprio, J., Kinnunen, L., Koskenvuo, M., and Tuomilehto, J. (2003) Genetic liability of type 1 diabetes and the onset age among 22,650 young Finnish twin pairs: a nationwide follow-up study. *Diabetes* **52**, 1052-1055

37. Redondo, M. J., Jeffrey, J., Fain, P. R., Eisenbarth, G. S., and Orban, T. (2008) Concordance for islet autoimmunity among monozygotic twins. *N. Engl. J. Med.* **359**, 2849-2850

38. Merten, M. J. (2010) Weight status continuity and change from adolescence to young adulthood: examining disease and health risk conditions. *Obesity (Silver Spring)* **18**, 1423-1428

39. Mozaffarian, D., Kamineni, A., Carnethon, M., Djoussé, L., Mukamal, K. J., and Siscovick, D. (2009) Lifestyle risk factors and new-onset diabetes mellitus in

older adults The cardiovascular health study. *Archives of Internal Medicine* **169**, 798-807

40. Eberhardt, M., Ogden, C., Engelgau, M., Cadwell, B., Hedley, A., and Saydah, S. (2004) Prevalence of overweight and obesity among adults with diagnosed diabetes-United States, 1988-1994 and 1999-2002. *Morbidity and Mortality Weekly Report* **53**, 1066-1068

41. Roberts, C. K., and Sindhu, K. K. (2009) Oxidative stress and metabolic syndrome. *Life Sci.* **84**, 705-712

42. Cho, Y. M., Kim, M., Park, K. S., Kim, S. Y., and Lee, H. K. (2003) S20G mutation of the amylin gene is associated with a lower body mass index in Korean type 2 diabetic patients. *Diabetes Research and Clinical Practice* **60**, 125-129

43. Sakagashira, S., Sanke, T., and Hanabusa, T. (1996) Missense mutation of amylin gene (S20G) in Japanese NIDDM patients. *Diabetes* **45**, 1279-1281

44. Skurk, T., Alberti-Huber, C., Herder, C., and Hauner, H. (2007) Relationship between adipocyte size and adipokine expression and secretion. *J. Clin. Endocrinol. Metab.* **92**, 1023-1033

45. Chen, X. H., Zhao, Y. P., Xue, M., Ji, C. B., Gao, C. L., Zhu, J. G., Qin, D. N., Kou, C. Z., Qin, X. H., Tong, M. L., and Guo, X. R. (2010) TNF-alpha induces mitochondrial dysfunction in 3T3-L1 adipocytes. *Mol. Cell. Endocrinol.* **328**, 63-69

46. Iida, A., Chen, S. T., Friedmann, T., and Yee, J. K. (1996) Inducible gene expression by retrovirus-mediated transfer of a modified tetracycline-regulated system. *J. Virol.* **70**, 6054-6059

47. Skurk, T., van Harmelen, V., Lee, Y. M., Wirth, A., and Hauner, H. (2002) Relationship between IL-6, leptin and adiponectin and variables of fibrinolysis in overweight and obese hypertensive patients. *Horm. Metab. Res.* **34**, 659-663

48. Mohamed-Ali, V., Goodrick, S., Rawesh, A., Katz, D. R., Miles, J. M., Yudkin, J. S., Klein, S., and Coppack, S. W. (1997) Subcutaneous adipose tissue releases interleukin-6, but not tumor necrosis factor-alpha, in vivo. *J. Clin. Endocrinol. Metab.* **82**, 4196-4200

49. Considine, R. V., Sinha, M. K., Heiman, M. L., Kriauciunas, A., T.W., S., Nyce, M. R., Ohannesian, J. P., Marco, C. C., McKee, L. J., and Bauer, T. L. (1996) Serum immunoreactive-leptin concentrations in normal-weight and obese humans. *N Engl J Med* **334**, 292–295

50. Lihn, A. S., Pedersen, S. B., and Richelsen, B. (2005) Adiponectin: action, regulation and association to insulin sensitivity. *Obes. Rev.* **6**, 13-21

51. Kobayashi, H., Matsuda, M., Fukuhara, A., Komuro, R., and Shimomura, I. (2009) Dysregulated glutathione metabolism links to impaired insulin action in adipocytes. *Am. J. Physiol. Endocrinol. Metab.* **296**, E1326-E1334

52. Day, C. P. (2006) Genes or environment to determine alcoholic liver disease and non-alcoholic fatty liver disease. *Liver Int.* **26**, 1021-1028

53. Lieber, C. S. (1993) Biochemical factors in alcoholic liver disease. *Semin. Liver Dis.* **13**, 136-153

54. Lieber, C. S. (1994) Alcohol and the liver: 1994 update. *Gastroenterology* **106**, 1085-1105

55. Zhao, L. F., Jia, J. M., and Han, D. W. (2004) The role of enterogenous endotoxemia in the pathogenesis of non-alcoholic steatohepatitis. *Zhonghua Gan Zang Bing Za Zhi* **12**, 632-638

56. Donohue, T. M., Jr. (2007) Alcohol-induced steatosis in liver cells. *World J. Gastroenterol.* **13**, 4974-4978

57. Desmet, V. J. (1985) Alcoholic liver disease. Histological features and evolution. *Acta Med. Scand. Suppl.* **703**, 111-126

58. MacSween, R. N., and Burt, A. D. (1986) Histologic spectrum of alcoholic liver disease. *Semin. Liver. Dis.* **6**, 221-232

59. Burt, A. D., and MacSween, R. N. (1986) Hepatic vein lesions in alcoholic liver disease: retrospective biopsy and necropsy study. *J. Clin. Pathol.* **39**, 63-67

60. Bykov, I., Jarvelainen, H., and Lindros, K. (2003) L-carnitine alleviates alcohol-induced liver damage in rats: role of tumor necrosis factor-alpha. *Alcohol & Alcoholism* **38**, 400-406

61. Fischer, M., You, M., Matsumoto, M., and Crabb, D. W. (2003) Peroxisome proliferator-activated receptor alpha (PPARalpha) agonist treatment reverses PPARalpha dysfunction and abnormalities in hepatic lipid metabolism in ethanol-fed mice. *J. Biol. Chem.* **278**, 27997-28004

62. Galli, A., Pinaire, J., Fischer, M., Dorris, R., and Crabb, D. W. (2001) The transcriptional and DNA binding activity of peroxisome proliferator-activated receptor alpha is inhibited by ethanol metabolism. A novel mechanism for the development of ethanol-induced fatty liver. *J. Biol. Chem.* **276**, 68-75

63. Teli, M. R., Day, C. P., Burt, A. D., Bennett, M. K., and James, O. F. (1995) Determinants of progression to cirrhosis or fibrosis in pure alcoholic fatty liver. *Lancet* **346**, 987-990

64. Colell, A., Garcia-Ruiz, C., Miranda, M., Ardite, E., Mari, M., Morales, A., Corrales, F., Kaplowitz, N., and Fernandez-Checa, J. C. (1998) Selective glutathione depletion of mitochondria by ethanol sensitizes hepatocytes to tumor necrosis factor. *Gastroenterology* **115**, 1541-1551

65. Yang, S. Q., Lin, H. Z., Lane, M. D., Clemens, M., and Diehl, A. M. (1997) Obesity increases sensitivity to endotoxin liver injury: implications for the pathogenesis of steatohepatitis. *Proc. Natl. Acad. Sci. U. S. A.* **94**, 2557-2562

66. Apte, U. M., McRee, R., and Ramaiah, S. K. (2004) Hepatocyte proliferation is the possible mechanism for the transient decrease in liver injury during steatosis stage of alcoholic liver disease. *Toxicol. Pathol.* **32**, 567-576

67. Bautista, A. P. (2002) Neutrophilic infiltration in alcoholic hepatitis. *Alcohol* **27**, 17-21

68. Jaeschke, H. (2002) Neutrophil-mediated tissue injury in alcoholic hepatitis. *Alcohol* **27**, 23-27

69. French, S. W. (2002) Alcoholic hepatitis: inflammatory cell-mediated hepatocellular injury. *Alcohol* **27**, 43-46

70. Diehl, A. M. (2002) Liver disease in alcohol abusers: clinical perspective. *Alcohol* **27**, 7-11

71. Galambos, J. T. (1972) Natural history of alcoholic hepatitis. 3. Histological changes. *Gastroenterology* **63**, 1026-1035

72. Ludwig, J., Viggiano, T. R., McGill, D. B., and Oh, B. J. (1980) Nonalcoholic steatohepatitis: Mayo Clinic experiences with a hitherto unnamed disease. *Mayo Clin. Proc.* **55**, 434-438

73. Chavez-Tapia, N. C., Mendez-Sanchez, N., and Uribe, M. (2006) The metabolic syndrome as a predictor of nonalcoholic fatty liver disease. *Ann. Intern. Med.* **144**, 379-380

74. Moseley, R. H. (2005) Progress in understanding the pathogenesis of nonalcoholic fatty liver disease. *Hepatology* **41**, 204-206

75. Bugianesi, E., McCullough, A. J., and Marchesini, G. (2005) Insulin resistance: a metabolic pathway to chronic liver disease. *Hepatology* **42**, 987-1000

76. Tilg, H., and Hotamisligil, G. S. (2006) Nonalcoholic fatty liver disease: Cytokine-adipokine interplay and regulation of insulin resistance. *Gastroenterology* **131**, 934-945

77. Nagata, K., Suzuki, H., and Sakaguchi, S. (2007) Common pathogenic mechanism in development progression of liver injury caused by non-alcoholic or alcoholic steatohepatitis. *J. Toxicol. Sci.* **32**, 453-468

78. Begriche, K., Igoudjil, A., Pessayre, D., and Fromenty, B. (2006) Mitochondrial dysfunction in NASH: causes, consequences and possible means to prevent it. *Mitochondrion* **6**, 1-28

79. Wigg, A. J., Roberts-Thomson, I. C., Dymock, R. B., McCarthy, P. J., Grose, R. H., and Cummins, A. G. (2001) The role of small intestinal bacterial overgrowth, intestinal permeability, endotoxaemia, and tumour necrosis factor alpha in the pathogenesis of non-alcoholic steatohepatitis. *Gut* **48**, 206-211

80. Weltman, M. D., Farrell, G. C., Hall, P., Ingelman-Sundberg, M., and Liddle, C. (1998) Hepatic cytochrome P450 2E1 is increased in patients with nonalcoholic steatohepatitis. *Hepatology* **27**, 128-133

81. Nelson, D. R., Zeldin, D. C., Hoffman, S. M., Maltais, L. J., Wain, H. M., and Nebert, D. W. (2004) Comparison of cytochrome P450 (CYP) genes from the mouse and human genomes, including nomenclature recommendations for genes, pseudogenes and alternative-splice variants. *Pharmacogenetics* **14**, 1-18

82. Aguiar, M., Masse, R., and Gibbs, B. F. (2005) Regulation of cytochrome P450 by posttranslational modification. *Drug Metab. Rev.* **37**, 379-404

83. Ioannides, C., and Parke, D. V. (1990) The cytochrome P450 I gene family of microsomal hemoproteins and their role in the metabolic activation of chemicals. *Drug Metab. Rev.* **22**, 1-85

84. Perrot, N., Nalpas, B., Yang, C. S., and Beaune, P. H. (1989) Modulation of cytochrome P450 isozymes in human liver, by ethanol and drug intake. *Eur. J. Clin. Invest.* **19**, 549-555

85. Dicker, E., McHugh, T., and Cederbaum, A. I. (1990) Increased oxidation of p-nitrophenol and aniline by intact hepatocytes isolated from pyrazole-treated rats. *Biochim. Biophys. Acta* **1035**, 249-256

86. Lu, Y., and Cederbaum, A. I. (2008) CYP2E1 and oxidative liver injury by alcohol. *Free Radic. Biol. Med.* **44**, 723-738

87. Dahlin, D. C., Miwa, G. T., Lu, A. Y., and Nelson, S. D. (1984) N-acetyl-p-benzoquinone imine: a cytochrome P-450-mediated oxidation product of acetaminophen. *Proc. Natl. Acad. Sci. U. S. A.* **81**, 1327-1331

88. Manibusan, M. K., Odin, M., and Eastmond, D. A. (2007) Postulated carbon tetrachloride mode of action: a review. *J. Environ. Sci. Health C. Environ. Carcinog. Ecotoxicol. Rev.* **25**, 185-209

89. Stadtman, E. R. (1992) Protein oxidation and aging. *Science* **257**, 1220-1224

90. Fridovich, I. (1995) Superoxide radical and superoxide dismutases. *Annu. Rev. Biochem.* **64**, 97-112

91. Reinke, L. A., and Moyer, M. J. (1985) p-Nitrophenol hydroxylation. A microsomal oxidation which is highly inducible by ethanol. *Drug Metab. Dispos.* **13**, 548-552

92. Liu, L. G., Yan, H., Yao, P., Zhang, W., Zou, L. J., Song, F. F., Li, K., and Sun, X. F. (2005) CYP2E1-dependent hepatotoxicity and oxidative damage after ethanol administration in human primary hepatocytes. *World J. Gastroenterol.* **11**, 4530-4535

93. Cederbaum, A. I., Wu, D., Mari, M., and Bai, J. (2001) CYP2E1-dependent toxicity and oxidative stress in HepG2 cells. *Free Radic. Biol. Med.* **31**, 1539-1543

94. Cederbaum, A. I., Lu, Y., and Wu, D. (2009) Role of oxidative stress in alcohol-induced liver injury. *Arch. Toxicol.* **83**, 519-548

95. Gorsky, L. D., Koop, D. R., and Coon, M. J. (1984) On the stoichiometry of the oxidase and monooxygenase reactions catalyzed by liver microsomal cytochrome P-450. Products of oxygen reduction. *J. Biol. Chem.* **259**, 6812-6817

96. Ekstrom, G., and Ingelman-Sundberg, M. (1989) Rat liver microsomal NADPH-supported oxidase activity and lipid peroxidation dependent on ethanol-inducible cytochrome P-450 (P-450IIE1). *Biochem. Pharmacol.* **38**, 1313-1319

97. Bansal, S., Liu, C. P., Sepuri, N. B., Anandatheerthavarada, H. K., Selvaraj, V., Hoek, J., Milne, G. L., Guengerich, F. P., and Avadhani, N. G. (2010) Mitochondria-targeted cytochrome P450 2E1 induces oxidative damage and augments alcohol-mediated oxidative stress. *J. Biol. Chem.* **285**, 24609-24619

98. Wu, D. F., Clejan, L., Potter, B., and Cederbaum, A. I. (1990) Rapid decrease of cytochrome P-450IIE1 in primary hepatocyte culture and its maintenance by added 4-methylpyrazole. *Hepatology* **12**, 1379-1389

99. Fridovich, I. (2004) Mitochondria: are they the seat of senescence? *Aging Cell* **3**, 13-16

100. Lieber, C. S. (1997) Cytochrome P-4502E1: its physiological and pathological role. *Physiol. Rev.* **77**, 517-544

101. Rashba-Step, J., Turro, N. J., and Cederbaum, A. I. (1993) Increased NADPH- and NADH-dependent production of superoxide and hydroxyl radical by microsomes after chronic ethanol treatment. *Arch. Biochem. Biophys.* **300**, 401-408

102. Raucy, J. L., Lasker, J. M., Kraner, J. C., Salazar, D. E., Lieber, C. S., and Corcoran, G. B. (1991) Induction of cytochrome P450IIE1 in the obese overfed rat. *Mol. Pharmacol.* **39**, 275-280

103. Woodcroft, K. J., Hafner, M. S., and Novak, R. F. (2002) Insulin signaling in the transcriptional and posttranscriptional regulation of CYP2E1 expression. *Hepatology* **35**, 263-273

104. Bellward, G. D., Chang, T., Rodrigues, B., McNeill, J. H., Maines, S., Ryan, D. E., Levin, W., and Thomas, P. E. (1988) Hepatic cytochrome P-450j induction in the spontaneously diabetic BB rat. *Mol. Pharmacol.* **33**, 140-143

105. Honchel, R., Ray, M. B., Marsano, L., Cohen, D., Lee, E., Shedlofsky, S., and McClain, C. J. (1992) Tumor necrosis factor in alcohol enhanced endotoxin liver injury. *Alcohol Clin. Exp. Res.* **16**, 665-669

106. Kamimura, S., and Tsukamoto, H. (1995) Cytokine gene expression by Kupffer cells in experimental alcoholic liver disease. *Hepatology* **22**, 1304-1309

107. Yin, M., Wheeler, M. D., Kono, H., Bradford, B. U., Gallucci, R. M., Luster, M. I., and Thurman, R. G. (1999) Essential role of tumor necrosis factor alpha in alcohol-induced liver injury in mice. *Gastroenterology* **117**, 942-952

108. Wheeler, M. D., Kono, H., Yin, M., Nakagami, M., Uesugi, T., Arteel, G. E., Gabele, E., Rusyn, I., Yamashina, S., Froh, M., Adachi, Y., Iimuro, Y., Bradford, B. U., Smutney, O. M., Connor, H. D., Mason, R. P., Goyert, S. M., Peters, J. M., Gonzalez, F. J., Samulski, R. J., and Thurman, R. G. (2001) The role of Kupffer cell oxidant production in early ethanol-induced liver disease. *Free Radic. Biol. Med.* **31**, 1544-1549

109. Koop, D. R., Klopfenstein, B., Iimuro, Y., and Thurman, R. G. (1997) Gadolinium chloride blocks alcohol-dependent liver toxicity in rats treated chronically with intragastric alcohol despite the induction of CYP2E1. *Mol. Pharmacol.* **51**, 944-950

110. Kono, H., Bradford, B. U., Yin, M., Sulik, K. K., Koop, D. R., Peters, J. M., Gonzalez, F. J., McDonald, T., Dikalova, A., Kadiiska, M. B., Mason, R. P., and Thurman, R. G. (1999) CYP2E1 is not involved in early alcohol-induced liver injury. *Am. J. Physiol.* **277**, G1259-1267

111. Bardag-Gorce, F., Yuan, Q. X., Li, J., French, B. A., Fang, C., Ingelman-Sundberg, M., and French, S. W. (2000) The effect of ethanol-induced cytochrome p4502E1 on the inhibition of proteasome activity by alcohol. *Biochem. Biophys. Res. Commun.* **279**, 23-29

112. Wu, D., and Cederbaum, A. I. (2008) Development and properties of HepG2 cells that constitutively express CYP2E1. *Methods Mol. Biol.* **447**, 137-150

113. Bardag-Gorce, F., French, B. A., Nan, L., Song, H., Nguyen, S. K., Yong, H., Dede, J., and French, S. W. (2006) CYP2E1 induced by ethanol causes oxidative

stress, proteasome inhibition and cytokeratin aggresome (Mallory body-like) formation. *Exp. Mol. Pathol.* **81**, 191-201

114. Bai, J., and Cederbaum, A. I. (2004) Adenovirus mediated overexpression of CYP2E1 increases sensitivity of HepG2 cells to acetaminophen induced cytotoxicity. *Mol. Cell Biochem.* **262**, 165-176

115. Zhang, J., Li, X., Mueller, M., Wang, Y., Zong, C., Deng, N., Vondriska, T. M., Liem, D. A., Yang, J. I., Korge, P., Honda, H., Weiss, J. N., Apweiler, R., and Ping, P. (2008) Systematic characterization of the murine mitochondrial proteome using functionally validated cardiac mitochondria. *Proteomics* **8**, 1564-1575

116. Wiesner, R. J., Ruegg, J. C., and Morano, I. (1992) Counting target molecules by exponential polymerase chain reaction: copy number of mitochondrial DNA in rat tissues. *Biochem. Biophys. Res. Commun.* **183**, 553-559

117. Alberts, B., Bray, D., Lewis, J., Raff, M., Roberts, K., and Watson, J. D. (1994) *Molecular Biology of the Cell*, 1408, Garland Science, New York

118. Zundorf, G., Kahlert, S., Bunik, V. I., and Reiser, G. (2009) alpha-Ketoglutarate dehydrogenase contributes to production of reactive oxygen species in glutamate-stimulated hippocampal neurons in situ. *Neuroscience* **158**, 610-616

119. Koopman, W. J., Nijtmans, L. G., Dieteren, C. E., Roestenberg, P., Valsecchi, F., Smeitink, J. A., and Willems, P. H. (2009) Mammalian mitochondrial complex I: biogenesis, regulation and reactive oxygen species generation. *Antioxid. Redox Signal.* **12**, 1431-1470

120. Murphy, M. P. (2009) How mitochondria produce reactive oxygen species. *Biochem J.* **417**, 1-13

121. Sazanov, L. A. (2007) Respiratory complex I: mechanistic and structural insights provided by the crystal structure of the hydrophilic domain. *Biochemistry* **46**, 2275-2288

122. Crofts, A. R. (2004) The cytochrome bc1 complex: function in the context of structure. *Annu. Rev. Physiol.* **66**, 689-733

123. Kramer, D. M., Roberts, A. G., Muller, F., Cape, J., and Bowman, M. K. (2004) Q-cycle bypass reactions at the Qo site of the cytochrome bc1 (and related) complexes. *Methods Enzymol.* **382**, 21-45

124. Muller, F. L., Liu, Y., and Van Remmen, H. (2004) Complex III releases superoxide to both sides of the inner mitochondrial membrane. *J. Biol. Chem.* **279**, 49064-49073

125. Zhang, H., Osyczka, A., Dutton, P. L., and Moser, C. C. (2007) Exposing the complex III Qo semiquinone radical. *Biochim. Biophys. Acta* **1767**, 883-887

126. Eaton, S. (2002) Control of mitochondrial beta-oxidation flux. *Prog. Lipid. Res.* **41**, 197-239

127. Moore, K. P., Holt, S. G., Patel, R. P., Svistunenko, D. A., Zackert, W., Goodier, D., Reeder, B. J., Clozel, M., Anand, R., Cooper, C. E., Morrow, J. D., Wilson, M. T., Darley-Usmar, V., and Roberts, L. J., 2nd (1998) A causative role for redox cycling of myoglobin and its inhibition by alkalinization in the

pathogenesis and treatment of rhabdomyolysis-induced renal failure. *J. Biol. Chem.* **273**, 31731-31737

128. Soreghan, B. A., Yang, F., Thomas, S. N., Hsu, J., and Yang, A. J. (2003) High-throughput proteomic-based identification of oxidatively induced protein carbonylation in mouse brain. *Pharm.. Res.* **20**, 1713-1720

129. Levine, R. L., Moskovitz, J., and Stadtman, E. R. (2000) Oxidation of methionine in proteins: roles in antioxidant defense and cellular regulation. *IUBMB Life* **50**, 301-307

130. Fridovich, I. (1997) Superoxide anion radical (O2-.), superoxide dismutases, and related matters. *J. Biol. Chem.* **272**, 18515-18517

131. Paul, R., Obermaier, B., Van Ziffle, J., Angele, B., Pfister, H. W., Lowell, C. A., and Koedel, U. (2008) Myeloid Src kinases regulate phagocytosis and oxidative burst in pneumococcal meningitis by activating NADPH oxidase. *J. Leukoc. Biol.* **84**, 1141-1150

132. Galkina, E., and Ley, K. (2009) Immune and inflammatory mechanisms of atherosclerosis. *Annu. Rev. Immunol.* **27**, 165-197

133. Tomas-Zapico, C., Alvarez-Garcia, O., Sierra, V., Vega-Naredo, I., Caballero, B., Joaquin Garcia, J., Acuna-Castroviejo, D., Rodriguez, M. I., Tolivia, D., Rodriguez-Colunga, M. J., and Coto-Montes, A. (2006) Oxidative damage in the livers of senescence-accelerated mice: a gender-related response. *Can. J. Physiol. Pharmacol.* **84**, 213-220

134. Klebanoff, S. J. (1968) Myeloperoxidase-halide-hydrogen peroxide antibacterial system. *J. Bacteriol.* **95**, 2131-2138

135. Beckman, J. S., Beckman, T. W., Chen, J., Marshall, P. A., and Freeman, B. A. (1990) Apparent hydroxyl radical production by peroxynitrite: implications for endothelial injury from nitric oxide and superoxide. *Proc. Natl. Acad. Sci. U.S.A.* **87**, 1620-1624

136. de Souza-Pinto, N. C., Eide, L., Hogue, B. A., Thybo, T., Stevnsner, T., Seeberg, E., Klungland, A., and Bohr, V. A. (2001) Repair of 8-oxodeoxyguanosine lesions in mitochondrial dna depends on the oxoguanine dna glycosylase (OGG1) gene and 8-oxoguanine accumulates in the mitochondrial dna of OGG1-defective mice. *Cancer Res.* **61**, 5378-5381

137. Negre-Salvayre, A., Coatrieux, C., Ingueneau, C., and Salvayre, R. (2008) Advanced lipid peroxidation end products in oxidative damage to proteins. Potential role in diseases and therapeutic prospects for the inhibitors. *Br. J. Pharmacol.* **153**, 6-20

138. Leray, D. C. (2011), *Cyberlipid Center*, www.cyberlipid.org

139. Stadtman, E. R., and Levine, R. L. (2003) Free radical-mediated oxidation of free amino acids and amino acid residues in proteins. *Amino Acids* **25**, 207-218

140. Lee, J. R., Kim, J. K., Lee, S. J., and Kim, K. P. (2009) Role of protein tyrosine nitration in neurodegenerative diseases and atherosclerosis. *Arch. Pharm. Res.* **32**, 1109-1118

141. Jacob, C., Holme, A. L., and Fry, F. H. (2004) The sulfinic acid switch in proteins. *Org. Biomol. Chem.* **2**, 1953-1956

142. Mirzaei, H., and Regnier, F. (2007) Identification of yeast oxidized proteins: chromatographic top-down approach for identification of carbonylated, fragmented and cross-linked proteins in yeast. *J. Chromatogr. A* **1141**, 22-31

143. Chaudhuri, A. R., de Waal, E. M., Pierce, A., Van Remmen, H., Ward, W. F., and Richardson, A. (2006) Detection of protein carbonyls in aging liver tissue: A fluorescence-based proteomic approach. *Mech. Ageing Dev.* **127**, 849-861

144. Stadtman, E. R. (1993) Oxidation of free amino acids and amino acid residues in proteins by radiolysis and by metal-catalyzed reactions. *Annu. Rev. Biochem.* **62**, 797-821

145. Walsh, G., and Jefferis, R. (2006) Post-translational modifications in the context of therapeutic proteins. *Nat. Biotechnol.* **24**, 1241-1252

146. Hermanson, G. T. (2008) *Bioconjugate Techniques*, 200-201, Academic Press, New York

147. Zhang, Q., Ames, J. M., Smith, R. D., Baynes, J. W., and Metz, T. O. (2009) A perspective on the Maillard reaction and the analysis of protein glycation by mass spectrometry: probing the pathogenesis of chronic disease. *J. Proteome Res.* **8**, 754-769

148. Tessier, F. J. (2010) The Maillard reaction in the human body. The main discoveries and factors that affect glycation. *Pathol. Biol. (Paris)* **58**, 214-219

149. Bluher, M. (2009) Adipose tissue dysfunction in obesity. *Exp. Clin. Endocrinol. Diabetes* **117**, 241-250

150. Bjorntorp, P., Karlsson, M., Pertoft, H., Pettersson, P., Sjostrom, L., and Smith, U. (1978) Isolation and characterization of cells from rat adipose tissue developing into adipocytes. *J. Lipid Res.* **19**, 316-324

151. Bjorntorp, P., Karlsson, M., and Pettersson, P. (1982) Expansion of adipose tissue storage capacity at different ages in rats. *Metabolism* **31**, 366-373

152. Hill, J. O., Peters, J. C., Lin, D., Yakubu, F., Greene, H., and Swift, L. (1993) Lipid accumulation and body fat distribution is influenced by type of dietary fat fed to rats. *Int J Obes Relat Metab Disord* **17**, 223-236

153. Johnson, P. R., Stern, J. S., Greenwood, M. R., and Hirsch, J. (1978) Adipose tissue hyperplasia and hyperinsulinemia on Zucker obese female rats: a developmental study. *Metabolism* **27**, 1941-1954

154. Faust, I. M., Johnson, P. R., Stern, J. S., and Hirsch, J. (1978) Diet-induced adipocyte number increase in adult rats: a new model of obesity. *Am. J. Physio.* **235**, E279-286

155. Vasselli, J. R., Fiene, J. A., and Maggio, C. A. (1992) Relationship of adipocyte size to hyperphagia in developing male obese Zucker rats. *Am. J. Physiol.* **262**, R33-38

156. Weyer, C., Foley, J. E., Bogardus, C., Tataranni, P. A., and Pratley, R. E. (2000) Enlarged subcutaneous abdominal adipocyte size, but not obesity itself, predicts type II diabetes independent of insulin resistance. *Diabetologia* **43**, 1498-1506

157. Carriere, A., MC, Fernandez, Y., Rigoulet, M., Wenger, R., Penicaud, L., and Casteilla, L. (2004) Mitochondrial reactive oxygen species control the transcription factor CHOP-10/GADD153 and adipocyte differentiation: a mechanism for hypoxia-dependent effect. *J Biol Chem* **279**, 40462-40469

158. Evans, J., Goldfine, I., Maddux, B., and Grodsky, G. (2003) Are oxidative stress-activated signaling pathways mediators of insulin resistance and beta-cell dysfunction? *Diabetes* **52**, 1-8

159. Schrauwen, P., and Hesselink, M. (2004) Oxidative capacity, lipotoxicity, and mitochondrial damage in type 2 diabetes. *Diabetes* **53**, 1412-1417

160. Paolisso, G., D (1996) Oxidative stress and insulin action. Is there a relationship? *Diabetalogica* **39**, 357-363

161. Yaworsky, K., Somwar, R., and Klip, A. (2000) Interrelationship between oxidative stress and insulin resistance. In *Antioxidants in Diabetes Management* (Packer, L., Rösen, P., Tritschler, H., and King, G., eds), Marcel Dekker, New York

162. Nishikawa, T., Edelstein, D., Du, X. L., Yamagishi, S., Matsumura, T., Kaneda, Y., Yorek, M. A., Beebe, D., Oates, P. J., Hammes, H. P., Giardino, I., and Brownlee, M. (2000) Normalizing mitochondrial superoxide production blocks three pathways of hyperglycaemic damage. *Nature* **404**, 787-790

163. West, I. (2000) Radicals and oxidative stress in diabetes. *Diabet Med* **17**, 171-180

164. Opara, E., Abdel-Rahman, E., Soliman, S., Kamel, W., Souka, S., Lowe, J., and Abdel-Aleem, S. (1999) Depletion of total antioxidant capacity in type 2 diabetes. *Metabolism* **48**, 1414-1417

165. Culotta, V. (2000) Superoxide dismutase, oxidative stress, and cell metabolism. *Curr Top Cell Reg* **36**, 117-132

166. Green, H., and Kehinde, O. (1975) An established preadipose cell line and its differentiation in culture. II. Factors affecting the adipose conversion. *Cell* **5**, 19-27

167. Si, Y., Palani, S., Jayaraman, A., and Lee, K. (2007) Effects of forced uncoupling protein 1 expression in 3T3-L1 cells on mitochondrial function and lipid metabolism. *J. Lipid Res.* **48**, 826-836

168. Senocak, F. S., Si, Y., Moya, C., Russell, W. K., Russell, D. H., Lee, K., and Jayaraman, A. (2007) Effect of uncoupling protein-1 expression on 3T3-L1 adipocyte gene expression. *FEBS Lett.* **581**, 5865-5871

169. Pallotti, F., and Lenaz, G. (2001) Isolation and subfractionation of mitochondria from animal cells and tissue culture lines. *Methods Cell Biol.* **65**, 1-35

170. Lim, P., North, R., and Vigh, G. (2007) Rapid isoelectric trapping in a micropreparative-scale multicompartment electrolyzer. *Electrophoresis* **28**, 1851-1859

171. Cologna, S. M., Russell, W. K., Lim, P. J., Vigh, G., and Russell, D. H. (2010) Combining Isoelectric Point-Based Fractionation, Liquid Chromatography and

Mass Spectrometry to Improve Peptide Detection and Protein Identification. *J. Am. Soc. Mass Spectrom.* **9**, 1612-1619

172. Shave, E., and Vigh, G. (2004) Preparative-scale, recirculating, pH-biased binary isoelectric trapping separations. *Electrophoresis* **25**, 381-387

173. Lalwani, S., Shave, E., Fleisher, H. C., Nzeadibe, K., Busby, M. B., and Vigh, G. (2004) Alkali-stable high-pI isoelectric membranes for isoelectric trapping separations. *Electrophoresis* **25**, 2128-2138

174. Lalwani, S., Shave, E., and Vigh, G. (2004) High-buffering capacity, hydrolytically stable, low-pI isoelectric membranes for isoelectric trapping separations. *Electrophoresis* **25**, 3323-3330

175. Fleisher, H. C., and Vigh, G. (2005) Hydrolytically stable, diaminocarboxylic acid-based membranes buffering in the pH range from 6 to 8.5 for isoelectric trapping separations. *Electrophoresis* **26**, 2511-2519

176. Fleisher-Craver, H. C., and Vigh, G. (2008) PVA-based tunable buffering membranes for isoelectric trapping separations. *Electrophoresis* **29**, 4247-4256

177. Rosas-Acosta, G., Russell, W. K., Deyrieux, A., Russell, D. H., and Wilson, V. G. (2005) A universal strategy for proteomic studies of SUMO and other ubiquitin-like modifiers. *Mol. Cell. Proteomics* **4**, 56-72

178. Kerlavage, A., Bonazzi, V., di Tommaso, M., Lawrence, C., Li, P., Mayberry, F., Mural, R., Nodell, M., Yandell, M., Zhang, J., and Thomas, P. (2002) The Celera Discovery System. *Nucleic Acids Res.* **30**, 129-136

179. Shilov, I. V., Seymour, S. L., Patel, A. A., Loboda, A., Tang, W. H., Keating, S. P., Hunter, C. L., Nuwaysir, L. M., and Schaeffer, D. A. (2007) The Paragon Algorithm, a next generation search engine that uses sequence temperature values and feature probabilities to identify peptides from tandem mass spectra. *Mol. Cell. Proteomics* **6**, 1638-1655

180. Chen, X., Sans, M. D., Strahler, J. R., Karnovsky, A., Ernst, S. A., Michailidis, G., Andrews, P. C., and Williams, J. A. (2010) Quantitative organellar proteomics analysis of rough endoplasmic reticulum from normal and acute pancreatitis rat pancreas. *J Proteome Res* **9**, 885-896

181. Tang, W. H., Shilov, I. V., and Seymour, S. L. (2008) Nonlinear fitting method for determining local false discovery rates from decoy database searches. *J. Proteome Res.* **7**, 3661-3667

182. Rook, G. A., Steele, J., Umar, S., and Dockrell, H. M. (1985) A simple method for the solubilisation of reduced NBT, and its use as a colorimetric assay for activation of human macrophages by gamma-interferon. *J. Immunol. Methods.* **82**, 161-167

183. Suissa, M., Suda, K., and Schatz, G. (1984) Isolation of the nuclear yeast genes for citrate synthase and fifteen other mitochondrial proteins by a new screening method. *Embo. J.* **3**, 1773-1781

184. Kim, J. J., and Miura, R. (2004) Acyl-CoA dehydrogenases and acyl-CoA oxidases. Structural basis for mechanistic similarities and differences. *Eur. J. Biochem.* **271**, 483-493

185. Kalinina, E. V., Chernov, N. N., and Saprin, A. N. (2008) Involvement of thio-, peroxi-, and glutaredoxins in cellular redox-dependent processes. *Biochemistry (Mosc)* **73**, 1493-1510

186. Sabelli, R., Iorio, E., De Martino, A., Podo, F., Ricci, A., Viticchie, G., Rotilio, G., Paci, M., and Melino, S. (2008) Rhodanese-thioredoxin system and allyl sulfur compounds. *Febs J.* **275**, 3884-3899

187. Wispe, J. R., Clark, J. C., Burhans, M. S., Kropp, K. E., Korfhagen, T. R., and Whitsett, J. A. (1989) Synthesis and processing of the precursor for human mangano-superoxide dismutase. *Biochim. Biophys. Acta* **994**, 30-36

188. Das, K., Lewis, R. Y., Combatsiaris, T. P., Lin, Y., Shapiro, L., Charron, M. J., and Scherer, P. E. (1999) Predominant expression of the mitochondrial dicarboxylate carrier in white adipose tissue. *Biochem. J.* **344 Pt 2**, 313-320

189. Yamasaki, M., Hasegawa, S., Yamanaka, H., Narishima, R., and Fukui, T. (2009) Ketone body utilization is regulated by male-specific factors in rat subcutaneous adipocytes. *Exp. Clin. Endocrinol. Diabetes* **117**, 170-174

190. Vinogradov, A. D. (1998) Catalytic properties of the mitochondrial NADH-ubiquinone oxidoreductase (complex I) and the pseudo-reversible active/inactive enzyme transition. *Biochim. Biophys. Acta* **1364**, 169-185

191. Hopper, R. K., Carroll, S., Aponte, A. M., Johnson, D. T., French, S., Shen, R. F., Witzmann, F. A., Harris, R. A., and Balaban, R. S. (2006) Mitochondrial matrix phosphoproteome: effect of extra mitochondrial calcium. *Biochemistry* **45**, 2524-2536

192. Hayashi, T., Rizzuto, R., Hajnoczky, G., and Su, T. P. (2009) MAM: more than just a housekeeper. *Trends Cell. Biol.* **19**, 81-88

193. Csordas, G., and Hajnoczky, G. (2009) SR/ER-mitochondrial local communication: calcium and ROS. *Biochim. Biophys. Acta* **1787**, 1352-1362

194. Fridlyand, L. E., and Philipson, L. H. (2006) Reactive species and early manifestation of insulin resistance in type 2 diabetes. *Diabetes Obes. Metab.* **8**, 136-145

195. Hoehn, K. L., Salmon, A. B., Hohnen-Behrens, C., Turner, N., Hoy, A. J., Maghzal, G. J., Stocker, R., Van Remmen, H., Kraegen, E. W., Cooney, G. J., Richardson, A. R., and James, D. E. (2009) Insulin resistance is a cellular antioxidant defense mechanism. *Proc. Natl. Acad. Sci. U. S. A.* **106**, 17787-17792

196. Alia, M., Ramos, S., Mateos, R., Bravo, L., and Goya, L. (2005) Response of the antioxidant defense system to tert-butyl hydroperoxide and hydrogen peroxide in a human hepatoma cell line (HepG2). *J. Biochem. Mol. Toxicol.* **19**, 119-128

197. Fiala, E. S., Conaway, C. C., and Mathis, J. E. (1989) Oxidative DNA and RNA damage in the livers of Sprague-Dawley rats treated with the hepatocarcinogen 2-nitropropane. *Cancer Res.* **49**, 5518-5522

198. Yang, C. S., Yoo, J. S., Ishizaki, H., and Hong, J. Y. (1990) Cytochrome P450IIE1: roles in nitrosamine metabolism and mechanisms of regulation. *Drug Metab. Rev.* **22**, 147-159

199. Yoo, J. S., Ishizaki, H., and Yang, C. S. (1990) Roles of cytochrome P450IIE1 in the dealkylation and denitrosation of N-nitrosodimethylamine and N-nitrosodiethylamine in rat liver microsomes. *Carcinogenesis* **11**, 2239-2243

200. Zhuge, J., and Cederbaum, A. I. (2006) Serum deprivation-induced HepG2 cell death is potentiated by CYP2E1. *Free Radic. Biol. Med.* **40**, 63-74

201. Kozak, M. (1984) Point mutations close to the AUG initiator codon affect the efficiency of translation of rat preproinsulin in vivo. *Nature* **308**, 241-246

202. Hudson, T. J. (2001) Construction of small-insert libraries from genomic DNA. *Curr. Protoc. Hum. Genet.* **2.1**, 1-6

203. Takeuchi, A., Matsumura, H., and Kano, Y. (2002) Cloning and expression in Escherichia coli of a gene, hup, encoding the histone-like protein HU of Bifidobacterium longum. *Biosci. Biotechnol. Biochem.* **66**, 598-603

204. Somia, N. (2004) Gene delivery to cells in culture using retroviruses. *Methods Mol. Biol.* **246**, 491-498

205. Wieder, K. J., King, K. R., Thompson, D. M., Zia, C., Yarmush, M. L., and Jayaraman, A. (2005) Optimization of reporter cells for expression profiling in a microfluidic device. *Biomed. Microdevices* **7**, 213-222

206. Huang, Z., Moya, C., Jayaraman, A., and Hahn, J. (2010) Using the Tet-On system to develop a procedure for extracting transcription factor activation dynamics. *Mol. Biosyst.* **6**, 1883-1889

207. Koop, D. R., and Laethem, C. L. (1992) Inhibition of rabbit microsomal cytochrome P-450 2E1-dependent p-nitrophenol hydroxylation by substituted benzene derivatives. *Drug Metab. Dispos.* **20**, 775-777

208. Welsch, F., and De Balbian Verster, F. (1971) A method for the rapid determination of arylsulfatase in nervous tissue. *Brain Res.* **26**, 375-383

209. Paulus, W., Baur, I., Boyce, F. M., Breakefield, X. O., and Reeves, S. A. (1996) Self-contained, tetracycline-regulated retroviral vector system for gene delivery to mammalian cells. *J. Virol.* **70**, 62-67

210. Khlistunova, I., Biernat, J., Wang, Y., Pickhardt, M., von Bergen, M., Gazova, Z., Mandelkow, E., and Mandelkow, E. M. (2006) Inducible expression of Tau repeat domain in cell models of tauopathy: aggregation is toxic to cells but can be reversed by inhibitor drugs. *J. Biol. Chem.* **281**, 1205-1214

211. Tang, H., Liu, L., Liu, F. J., Chen, E. Q., Murakami, S., Lin, Y., He, F., Zhou, T. Y., and Huang, F. J. (2009) Establishment of cell lines using a doxycycline-inducible gene expression system to regulate expression of hepatitis B virus X protein. *Arch. Virol.* **154**, 1021-1026

212. Moya, C., Huang, Z., Cheng, P., Jayaraman, A., and Hahn, J. (2010) Investigation of IL-6 and IL-10 signalling via mathematical modelling. *IET Syst. Biol.* **5**, 15

213. Acosta, D., Anuforo, D. C., and Smith, R. V. (1980) Cytotoxicity of acetaminophen and papaverine in primary cultures of rat hepatocytes. *Toxicol. Appl. Pharmacol.* **53**, 306-314

214. Zhao, P., Kalhorn, T. F., and Slattery, J. T. (2002) Selective mitochondrial glutathione depletion by ethanol enhances acetaminophen toxicity in rat liver. *Hepatology* **36**, 326-335

215. Korzeniewski, C., and Callewaert, D. M. (1983) An enzyme-release assay for natural cytotoxicity. *J. Immunol. Methods* **64**, 313-320

216. Sasaki, T., Kawai, K., Saijo-Kurita, K., and Ohno, T. (1992) Detergent cytotoxicity: simplified assay of cytolysis by measuring LDH activity. *Toxicol. In Vitro.* **6**, 451-457

217. Henderson, C. J., Wolf, C. R., Kitteringham, N., Powell, H., Otto, D., and Park, B. K. (2000) Increased resistance to acetaminophen hepatotoxicity in mice lacking glutathione S-transferase Pi. *Proc. Natl. Acad. Sci. U. S. A.* **97**, 12741-12745

218. Laval, F., and Laval, J. (1984) Adaptive response in mammalian cells: crossreactivity of different pretreatments on cytotoxicity as contrasted to mutagenicity. *Proc. Natl. Acad. Sci. U. S. A.* **81**, 1062-1066

219. Marabini, L., Frigerio, S., Chiesara, E., and Radice, S. (2006) Toxicity evaluation of surface water treated with different disinfectants in HepG2 cells. *Water Res.* **40**, 267-272

220. Liu, Q., Bengmark, S., and Qu, S. (2010) The role of hepatic fat accumulation in pathogenesis of non-alcoholic fatty liver disease (NAFLD). *Lipids Health Dis.* **9**, 34-42

221. Negro, F. Hepatitis C virus-induced steatosis: an overview. *Dig. Dis.* **28**, 294-299

222. Niemela, O., Parkkila, S., Juvonen, R. O., Viitala, K., Gelboin, H. V., and Pasanen, M. (2000) Cytochromes P450 2A6, 2E1, and 3A and production of protein-aldehyde adducts in the liver of patients with alcoholic and non-alcoholic liver diseases. *J. Hepatol.* **33**, 893-901

223. Esterbauer, H., Schaur, R. J., and Zollner, H. (1991) Chemistry and biochemistry of 4-hydroxynonenal, malonaldehyde and related aldehydes. *Free Radic. Biol. Med.* **11**, 81-128

224. Shang, F., Nowell, T. R., Jr., and Taylor, A. (2001) Removal of oxidatively damaged proteins from lens cells by the ubiquitin-proteasome pathway. *Exp. Eye Res.* **73**, 229-238

225. Marques, C., Pereira, P., Taylor, A., Liang, J. N., Reddy, V. N., Szweda, L. I., and Shang, F. (2004) Ubiquitin-dependent lysosomal degradation of the HNE-modified proteins in lens epithelial cells. *Faseb J.* **18**, 1424-1426

226. Gomez-Lechon, M. J., Donato, M. T., Martinez-Romero, A., Jimenez, N., Castell, J. V., and O'Connor, J. E. (2007) A human hepatocellular *in vitro* model to investigate steatosis. *Chem. Biol. Interact.* **165**, 106-116

227. Sung, M., Kim, I., Park, M., Whang, Y., and Lee, M. (2004) Differential effects of dietary fatty acids on the regulation of CYP2E1 and protein kinase C in human hepatoma HepG2 cells. *J. Med. Food* **7**, 197-203

228. Mirzaei, H., and Regnier, F. (2005) Affinity chromatographic selection of carbonylated proteins followed by identification of oxidation sites using tandem mass spectrometry. *Anal. Chem.* **77**, 2386-2392

229. Morrill, G. A., Kostellow, A., Resnick, L. M., and Gupta, R. K. (2004) Interaction between ferric ions, phospholipid hydroperoxides, and the lipid phosphate moiety at physiological pH. *Lipids* **39**, 881-889

230. Nanji, A. A., Mendenhall, C. L., and French, S. W. (1989) Beef fat prevents alcoholic liver disease in the rat. *Alcohol Clin. Exp. Res.* **13**, 15-19

231. Rabek, J. P., Boylston, W. H., 3rd, and Papaconstantinou, J. (2003) Carbonylation of ER chaperone proteins in aged mouse liver. *Biochem. Biophys. Res. Commun.* **305**, 566-572

232. Cutler, P. (2004) Affinity chromatography. *Methods Mol. Biol.* **244**, 139-149

233. Zachariou, M. (2008) Affinity chromatography: methods and protocols. Preface. *Methods Mol. Biol.* **421**, vii-viii

APPENDIX

S1. Supplemental adipocyte protein table

Protein Name	Accession #	Fig. Abbrev.	N First Run	Un-used	% Cov-erage	Pep-tides (≥95%)	iTRAQ Quantitation Ratios (averaged) [3.] 115: 113	117: 113	118: 113	119: 113	121: 113
TCA Cycle											
Pyruvate dehyd	P35486	PDHA1	57	16.9	30.0	8			2.7	2.8	2.9
Pyruvate dehyd	Q9D051	PDHB1	75	14.2	39.6	6			2.0	2.2	2.2
Dihydrolipoamid	Q8R339	DLAT	79	14.0	25.1	6		1.8	2.3	2.7	2.3
dihydrolipoamid	O08749	DLD	22	27.2	45.0	14			2.1	2.3	
Pyruvate carbox	Q05920	PCB	1	112.7	65.4	57	1.9	2.5	3.2	3.7	3.7
Citrate synthase	Q9CZU6	CS	31	24.4	47.0	11		1.8	2.3	2.9	2.9
Aconitase 2, mit	Q99KI0	ACO2	9	42.5	55.4	19			2.6	3.1	3.4
Isocitrate dehyd	P70404	IDH	110	9.8	23.4	4		1.5	1.4	1.6	1.6
NADP+-specific	Q9EQK1	ICDPH	30	24.5	39.8	13			1.5		1.7
Dihydrolipoyllysi	Q9D2G2	ODO2	92	11.9	32.4	6				2.6	2.4
Succinyl-CoA lig	Q9WUM5	SUCLG1	141	7.1	18.6	3				1.5	1.7
Succinyl-CoA lig	Q9Z2I8	SUCLG2	142	7.0	20.8	3					
Sdha protein (Fr	Q921P5	SDHA	43	21.1	38.7	10			2.4	2.6	2.5
Succinate dehyd	Q9CQA3	SDHB	60	16.6	48.9	6					1.8
Fumarate hydra	P97807	FH1	38	22.3	37.1	11					
Malate dehydrog	Q8R1P0	MDH2	12	34.4	67.5	19		1.9	2.4	2.8	3.1
Solute carrier fa	Q8JZU2	CTP	42	21.3	51.5	10			2.8	3.3	3.0
Mitochondrial di	Q9QZD8	DIC	116	9.3	33.5	4		3.1	4.2	4.2	4.1
Mitochondrial 2-	Q9CR62	OGCP	155	6.5	26.5	3					
Mitochondrial gl	Q9D6M3	GC1	254	3.5	17.3	1					
Fatty acid metabolism											
acyl-CoA synthe	P41216	ACSL1	4	58.9	51.5	31	3.5	6.9	6.5	5.7	5.5
Carnitine acetylt	Q923A6	CAT	26	25.4	33.1	12		2.3	2.8	3.2	3.2
carnitine palmitc	P52825	CPT1	36	22.8	29.3	10					
Nonspecific lipic	P32020	SCP2	95	11.6	19.7	6					
Acyl-Coenzyme	Q91W85	SCAD	47	19.0	38.6	9					
Acetyl-Coenzym	Q91WS8	MCAD	41	21.5	45.6	10					
Acyl-CoA dehyd	P51174	LCAD	35	23.7	39.5	12					
Acyl-CoA dehyd	P50544	VCAD	72	14.7	22.3	8					
Delta3,5-delta2,	O35459	ECH1	212	4.3	31.8	2					
Dodecenoyl-Co	Q8QZV3	DCI	249	3.6	12.8	1					
2,4-dienoyl CoA	Q9DCI7	DECR1	89	12.2	36.1	5		1.6		2.2	2.5
Enoyl-CoA hydr	Q99LX7	ECHS1	25	26.0	61.5	13			3.1	3.9	4.3
Hydroxyacyl-Co	Q8BMS1	HADHA	10	40.7	43.9	21		1.9	2.3	2.7	2.9
Short chain 3-hy	Q61425	HADHSC	132	7.7	32.5	3					
Trifunctional en	Q99JY0	HADHB	19	28.0	42.1	14			2.3	2.5	3.0
Acetyl-CoA acet	Q8QZT1	ACAT1	46	19.8	59.2	13			3.3	3.7	3.8
ETC Complex 1											
NADH-ubiquinor	Q91VD9	NDUFS1	104	10.2	19.5	5					
NADH dehydrog	Q9CQ75	NDUFA2	281	2.9	24.3	1					
NADH-ubiquinor	Q9DC69	NDUFA9	185	5.0	19.4	3					

NADH-ubiquino	Q91YT0	NDUFV1	244	3.7	14.9	2				0.1	
NADH-ubiquino	Q62425	NDUFA4	168	6.0	30.5	3					
NDUFAF2, RIKI	Q59J78	NDUFAF2	300	2.5	28.0	1					
Auxillary Electron Carriers											
Electron transfe	Q99LC5	ETFA	20	27.6	59.5	13			2.5	3.0	3.4
Electron transfe	Q810V3	ETFB	77	14.1	51.0	6				2.4	2.7
Electron transfe	Q921G7	ETF-QO	96	11.4	22.9	4			2.1	2.3	2.8
ETC Complex 2*											
Sdha protein (F	Q921P5	SDHA	43	21.1	38.7	10			2.4	2.6	2.5
Succinate dehy	Q9CQA3	SDHB	60	16.6	48.9	6					1.8
ETC Complex 3											
Ubiquinol-cytocl	P99028	UQCRH	139	7.3	67.4	4					
Ubiquinol-cytocl	Q9DB77	UQCRC2	149	6.8	24.3	3					
Ubiquinol-cytocl	Q9CZ13	UQCRC1	161	6.1	18.3	1					
ETC Complex 4											
Cytochrome c o	Q8BJ03	COX15	285	2.8	9.4	1					
Cytochrome c o	Q9D2W1	COX5A	233	4.0	26.7	2					
Cytochrome c o	P56391	COX6B	222	4.1	42.4	2					
Cytochrome c o	Q9CPQ1	COX6C	255	3.5	56.0	1	1.5				
Cytochrome c o	P19783	COX4A	98	10.9	50.3	5					
Cytochrome c, s	P62897	CYCS	159	6.2	51.9	4				3.3	
ATP Synthase											
ATP synthase a	Q03265	ATP5A1	5	53.6	67.5	27	1.5	1.9	2.3	2.2	2.2
ATP synthase b	Q8CI65	ATP5B	6	50.5	72.8	27		1.8	2.3	2.1	2.3
ATP synthase B	Q9CQQ7	ATP5F1B	216	4.2	20.7	2					
ATP synthase D	Q9DCX2	ATP5H	137	7.4	51.9	4					
ATP synthase d	Q9DCZ0	ATP5D	197	4.7	29.2	2					
ATP synthase o	Q9DB20	ATP5O	113	9.6	42.3	6			2.3	2.3	
ATP synthase f	P56135	ATP5F	194	4.8	50.6	2					
ATP synthase g	Q91VR2	ATP5C1	78	14.1	34.2	6					
ATP synthase g	Q9CPQ8	ATP5L	239	3.9	31.8	2					
ATP synthase c	P97450	ATP5J	182	5.2	45.4	3					
ATP/ADP, Phosphate Transporters											
ADP,ATP carrie	P51881	ANT2	11	34.4	59.9	21		3.2	4.3	4.0	3.8
Phosphate carri	Q8VEM8	PCP	53	17.6	41.9	8			1.9		
Antioxidant Proteins											
Lung carbonyl r	P08074		70	14.8	32.4	7			2.7	3.5	3.7
Thiosulfate sulf	P52196		81	13.6	47.3	6		1.3	1.6	2.4	2.3
Superoxide disr	P09671		123	8.5	41.9	5	0.6	0.7			
Aldehyde dehyc	P47738		24	26.6	35.7	13					
MOSC domain-(	Q922Q1		87	12.7	30.5	7					
Peroxiredoxin 3	P20108		101	10.5	32.3	6					
Peroxiredoxin 5	P99029		163	6.0	29.5	3					
Mutant catalase	Q91XI2		150	6.7	16.5	2					
Cytochrome B5	Q9D8R3		170	5.7	33.6	2					
Microsomal glut	Q91VS7		286	2.8	31.6	1					
Other Proteins											
Ribosome-bindi	Q99PL5		2	73.5	50.6	38		0.9	0.7	0.6	0.6

60 kDa heat sh	P63038	3	73.4	88.5	38					
Stress-70 protei	P38647	7	49.7	58.9	23			2.2	2.2	2.1
Methylmalonate	Q8CIB4	8	44.8	56.3	20				4.7	
dnaK-type mole	P20029	13	34.2	45.8	14					
Protein disulfide	P09103	14	33.8	42.8	15	1.5	1.6			
Glutamate dehy	P26443	15	33.3	48.2	16					
Actin, cytoplasn	P63260	16	32.3	64.0	19					
alpha 3 type VI	O88493	17	31.4	18.9	12	1.2				
Programmed ce	Q9Z0X1	18	28.4	35.0	13					
Voltage-depend	Q60932	21	27.5	61.8	13		1.8	2.0	1.8	1.9
Glucose regulat	Q99LF6	23	26.7	45.5	12					
NRAA Best Hit:	Q9D6R2	27	25.0	47.1	12					
BAP (Represso	Q61336	28	25.0	68.6	11		1.9	2.2	1.9	2.2
Aspartate amin	P05202	32	24.3	39.3	11					
Serpin H1, 47 k	P19324	33	24.2	53.7	13					
Isovaleryl dehyc	Q9CYI3	34	24.2	41.0	11				2.7	2.4
Histone H2b (Hi	Q6ZWY9	37	22.7	91.3	16					
Mitofilin; motor	cra|mCP110172	39	22.2	36.2	9					
Calreticulin prec	P14211	40	21.7	40.4	12					
Tumor rejection	P08113	44	21.0	25.9	7		1.7			
Acetyl-Coenzyn	Q8JZR8	45	19.8	42.3	10					
Calnexin precur	P35564	48	18.7	25.6	8					
Aldh4a1 protein	Q8CHT0	49	18.3	34.9	9					
Branched-chain	O35855	50	18.1	31.6	8					
Histone protein	P10812	51	18.1	56.9	11					
Polymerase I ar	O54724	52	18.0	40.3	10					
Mitochondrial A	Q9DBP9	54	17.4	29.1	8					
Prohibitin (B-cel	P67778	55	17.0	58.8	9			2.1		
Fibronectin prec	P11276	56	16.9	12.8	6					
Voltage-depend	Q60931	58	16.9	52.7	9					
AHNAK (Fragm	Q6UL10	59	16.8	26.5	9			0.6		
Lipoprotein lipa	P11152	61	16.4	39.0	7					
Annexin A2 (An	P07356	62	16.0	45.9	7					
Cai protein (Fra	P08003	63	15.7	30.9	9					1.8
Acetyl-Coenzyn	Q921H8	64	15.7	35.1	7					
SERINE HYDR	Q99K87	65	15.6	30.8	7					
Caveolin-1	P49817	66	15.5	47.8	9					
ADP,ATP carrie	P48962	67	15.3	63.6	19					
similar to glycer	P16858	68	15.3	36.1	8					
Mus musculus 1	Q8QZS1	69	15.1	40.5	8				2.5	
Mus musculus a	Q91YQ5	71	14.7	24.0	7					
Txndc7 protein	Q922R8	73	14.5	35.7	6					
Phosphoenolpy	Q8BH04	74	14.5	29.1	6					
Hist1h4i protein	P62806	76	14.2	69.6	9				0.7	0.5
10 kDa heat sh	Q64433	80	13.8	84.2	6					
RIKEN cDNA 11	cra|mCP20737.1	82	13.5	31.1	6					
Semicarbazide-	Q66JM4	83	13.4	23.7	5					
NRAA Best Hit:	Q60597	84	13.3	19.0	6					
Voltage-depend	Q99L98	85	13.2	34.6	8		1.6	1.8	1.7	1.7
Vimentin	P20152	86	12.9	28.0	6		0.5	0.5	0.5	0.7
ERO1-like prote	Q8R180	88	12.2	29.5	5					

Ribophorin II	Q61833	90	12.0	24.3	5		
NRAA Best Hit:	cra|mCP23754.1	91	11.9	26.3	6		
Mus musculus a	Q9DCN2	93	11.9	32.9	7		
Lamin A, full ins	P48678	94	11.7	30.4	5		
Histone protein	P68433	97	11.0	47.5	5		0.5
Succinyl-CoA:3-	Q9D0K2	99	10.8	35.0	5		
hydroxysteroid (	P51660	100	10.5	22.9	4		
GrpE protein ho	Q99LP6	102	10.4	44.2	5		
Tumor-related p	Q91VA7	103	10.3	24.2	5		
Serum deprivati	Q63918	105	10.1	18.4	5		
Dihydrolipoamid	Q7TND9	106	10.1	22.4	5		
Propionyl Coen	Q8CFZ3	107	10.1	21.4	5		
NRAA Best Hit:	Q922Q8	108	10.1	28.5	5		
Procollagen, typ	P08121	111	9.8	12.6	4		
unnamed protei	Q63ZW4	112	9.8	32.9	5		
ELONGATION F	Q8BFR5	114	9.6	28.8	4		
Trap1 protein (F	Q9CQN1	115	9.3	20.7	4		
Growth and trar	Q9D6U8	117	9.2	46.5	4		
RIKEN cDNA D	Q8K009	118	9.0	19.3	4		
Ornithine amino	P29758	119	8.9	22.8	4		
Mus musculus 1	Q8BIJ6	120	8.8	16.0	4		
Peptidylprolyl is	P24369	121	8.6	36.1	4		
Protein kinase C	Q91VJ2	122	8.5	30.8	4		
Procollagen, typ	Q8K229	124	8.5	14.7	3		
NRAA Best Hit:	O35857	125	8.4	35.0	4		
Succinyl-CoA lig	Q9Z2I9	126	8.4	17.7	4		
Collagen alpha	P11087	127	8.1	11.4	4		
AFG3(ATPase f	Q8JZQ2	128	8.1	16.7	3		
Histone H1' (H1	P10922	129	8.1	35.8	3		
ES1 protein hor	Q9D172	130	7.9	27.4	4		
Sideroflexin 1	Q99JR1	131	7.9	23.0	4		
Acyl-Coenzyme	Q9DBL1	133	7.6	16.9	4		
UBQ-2 protein (	Q8R0Z9	134	7.6	42.5	3		
Hexokinase type	O08528	135	7.6	12.8	4		
Histone H1.5 (H	P43276	136	7.5	55.0	7		
Delta-1-pyrroline	Q9Z110	138	7.4	18.8	3		0.6
Histone H1.4 (H	P43274	140	7.3	67.4	11		
Mitochondrial in	Q9CPQ3	143	7.0	66.9	3		
NRAA Best Hit:	P08122	144	6.9	8.7	3		
60S ribosomal p	P47963	145	6.9	36.7	2		
Mus musculus a	Q8R4N0	146	6.9	19.2	3		
adenylate kinas	Q9WTP7	147	6.9	37.9	3		
plasma membra	O88492	148	6.8	23.0	3		
Acyl-CoA desatu	P13011	151	6.7	23.1	4		
B-cell receptor-a	Q61335	152	6.7	23.0	3	1.7	
RIKEN cDNA 15	Q91WP8	153	6.6	24.4	3		
Mus musculus a	Q9WTP6	154	6.6	35.6	3		
P32-RACK (Cor	O35658	156	6.4	26.5	4		
Histone H1.2 (H	P15864	158	6.2	70.1	11		
NADPH--cytoch	P37040	160	6.1	13.9	2		
Prostaglandin E	Q8BWM0	162	6.1	15.1	3		

TIM9, Mitochon	Q9WV98	164	6.0	57.3	3	
Ras-related pro	P51150	165	6.0	28.0	3	
Adiponectin pre	Q60994	166	6.0	19.4	3	
Mitochondrial ca	Q9D050	167	6.0	21.5	2	
60S ribosomal p	P14148	169	5.8	29.3	2	
NRAA Best Hit:	P68040	171	5.7	23.1	3	
Mus musculus 1	Q91VG6	172	5.7	24.2	2	
alpha glucosida	Q9R1N7	173	5.6	12.6	3	
MKIAA0719 pro	Q9CZW5	174	5.6	15.3	2	
Mus musculus a	P46978	175	5.6	10.4	2	
AAA-ATPase T(	Q8C6C6	176	5.5	26.1	2	
Sideroflexin 3	Q91V61	177	5.5	26.2	2	
translation elon	P10126	178	5.5	16.7	2	
Single-stranded	Q9CYR0	179	5.5	28.3	3	
Basement mem	Q05793	180	5.4	8.4	2	
Sarcoplasmic/e	O55143	181	5.3	10.3	1	
3-hydroxyisobut	Q99L13	183	5.1	27.2	2	
Calumenin prec	O35887	184	5.1	26.0	2	
Mitochondrial in	P62075	186	5.0	47.4	2	1.3
NRAA Best Hit:	Q6PHZ1	187	4.9	24.5	2	
Vesicle traffickir	O08547	188	4.9	24.7	2	
Neutral amino a	Q5U647	189	4.9	16.2	2	
Dolichyl-diphos	O54734	190	4.9	18.1	2	
60S ribosomal p	P62918	191	4.9	30.5	1	
similar to Rpl7a	P12970	192	4.9	27.6	2	
hydroxysteroid	P50172	193	4.9	20.4	2	
Leucine aminop	Q9CPY7	195	4.8	16.4	2	
Trimethyllysine	Q91ZE0	196	4.7	14.7	2	
MKIAA0152 pro	Q6ZQI3	198	4.7	21.6	2	
40S ribosomal p	P62281	199	4.7	26.6	2	
prolyl 4-hydroxy	Q60715	200	4.6	17.1	2	
60S ribosomal p	Q9CZM2	201	4.6	23.7	2	
CD63 antigen	P41731	202	4.6	13.1	2	
NRAA Best Hit:	Q99M87	203	4.6	13.4	2	
Guanine nucleo	P62880	204	4.5	15.0	2	
Mus musculus C	P97461	205	4.5	35.3	2	
60S ribosomal p	P62717	207	4.4	39.8	1	
Nuclear transpla	Q6ZPX6	208	4.4	12.6	1	
hypothetical pro	Q922H2	209	4.4	17.4	2	
RAB1, member	P62821	210	4.3	27.2	2	
40S ribosomal p	P62702	211	4.3	22.5	2	
hypothetical pro	P02468	213	4.3	9.7	2	
RIKEN cDNA 2(	Q8JZN5	214	4.2	12.3	2	
NRAA Best Hit:	Q8BSY0	215	4.2	8.5	2	
60S ribosomal p	Q811L0	217	4.2	27.3	2	
Collagen alpha	Q99LW4	218	4.1	12.6	2	
60S ribosomal p	P19253	219	4.1	27.7	1	
RIKEN cDNA 9(	Q9CZB4	220	4.1	26.8	2	
transmembrane	Q6P227	221	4.1	23.3	2	
ribosomal protei	P61358	223	4.1	23.2	2	0.6
Adipocyte plasn	Q9D7N9	224	4.1	18.3	2	

17beta-hydroxy	Q9CYT3	225	4.0	23.4	2
Mus musculus 1	P17742	226	4.0	31.7	2
Calpactin I light	P08207	227	4.0	33.3	2
triosephosphate	P17751	228	4.0	17.1	2
similar to riboso	P62900	229	4.0	20.0	2
Histone H2A.X	P27661	230	4.0	56.3	8
60S acidic ribos	P99027	231	4.0	27.8	2
Ras-related prot	Q9D1G1	232	4.0	20.1	2
Putative ATP-de	O88696	234	4.0	9.6	2
60S ribosomal p	P41105	235	4.0	32.4	1
40S ribosomal p	P62245	236	3.9	39.5	1
myosin heavy chain IX		237	3.9	14.0	1
NADP transhydı	Q61941	238	3.9	7.8	2
60S ribosomal p	Q8BP67	240	3.8	29.3	2
Gbas protein	O55126	241	3.8	24.2	1
cytochrome b-5	P56395	242	3.8	32.0	2
RIKEN cDNA 23	Q8K1Z0	243	3.7	16.3	2
DNA segment, (	Q8R3K4	245	3.6	22.3	1
carbonic anhydı	Q9QZA0	246	3.6	15.7	2
Mannosyl-oligos	Q80UM7	247	3.6	10.0	2
glycerol-3-phosp	Q64521	248	3.6	17.5	2
septin 7	O55131	250	3.6	16.7	1
Synaptic glycop	Q9CY27	251	3.6	12.0	1
Heme oxygenas	O70252	252	3.5	21.0	2
60S ribosomal p	P47962	253	3.5	29.1	1
Membrane assc	Q80UU9	256	3.4	22.2	2
QIL1 (Mus musc	Q8R404	257	3.4	26.1	2
Leucine zipper-l	Q8CGJ3	258	3.4	18.6	1
Putative steroid	O70503	259	3.4	8.0	2
Ribosomal prote	P47911	261	3.4	17.9	1
hypothetical pro	Q80VY8	262	3.3	23.9	1
60S ribosomal p	Q9D8E6	263	3.3	20.5	1
Collagen alpha	P02463	264	3.3	10.2	1
Ribosomal prote	P53026	265	3.2	14.8	1
Histone H2a(A)-	Q8CGP4	266	3.2	55.0	7
similar to 60S ril	P61255	267	3.2	28.4	1
NRAA Best Hit:	Q6P8N6	268	3.2	16.1	1
Collagen alpha	Q01149	269	3.2	10.4	1
Ribosomal prote	P27659	270	3.2	21.1	1
low molecular m	Q9CQ69	271	3.1	20.3	1
laminin B1 subu	P02469	272	3.1	10.0	1
Pdk1 protein	Q8R2U8	273	3.0	13.0	1
Mus musculus 1	P97351	274	3.0	25.4	2
Aquaporin-CHIF	Q02013	275	3.0	17.2	1
Lrpap1 protein (	P55302	276	2.9	20.9	1
Mus musculus a	O35143	277	2.9	49.1	1
UBX domain-co	Q6ZQF6	278	2.9	15.4	1
similar to riboso	P63323	279	2.9	20.5	1
splicing factor, a	Q62093	283	2.9	32.8	1
mitochondrial o	Q9QYA2	288	2.8	17.1	1
similar to 40S ril	P14206	289	2.8	26.3	1

PREDICTED: si	P14869	290	2.7	10.8	1	
Sodium/potassi	Q8VDN2	291	2.7	7.6	1	
60S ribosomal p	P62830	292	2.7	18.6	1	
Mitochondrial ac	Q9QYR9	294	2.7	21.4	1	
Methylmalonyl-C	P16332	295	2.7	9.1	1	
40S ribosomal p	P62082	296	2.6	17.0	1	
ribosomal protei	P62908	297	2.6	17.1	1	
Thioredoxin dor	Q8VBT0	298	2.6	16.6	1	
Mus musculus a	Q69ZW0	299	2.6	12.7	1	
Fatty acid-bindi	P04117	303	2.5	26.0	1	1.9
Glucosidase II b	O08795	306	2.4	11.3	1	
L-gicerin/MUC1	Q9ESS7	308	2.4	7.3	1	
Mus musculus a	P55096	309	2.4	13.2	1	
RIKEN cDNA 2	Q99KF1	310	2.4	26.8	1	
Fech protein	P22315	311	2.4	17.5	1	
methylcrotonoyl	Q99MR8	312	2.4	14.9	1	
similar to 60S ril	Q6ZWV3	313	2.4	30.4	1	
RIKEN cDNA 4	cra|mCP13941.2	314	2.4	9.9	1	
OVARIAN CAR	Q9CRD0	315	2.4	23.9	1	
Mus musculus 1	Q9CQN3	316	2.4	55.4	1	
leucine-rich PPI	Q6PB66	317	2.4	12.1	1	
hypothetical pro	Q8CGN5	319	2.3	11.6	1	
Plasminogen ac	Q9CY58	321	2.3	18.9	1	
Calcium-binding	P61022	322	2.3	24.7	1	
Thioesterase su	Q9CQR4	323	2.3	26.4	1	
60S ribosomal p	P62911	324	2.3	11.3	1	
Propionyl-Coen	Q91ZA3	326	2.3	12.9	1	
P100 co-activat	Q78PY7	327	2.2	14.2	1	
NRAA Best Hit:	Q8R3N9	328	2.2	19.3	1	
Aldolase 1, A is	P05064	329	2.2	15.1	1	
similar to 40S ril	P62852	330	2.2	27.1	1	
similar to Mitoch	Q9DB15	331	2.2	9.1	1	
ribosomal protei	P35980	332	2.2	24.5	1	
Mus musculus 2	Q9QY76	333	2.2	15.2	1	
Epoxide hydrola	P97869	334	2.2	10.8	1	
Hypothetical pro	Q91VT4	335	2.2	8.9	1	
Oligosaccharyl t	Q921E3	336	2.2	9.2	1	
Mitochondrial pr	Q9DC61	337	2.2	18.1	1	
Mus musculus 1	Q9D1L0	345	2.1	28.1	1	
Acyl coenzyme	Q9R0X4	347	2.1	13.0	1	
Bcl-2-like 13 pro	P59017	349	2.1	9.7	1	
Mus musculus a	P18155	351	2.1	13.4	1	
Dynamin-like 12	P58281	352	2.1	15.1	1	
similar to 40S ril	P62242	353	2.1	23.6	1	
Phospholipid an	Q8C0N2	354	2.1	13.5	1	
Hmgcl protein	P38060	355	2.1	8.9	1	
Mitochondrial in	Q9DCC8	356	2.1	24.8	1	
Rps13 protein	P62301	357	2.1	12.1	1	
Mus musculus 1	Q99MP2	358	2.1	13.3	1	
Cytochrome c o	P56394	360	2.1	43.6	1	
Mus musculus a	Q9JKK7	362	2.1	14.3	1	

RIKEN cDNA C	Q8R127	363	2.1	10.5	1
NRAA Best Hit:	Q8R029	365	2.1	23.5	1
Fe-containing a	Q78SV3	366	2.1	9.0	1
Bifunctional me	P18155	367	2.0	15.4	1
similar to riboso	Q9CZX8	368	2.0	18.0	1
PREDICTED: si	Q60605	369	2.0	38.8	1
Mitsugumin 23	Q8R006	370	2.0	16.1	1
MKIAA1181 pro	Q9DC16	371	2.0	10.6	1
Ribosomal prote	P62264	372	2.0	17.5	1
Alpha-globin	P01942	373	2.0	24.7	1
ATP-dependent	Q6P8N8	374	2.0	13.3	1
Hnrpc protein	Q9Z204	375	2.0	20.6	1
Nsep1 protein	P62960	376	2.0	23.0	1
NRAA Best Hit:	P47915	378	2.0	17.5	1
hypothetical pro	Q9ES97	381	2.0	12.3	1
Superoxide disn	P08228	385	2.0	12.4	1
Transmembrane	Q8C1E7	386	2.0	10.5	1
Ras-related prot	Q9D1G1	388	2.0	21.4	2
Ras-related prot	P61027	389	2.0	20.0	1
RAB35, membe	Q6PHN9	392	2.0	17.4	1
22 kDa neurona	Q91XV3	398	2.0	16.4	1
Diacylglycerol C	Q9Z2A7	401	2.0	9.4	1
Hydroxysteroid	Q8K5C9	402	2.0	9.9	1
Mus musculus 1	Q9CTC5	406	2.0	11.2	1
Heme binding p	O88814	409	2.0	15.3	1
Cop-coated ves	Q9R0Q3	410	2.0	11.0	1
Ras-related prot	P35278	412	2.0	15.7	1
Tyrosine phospl	Q9D3B1	413	2.0	19.7	1
Mus musculus 1	Q9D3P8	414	2.0	19.7	1
similar to acidic	P47955	416	2.0	19.0	1
NRAA Best Hit:	Q9JJA0	417	2.0	11.6	1
Mus musculus a	Q9CQN5	418	2.0	15.4	1
Uncharacterizec	Q91WS0	419	2.0	15.7	1
Transcription fa	P40630	420	2.0	18.5	1
Acyl carrier prot	Q9CR21	421	2.0	16.7	1
60S ribosomal p	P83882	422	2.0	20.0	1
DnaJ homolog s	P60904	423	2.0	12.6	1
Cytochrome c o	P17665	424	2.0	27.0	1
NRAA Best Hit:	P62855	425	2.0	23.5	1
Microsomal glut	Q9CPU4	426	2.0	19.6	1
ATP synthase li	P56383	427	2.0	11.0	1
Mus musculus a	Q8C0Z8	428	2.0	11.9	2
Thy-1 membran	P01831	429	2.0	14.2	1
Mus musculus 1	Q920S6	431	2.0	5.0	1
vesicle-associat	Q9WV55	437	2.0	23.0	1
Solute carrier fa	P17809	438	2.0	9.4	1
CD9 antigen	P40240	440	1.9	12.9	1
hypothetical pro	Q80WJ7	451	1.8	10.7	1
Metaxin 2, full ir	Q8C454	452	1.8	9.1	1
Ndufv2 protein (	Q9D6J6	456	1.7	23.4	1
Ubiquinol-cytocl	Q9CR68	461	1.7	13.1	1

Histone macroH	Q91VZ2	467	1.7	16.1	1
Expressed sequ	Q80ZS3	470	1.7	19.0	1
similar to 40S ril	P62754	471	1.6	26.1	1
similar to 60S ril	P51410	479	1.6	26.0	1
Acyl-CoA dehyd	Q9D7B6	480	1.6	5.8	1
NRAA Best Hit:	Q9WVA2	481	1.5	9.5	1
Trypsinogen 16	Q9Z1R9	489	1.5	13.4	1
ATP synthase e	Q06185	492	1.5	15.7	1
Fdxr protein (Fr	Q61578	498	1.5	15.2	1
Fatty acid-bindi	Q05816	503	1.4	23.7	1
sulfite oxidase	Q8R086	504	1.4	8.2	2
Heat shock prot	P11499	507	1.4	14.5	1
Rps16 protein (I	P14131	514	1.4	19.1	1

1. N number corresponds to overall Protein Pilot score (N=1 is highest score)
2. These proteins are also listed in the TCA Cycle
3. These protein quantitations are based on peptides that are found in both experimental data sets for each protein. Each protein was found to have a quantitation p-value <= 0.05 in each data set respectively

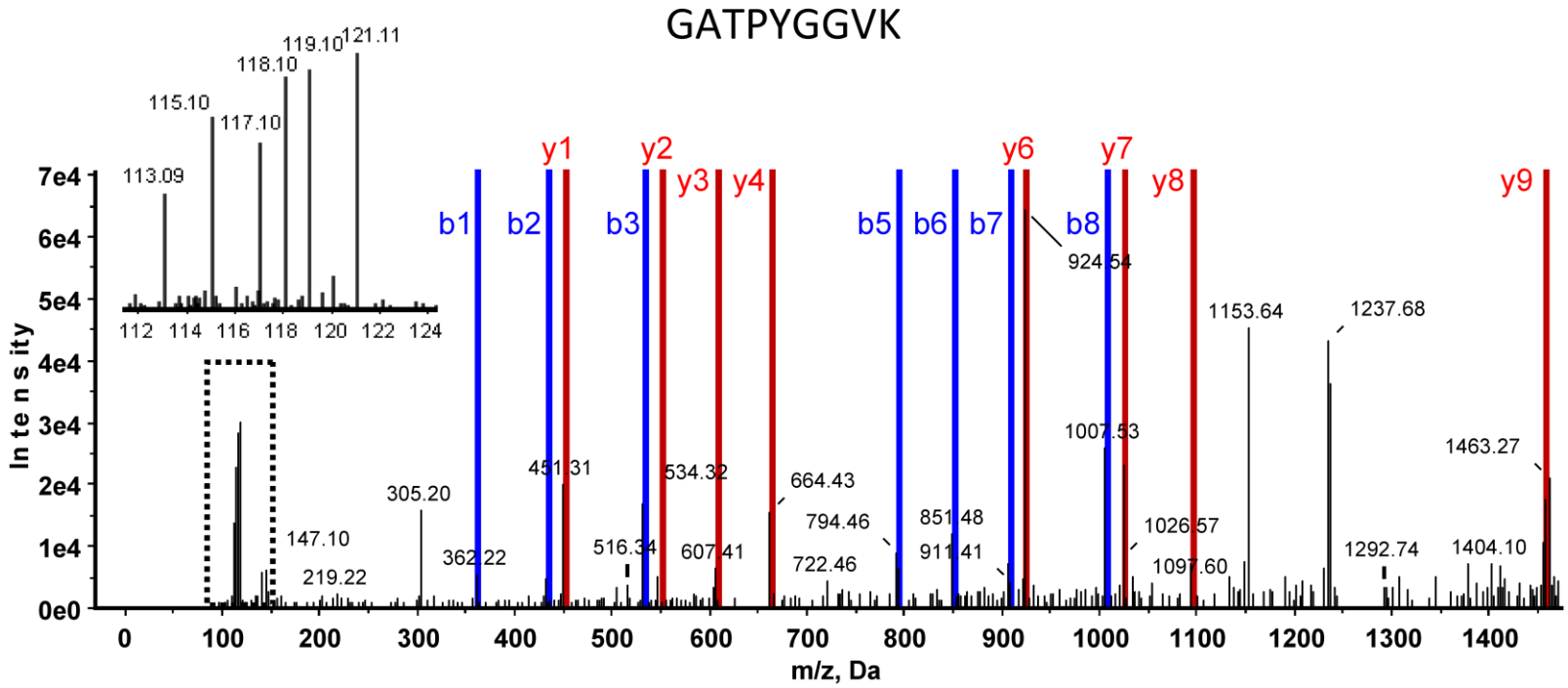

Figure S.3. Representative tandem mass spectrum of iTRAQ labeled tryptic peptides. Ion signals corresponding to b-type and y-type fragment ions from the tryptic peptide GATPYGGVK (acetyl CoA-acetyl transferase) are labeled in blue and red, respectively. Inserted is a zoom-in of the spectrum in the low mass range displaying the iTRAQ reporter ions.

VITA

Name: Billy Walker Newton

Address: Chemical Engineering Department, Texas A&M University
c/o Arul Jayaraman
Jack E. Brown Building, MS 3122
College Station, TX 77843-3122

Email Address: bnewton2k@yahoo.com

Education: B.S., Chemical Engineering, Texas A&M University, 2000
M.S., Chemical Engineering, Texas A&M University, 2008
Ph.D., Chemical Engineering, Texas A&M University, 2011

Research Interests: proteomics, sources of reactive oxygen species, biological effects of oxidative stress, especially in adipocytes and hepatocytes, and oxidative protein modifications.